IN THE UNITED STATES PATENT AND TRADEMARK OFFICE

Applicants:	Benvenisty	Atty Docket:	1822/113
Serial No.:	09/918,702	Art Unit:	1632
Date Filed:	July 31, 2001	Examiner:	Crouch, D.

Invention: Directed Differentiation of Embryonic Stem cells

****

CERTIFICATE OF MAILING

I hereby certify that this document, along with any other papers referred to as being attached or enclosed, is being deposited with the United States Postal Service as first class mail in an envelope addressed to: Commissioner for Patents, P.O. Box 1450, Alexandria, VA 22313-1450 on March 17, 2005.

Barbara J. Carter, Ph.D.

****

Commissioner for Patents
P.O. Box 1450
Alexandria, VA 22313-1450

DECLARATION OF BENVENISTY, M.D., PH.D. IN SUPPORT OF APPLICANT'S RESPONSE
[37 C.F.R. § 1.132]

Dear Sir:

In support of the accompanying response to the Office Action mailed December 17, 2004 in the above-reference matter, I hereby declare as follows:

1. My name is Nissim Benvenisty, M.D., Ph.D. I am a Professor at The Hebrew University in Jerusalem, Israel, in the Department of Genetics. I was formerly the Vice Chair of the Institute of Life Sciences at The Hebrew University, and have been a visiting Professor in the Department of Genetics at Harvard University in Boston, MA, among

other positions. I have been awarded numerous prizes and fellowships, including the Teva Prize for excellent research in stem cells in 2003, the Herbert Cohn Chair in Cancer Research during 1999, the Rom Prize in Genetics in 1998, a Howard Hughes Postdoctoral Fellowship from 1991-1993, and a Fulbright Postdoctoral Fellowship from 1990-1991. I have published extensively in the field of stem cell research, and other areas, with over 65 publications, to date. I am also an inventor or co-inventor of a substantial number of patents involving (among other things) human embryonic stem cell research, and I am the sole inventor of the invention claimed in the current application. My further credentials are set forth in my Curriculum Vitae, which is attached hereto as Exhibit A.

2. I have read the action of December 17, 2004. This declaration is provided to distinguish, on a technical level, why the claims in the above-referenced application as novel and non-obvious relative to the prior art references cited in the Office Action. This declaration is also provided to show that all of the pending claims for directing differentiation to specific cell types are enabled, by citing additional publications which rely on my protocols for preparing human embryoid bodies to direct differentiation of human embryonic cells into functional specific cell types.

Consideration of the Prior Art

3. The Examiner rejected claims 8, 9, 11, 12, 60 and 65 under 35 U.S.C. 103(a) as being unpatentable over Thomson et al. (1998) in view of Shamblott et al. (1998) and further in view of Yuen et al. (1998). As discussed in the March 3, 2005 interview, Thomson never satisfactorily verified that the human ES cell lines that were generated "maintained the potential to form derivatives of all three embryonic germ layers" (see

Thomson p. 1146, 1st column, lines 30-32), because he relied on evidence of teratomas generated in SCID mice injected with said cell lines (*id.*, p. 1147, Figure 4) to conclude that his cells actually were pluripotent human ES cells. As pointed out by Shamblott on the first page of the cited reference (see Shamblott, p. 13726, col. 2) "ES and EG cells from some species can form teratocarcinomas when injected into histocompatible or immunologically comprised mice. This property alone may not be a definitive test of stem cell pluripotency, as it has been demonstrated that rat and mouse visceral (yolk sac) endoderm are capable of forming highly differentiated teratomas containing cells of all three embryonic germ layers." Nonetheless, assuming Thomson's cells actually are pluripotent hES cells, if one starts with Thomson's cells, and tries to apply the methods of Shamblott for hEG cells to form hEBs, and then use mouse protocols such as Yuen et al. to direct differentiation, one will not get the results we have seen, not would one in the art even combine these technologies.

4. As already presented in my declaration of September 20, 2004 (Declaration 1) the human EG cells in Shamblott are very different from hES cells, with respect to many features. Any cell line deriving from hEG cells will be dissimilar from cell lines derived from hES cells. More importantly, my methods for forming hEBs and directing differentiation of human embryonic cells derived from those hEBs *require* dissociation of the hES cells initially used, followed by aggregation to hEBs, followed by additional dissociation of the hEBs to obtain dissociated human embryonic cells that can be treated with various factors to direct differentiation.

5. As acknowledged in a News Focus in Science magazine (Vogel, G., (2002) *Science*, Vol. **295**, pp. 1818-1820 – see Exhibit D of Declaration 1) under a section entitled

"Fundamental Firsts", my achievements of both embryoid bodies formation and directed differentiation of human ES cells are highlighted (see p. 1819, column 2, first full paragraph ("Their first project was to test whether human ES cells, like those from mice, can form ... embryoid bodies. Initial studies by Thomson's group suggested they didn't.... But by learning how to grow the cells suspended in liquid ... [they] found that they could."

6. Without the ability to start with actual pluripotent human ES cells, dissociate the hES cells and allow them to aggregate and form true human EBs, and then dissociate the hEBs into dissociated human embryonic cells, one would never be able to look to Yuen et al. and mouse protocols for directing differentiation of the dissociated EB-derived human embryonic cells.

7. Later in the same section of the News Focus article in Science, my laboratory is credited with other firsts, verifying that I was first to successfully produce human differentiated ES cells. See last line of column 2 through column 3, line 10 – "Benvenisty and company scored several other firsts. In October 2000 the team ... published the first paper on how growth factors ... prompt human ES cells to mature into different types.")

8. Moreover, Shamblott admits that their EB-like aggregates formed from human EG cells cannot be sufficiently dissociated after aggregating to form the EB-like bodies (see Shamblott et al., p.13729 col. 1, para. 1 and col. 2, para.4 - "Alternative disaggregation enzymes are currently under investigation" because trypsin/EDTA is not effective, a step essential for directing differentiation into specific cell types.) This second dissociation step is essential for directing differentiation of human embryonic cells derived from

hEBs. For these reasons, it was not obvious to produce differentiated cells from human EBs and the establishment of embryoid bodies from human ES cells may be considered a new and not obvious technology since it was developed at a time when all the research reported that such technology was not possible (Reubinoff et al, 2000). As stated in Declaration 1, when I attended a conference in 2001 and presented my results showing human embryoid body formation from human ES cells and subsequent directed differentiation of the human embryonic cells, and many experts in the field simply did not believe me (including Reubinoff), questioning my results intensely. Therefore, the combination of Thomson, Shamblott and Yuen would never be made by someone on the field trying to form true human EBs and then dissociate them to dissociated human embryonic cells that can be treated with various factors to direct differentiation. And even if such a combination were attempted, it would not be successful.

9. With respect to enablement for the specific differentiated cell types claimed, and whether our methods for directing differentiation lead to functional cells, I have provided, with this declaration, several articles (see Exhibits B-E, attached hereto) -published by others in the field using my methodologies for forming hEBs and then directing their differentiation into functional cells. These article support our pending claims for directing differentiation of human embryonic cells derived from hEBs into specific cell types wherein the differentiated cells so obtained are functional. The results by these other researchers show that someone in the field who uses the methodologies we claim in the instant application obtain differentiated cells that are functional. Therefore, our methods and claims are enabled for directing differentiation into specific cell types.

10. For example, Carpenter et al. (*Exp Neurol* (2001) **172**:383-397, "Enrichment of Neurons and Neural Precursors from Human Embryonic Stem Cells"- attached hereto as Exhibit B) used undifferentiated hES cells (H1, H7 and H9 cells) to produce human EBs using a protocol nearly identical to mine, and then directed differentiation of dissociated ES from the EBs using retinoic acid followed by culturing in differentiation medium (containing human neurotrophin-3 (hNT-3) and human brain-derived neurotrophic factor (hBDNF)). Analysis indicated that the resulting differentiated hES cell-derived neurons could synthesize neurotransmitters, respond to neurotransmitters, make synapses, and generate electrical activity (see pp. 390-392 and Figs. 3-7).

11. In addition, Kehat et al (*J Clin Invest* (2001) **108**(3):407-414 "Human embryonic stem cells can differentiate into myocytes with structural and functional properties of cardiomyocytes" – attached hereto as Exhibit C) cite and follow my protocols for both formation of human EBs from hES cells (reference 12 - Itskovitz-Eldor et al. - in Kehat et al.) and directed differentiation (reference 13 - Schulbinder et al – in Kehat et al.) (see col. 1, p. 408 of Kehat et al.). Kehat et al. show in this paper that hES cell-derived differentiated myocytes form spontaneously contracting areas (see pp. 410 – 412, Figs. 1b, and 3-6)

12. Following this initial study, Kehat et al. showed that hES cell-derived cardiomyocytes were able to form structural and electromechanical connections with cultured rat cardiomyocytes (see Kehat et al., *Nature Biotech* (2004) **22**(10):1282-1289 "Electromechanical integration of cardiomyocytes derived from human embryonic stem cells" – attached hereto as Exhibit D) The two Kehat papers rely on my previous published procedures for generating EBs from hES cells and directing differentiation of

dissociated hES cells, and verify that using my differentiation procedures, functional myocytes, particularly cardiomyocytes, are formed."

13. Finally, Assady et al. (*Diabetes* (2001) **50**:1691-1697 "Insulin Production by Human Embryonic Stem Cells" – attached hereto as Exhibit E) cite my protocols as references 16 and 19 and use my protocols to generate EBs (see "Research Design and Methods," p. 1692 of Assady – ref. 19 – for production of EBs). Assady et al. specifically cite my PNAS paper, one of the publications that forms the basis of this application, as having used RT-PCR to detect a wide variety of differentiated cell markers, including insulin (see Assady et al., p. 1691, col. 1). Assady et al. then use protocols I developed for generating EBs from hES cells (*id.*, p. 1692, col. 2) and verify that one can direct differentiation of hES cells after forming EBs into human pancreatic cells that are functional, as verified by their ability to secrete insulin, and are probably also glucose responsive (although that could not be absolutely confirmed because of the experimental parameters.)

14. Therefore, based on our specification and disclosed protocols, and supported by other researchers using my protocols to direct differentiation of human embryonic cells derived from hEBs into functional specific cell types, which confirm that the protocols disclosed in the present application, if followed, will in fact lead to functional differentiated cells, I believe that our methods and claims for directing differentiation of human embryonic cells into specific cell types are fully enabled.

15. I hereby declare that all statements made herein are of my own knowledge and that all statements made on information and belief are true; and further that these statements are being made with the knowledge that willful false statements and the like so made are

punishable by fine or imprisonment or both under Section 1001 of Title 18 of the United States Code and that such willful false statements may jeopardize the validity of the application or any patent issued thereon.

_____

Benvenisty, M.D., Ph.D.

Dated: March ____, 2005

371498v1

Exhibits:

A - Curriculum Vitae of Nissim Benvenisty, M.D., Ph.D.

B - Carpenter et al., *Exp Neurol* (2001) **172**:383-397, "Enrichment of Neurons and Neural Precursors from Human Embryonic Stem Cells."

C - Kehat et al., *J Clin Invest* (2001) **108**(3):407-414 "Human embryonic stem cells can differentiate into myocytes with structural and functional properties of cardiomyocytes.

D - Kehat et al., *Nature Biotech* (2004) **22**(10):1282-1289 "Electromechanical integration of cardiomyocytes derived from human embryonic stem cells."

E - Assady et al., *Diabetes* (2001) **50**:1691-1697 "Insulin Production by Human Embryonic Stem Cells."

NISSIM BENVENISTY

CURRICULUM VITAE

Date and Place of Birth : 9.10.1958; Israel.

Marital Status: Married + 3.

Education :

1983	M.D.	Faculty of Medicine, Hebrew University.
1986	Ph.D.	Department of Developmental Biochemistry, Hadassah Medical School, Hebrew University.

Employment and Related Training :

2002-	Professor, Department of Genetics, The Hebrew University, Jerusalem, Israel.
2002-2003	Head of Biology Teaching and Vice Chair, Institute of Life Sciences The Hebrew University, Jerusalem, Israel
1999-2000	Visiting Professor, Department of Genetics, Harvard University, Boston, USA
1998-2002	Associate Professor, Department of Genetics, The Hebrew University, Jerusalem, Israel.
1993-1998	Senior Lecturer, Department of Genetics, The Hebrew University, Jerusalem, Israel.
1990-1993	Research Fellow, Department of Genetics, Harvard Medical School, Boston, USA. Under supervision of Professor Philip Leder.
1986-1990	Israeli Army Medical Service.
1983-1986	Graduate Student, Department of Developmental Biochemistry, The Hebrew University, Jerusalem, Israel.
1985	Research Associate, Case Western Reserve University, Cleveland, USA.

1983-1984	Internship, Hadassah Hospital, Jerusalem, Israel.
1982-1985	Teaching biochemistry and molecular biology to medical students at The Hebrew University.

Awards and Fellowships :

1981	Awarded the Faculty Prize.
1982	Awarded a Fellowship at the Mount Sinai Hospital, New York - Program for outstanding students.
1982-1985	Foulkes Foundation Fellowship.
1985	Best Teacher Award for teaching biochemistry and molecular biology.
1988	Awarded the Senta Foulkes Prize (London).
1990-1991	Awarded the Weizmann Postdoctoral Fellowship.
1990-1991	Awarded the Fulbright Postdoctoral Fellowship.
1991-1993	Awarded the Howard Hughes Postdoctoral Fellowship.
1993-1996	Awarded the Alon Fellowship.
1994	The Joseph H. and Belle R. Braun Senior Lectureship in Life Sciences.
1995-1998	Awarded Best Teacher in Genetics.
1995	Awarded the Hebrew University Prize for Young Scientist.
1996	Awarded the Naftali Prize.
1997	Awarded the Hestrin Prize in Biochemistry and Molecular Biology.
1998	Awarded the Rom Prize in Genetics
1999	The Herbert Cohn Chair in Cancer Research
1999-2000	Awarded the Yamagiwa-Yoshida Memorial International Cancer Study Fellowship.
2003	Awarded the Teva Prize for excellent research in stem cells

List of publications

1. **Benvenisty, N.**, Ben-Simchon, E., Cohen, H. Mencher, D., Meyuhas, O. and Reshef, L. : Control of the activity of phosphoenolpyruvate carboxykinase and the level of its mRNA in livers of newborn rats. Eur. J. Biochem. 132: 663-668 (1983).

2. Mencher, D., Cohen, H., **Benvenisty, N.**, Meyuhas, O. and Reshef, L. : Primary activation of cytosolic phosphoenolpyruvate carboxykinase gene in fetal liver and the biogenesis of its mRNA. Eur. J. Biochem. 141: 199-203 (1984).

3. **Benvenisty, N.**, Cohen, H., Gidoni, B., Mencher, D., Meyuhas, O., Shouval, D. and Reshef, L. : Insulin deficient diabetes in the perinatal period: ontogeny of gluconeogenesis and phosphoenolpyruvate carboxykinase. In : Lessons from Animal Diabetes, E. Shafrir and A.E. Renold eds., John Libby & Company, London, pp. 717-733 (1984).

4. **Benvenisty, N.**, Mencher, D., Meyuhas, O., Razin, A. and Reshef, L. : Sequential changes in the methylation patterns of the rat phospho-enolpyruvate carboxykinase gene during development. Proc. Natl. Acad.Sci. USA 82: 267-271 (1985).

5. **Benvenisty, N.**, Szyf, M., Mencher, D., Razin, A. and Reshef, L. : Tissue-Specific hypomethylation and expression of rat phosphoenolpyruvate carboxykinase gene induced by in-vivo treatment of fetuses and neonates with 5-azacytidine. Biochemistry 24: 5015-5019 (1985).

6. Cohen, H., Gidoni, B., Shouval, D., **Benvenisty, N.**, Mencher, D., Meyuhas, O. and Reshef, L. : Conservation from rat to human of cytosolic phosphoenolpyruvate carboxykinase and the control of its gene expression. FEBS Lett. 180: 175-180 (1985).

7. **Benvenisty, N.**, Razin, A. and Reshef, L. : Developmental changes in the methylation pattern, chromatin conformation and expression of the rat phosphoenolpyruvate carboxykinase gene. In : Biochemistry and Biology of DNA Methylation, G.L. Cantoni and A. Razin, eds. , Alan R. Liss, Inc., New York, pp. 185-199 (1985).

8. **Benvenisty, N.**, Mencher, D., Meyuhas, O., Razin, A. and Reshef, L. :

Sequential changes in the methylation patterns of the rat phospho-enolpyruvate carboxykinase gen during development. Gent. Abstr. 17: 115 (1985).

9. **Benvenisty, N.** and Reshef, L. : Direct introduction of genes into rats and the expression of the genes. Proc. Natl. Acad. Sci. USA 83: 9551-9555
(1986).

10. Nechushtan, H., **Benvenisty, N.**, Brandes, R. and Reshef, L. : Glucocorticoids control phosphoenolpyruvate carboxykinase gene expression in a tissue-specific manner. Nucl. Acids Res. 15: 6405-6417 (1987).

11. **Benvenisty, N.** and Reshef, L.: Developmental expression and modification of genes. Biol. Neonate 52 : 61-69 (1987).

12. **Benvenisty, N.** and Reshef, L. : Developmental acquisition of DNAse I sensitivity of phosphoenolpyruvate carboxykinase (GTP) gene in rat liver. Proc. Natl. Acad. Sci. USA 84: 1132-1136 (1987).

13. Cohen, H., **Benvenisty, N.** and Reshef, L. : Fate of polyoma origin of replication after its direct introduction into mice. FEBS Lett. 223: 347-351 (1987).

14. **Benvenisty, N.**, Nechushtan, H., Cohen, H. and Reshef, L. : Separate cis regulatory elements confer expression of phosphoenolpyruvate carboxykinase (GTP) gene in different cell lines. Proc. Natl. Acad. Sci. USA 86: 1118-1122 (1989).

15. **Benvenisty, N.** : A molecular view of tissue differentiation and development. J. Royal Coll. Phys. London 23: 156-160 (1989).

16. **Benvenisty, N.**, Nechushtan, H., Shoshani, T., Cohen, H. and Reshef, L. : Cell specific expression of rat PEPCK gene in tissues from different embryonal origin. Cell Differ. Dev. 27: S219 (1989).

17. **Benvenisty, N.**, Shoshani, T., Farkash, Y., Soreq, H. and Reshef, L. : Trans activation of rat phosphoenolpyruvate carboxykinase (GTP) gene expression by micro-injection of rat liver mRNA in Xenopus laevis oocytes. Mol. Cell. Biol. 9: 5244-5247 (1989).

18. Brandes, R., Arad, R., **Benvenisty, N.** Weil, S. and Bar-Tana, J. : The induction of adipose conversion by bezafibrate in 3T3-L1. Synergism

with dibutiryl-cAMP. Biochem. Biophys. ACTA 1054: 219-224 (1990).

19. Trus, M., **Benvenisty, N.**, Cohen, H. and Reshef, L. : Developmentally regulated interactions of liver nuclear factors with the rat phospho-enolpyruvate carboxykinase promoter. Mol. Cell. Biol. 10: 2418-2422 (1990).

20. **Benvenisty, N.** and Reshef, L. : Regulation of tissue- and development-specific gene expression in the liver. Biol. Neonate 59: 181-189 (1991).

21. Shoshani, T., **Benvenisty, N.**, Trus, M. and Reshef, L. : Cis regulatory elements that confer differential expression upon the rat gene encoding phosphoenolpyruvate carboxykinase in the kidney and liver. Gene 101: 279-283 (1991).

22. **Benvenisty, N.**, Ornitz, D.M., Bennett, G.L., Sahagan, B.G., Kuo, A., Cardiff, R.D. and Leder, P.: Brain tumors and lymphomas in transgenic mice that carry HTLV-I LTR/c-myc and Ig/ tax genes. Oncogene 7: 2399-2405 (1992).

23. **Benvenisty, N.** , Leder, A., Kuo. A., and Leder, P.: An embryonically expressed gene is a target for c-Myc regulation via the c-Myc binding sequence. Genes & Development 6: 2513-2523 (1992).

24. Yanuka-Kashless, O., Cohen. H., Trus, M., Aran, A., **Benvenisty, N.** and Reshef, L.: Transcriptional regulation of the phosphoenolpyruvate carboxykinase (GTP) gene by cooperation between hepatic nuclear factors. Mol. Cell. Biol. 14: 7124-7133 (1994).

25. Dushnik-Levinson, M. and **Benvenisty, N.**: Embryogenesis *in vitro*: The study of differentiation of embryonic stem cells. Biol. Neonate 67: 77-83 (1995).

26. **Benvenisty, N.** and Ornitz, D.M.: BK1: An FGF-responsive central nervous system-derived cell line. Growth Factors 12: 49-55 (1995).

27. Schuldiner, O., Eden, A., Ben-Yosef, T., Yanuka, O., Simchen, G. and **Benvenisty, N.**:*ECA39*, a conserved gene regulated by c-Myc in mice, is involved in G1/S cell cycle regulation in yeast. Proc. Natl. Acad. Sci. USA 93: 7143-7148 (1996).

28. Ben-Yosef, T. Yanuka, O. and **Benvenisty, N.**: *ECA39* is regulated by c-Myc in human and by a Jun/Fos homolog, Gcn4, in yeast. Oncogene 13: 1859-1866 (1996).

29. Eden, A., Simchen, G. and **Benvenisty, N.**: Two yeast homologs of *ECA39*, a target for c-Myc regulation, code for cytosolic and mitochondrial branched-chain amino acid aminotransferases. J. Biol. Chem. 271: 20242-20245 (1996).

30. Cohen, H., Trus, M., **Benvenisty, N.** and Reshef, L.: Characterization of expression of several hepatoma specific genes during liver development and upon premature induction by hormones. Eur. J. Biochem. 242: 550-556 (1996).

31. Ben-Porath, I. and **Benvenisty, N.**: Characterization of a tumor associated gene, a member of a novel family of genes encoding membrane glycoproteins. Gene 183: 69-75 (1996).

32. Dushnik-Levinson, M. and **Benvenisty, N.**: Hepatocyte nuclear factor 3 is involved in endodermal differentiation of embryonic stem cells. Mol. Cell. Biol. 17: 3817-3822 (1997).

33. Eden, A. and **Benvenisty, N.**: Charactrization of branched-chain amino acid aminotransferase in *S. pombe.* Yeast 14: 189-194 (1998).

34. Schuldiner, O., Yanover, C. and **Benvenisty, N.**: Computer analysis of the entire budding yeast genome for putative targets of the GCN4 transcription factor. Current Genetics 33: 16-20 (1998).

35. Ben-Porath, I., Kozak, C.A. and **Benvenisty, N.**: Chromosomal mapping of *Tmp (EMP1)* , *Xmp (EMP2)* and *Ymp (EMP3)*, genes encoding membrane proteins related to *Pmp22*. Genomics 49: 433-437 (1998)

36. Ben-Yosef, T., Eden, A. and **Benvenisty, N.**: Characterization of Murine BCATs: *Bcat1*, a target for c-Myc oncogene, and its homolog *Bcat2*. Mamm. Genome 9: 595-597 (1998).

37. Ben-Yosef, T., Yanuka, O. and **Benvenisty, N.**: Involvement of Myc targets in c-*myc* and N-*myc* induced human tumors. Oncogene 17: 165-172 (1998).

38. Ben-Porath, I., Yanuka, O. and **Benvenisty, N.**: The *Tmp* gene, encoding a membrane protein, is a c-Myc target with a tumorigenic activity. Mol. Cell. Biol. 19: 3529-3539 (1999).

39. Eden, A. and **Benvenisty, N.**: Involvement of branched-chain amino

acid amino transferase, a target for c-Myc activity, in apoptosis. FEBS Lett. 457: 255-261 (1999).

40. Ben-Yosef, T. and **Benvenisty, N.**: Hereditary cancer and Developmental abnormalities. Biol. Neonate 77:1-11 (2000).

41. Itskovitz-Eldor, J., Schuldiner, M., Karsenti, D., Eden, A., Yanuka, O., Amit, M., Soreq, H. and **Benvenisty, N.**: Differentiation of human ES cells into embryoid bodies comprising the three embryonic germ layers. Mol. Med. 6:88-95 (2000) (Cover).

42. Schuldiner, M., Yanuka, O., Itskovitz-Eldor, J., Melton, D.A. and **Benvenisty, N.**: Effects of eight growth factors on the differentiation of cells derived from human embryonic stem cells. Proc. Natl. Acad. Sci. USA 97:11307-11312 (2000) (Cover).

43. Eden, A., Van Nedervelde, L., Drukker, M., **Benvenisty, N.** and Debourg, A.: Involvement of branched-chain amino acid aminotransferase in the production of fusel alcohols during fermentation in yeast. Appl. Microbiol.Biotechnol. 55:296-300 (2001).

44. Eiges, R., Schuldiner, M., Drukker, M., Yanuka, O., Itskovitz-Eldor, J. and **Benvenisty, N.** (PI): Establishment of transfected clones of human embryonic stem cells carrying a marker for undifferentiated cells. Current Biology 11:514-518 (2001).

50. Schuldiner, O. and **Benvenisty, N.**: A DNA microarray screen for genes involved in c-*MYC* and N-*MYC* oncogenesis in human tumors. Oncogene 20:4984-4994. (2001).

46. Schuldiner, M., Eiges, R., Eden, A. Yanuka, O., Itskovitz-Eldor, J., Goldstein, R. and **Benvenisty, N.** (PI): Induced neuronal differentiation of human embryonic stem cells. Brain Research 913:201-205 (2001) (Cover).

47. Schuldiner, M. and **Benvenisty, N.**: Human embryonic stem cells: From human embryogenesis to cell therapy. In Recent Research Developments in Molecular & Cellular Biology Research Signpost Press. pp. 223-231 (2001).

48. **Benvenisty, N.**: Europe and the stem cells question. Trends in Biotech. 20: 183 (2002).

49. Goldstein, R., Drukker, M., Reubinoff, B. and **Benvenisty, N.**: Integration and differentiation of human embryonic stem cells transplanted to the chick embryo. Dev. Dyn. 225:80-86 (2002).

50. Schuldiner, O., Shor, S. and **Benvenisty, N.**: A computerized database-scan
to identify c-MYC targets. Gene 292:91-99 (2002).

51. Eiges, R. (S) and **Benvenisty, N.** (PI): A molecular view on pluripotent stem cells. FEBS Lett. 529: 135-141 (2002).

52. Drukker, M., Katz, G., Urbach, A., Schuldiner, M., Markel, G., Itskovitz-Eldor, J., Reubinoff, B., Mandelboim, O. and **Benvenisty, N.**: Characterization of the major histocompatibility complex proteins expression in human embryonic stem cells. Proc. Natl. Acad. Sci. USA 99: 9864-9869 (2002).

53. Lavon, N. and **Benvenisty, N.**: Differentiation and genetic manipulation of human embryonic stem cells. Trends Cardiovas. Med. 13: 47-52 (2003).

54. Drukker, M. and **Benvenisty, N.**: Genetic manipulation of human embryonic stem cells. In: Human embryonic stem cells and other pluripotent cells. M.S. Rao and Chiu, eds. Humana Press Inc., Totowa, NJ, 265-284 (2003).

55. Schuldiner, M., Itskovitz-Eldor, J. and **Benvenisty, N.**: Selective ablation of human embryonic stem cells expression a suicide gene. Stem Cells 21: 257-265 (2003).

56. Schuldiner, M. and **Benvenisty, N.**: Factors controlling human ES cell differentiation differentiation of In: Methods in Enzymology, P.M. Wassarman and G.M. Keller, eds. , Academic Press, New York. 365: 446-461 (2003).

57. Drukker, M. and **Benvenisty, N.**: The immunogenicity of human embryonic stem-derived cells. Trends in Biotech. 22:136-141 (2004).

58. Hornstein, E. and **Benvenisty, N.**: The "brainy side" of human embryonic stem cells. Journal of Neuroscience Research 76:169-173 (2004).

59. Schuldiner, M. and **Benvenisty, N.**: In vitro culture and differentiation of human ES cells. In: Methods in mammalian gene targeting and embryonic stem cells, J. McWhir and A. Thomson, eds. , BIOS, London pp. 141-156 (2004).

60. Drukker, M., Dhara, S. and **Benvenisty, N.**: Genetic engineering of human embryonic stem cells. In: Human embryonic stem cells. J. Odorico, R. Pedersen, S.C. Zhang, eds. BIOS, London (in press) (2004).

61. Drukker, M. and **Benvenisty, N.**: Immunogenicity of embryonic stem cells. In: Handbook of embryonic stem cells. R. Lanza, ed. Academic Press, (in press) (2004).

62. Meyshar, Y. and **Benvenisty, N.**: Genetic manipulation of human embryonic stem cells. In: Handbook of embryonic stem cells. R. Lanza, ed. Academic Press, (in press) (2004).

63. Dvash, T. and **Benvenisty, N.**: Human embryonic stem cells as a model for the study of early human development Clin. Obst. Gyn.(in press) (2004)

64. Urbach, A., Schuldiner, M. and **Benvenisty, N.**: Modeling for Lesch-Nyhan Disease by gene targeting in human embryonic stem cells. Stem Cells 22:635-641 (2004).

65. Lavon, N. and **Benvenisty, N.**: Embryonic stem cell and the cardiovascular system. Cardiovascular Genomics Human Press, M.K. Raizada ed. (in press) (2004).

66. Meyshar, Y. and **Benvenisty, N.**: Genetic manipulation of human embryonic stem cells. In: Essentials of Stem Cell Biology. R. Lanza, ed. Academic Press, (in press) (2004).

67. Lavon, N., Yanuka, O. and **Benvenisty, N.**: Differentiation and isolation of hepatic-like cells from human embryonic stem cells. Differentiation 72:230-238 (2004).

68. Dhara, S.K. and **Benvenisty, N.**: Gene trap as a tool for genome annotation and analysis of X chromosome inactivation in human embryonic stem cells. Nucleic Acids Res. 32:3995-4002 (2004).

Experimental Neurology 172, 383–397 (2001)
doi:10.1006/exnr.2001.7832, available online at http://www.idealibrary.com on IDEAL®

Enrichment of Neurons and Neural Precursors from Human Embryonic Stem Cells

Melissa K. Carpenter,*[,1] Margaret S. Inokuma,* Jerrod Denham,* Tahmina Mujtaba,† Choy-Pik Chiu,* and Mahendra S. Rao†[,2]

*Geron Corporation, 230 Constitution Drive, Menlo Park, California 94025; and †Department of Neurobiology and Anatomy, University of Utah Medical School, 50 North Medical Drive, Salt Lake City, Utah 84132

Received May 4, 2001, accepted September 27, 2001

Human embryonic stem (hES) cells proliferate and maintain their pluripotency for over a year *in vitro* (M. Amit, M. K. Carpenter, M. S. Inokuma, C. P. Chiu, C. P., Harris, M. A. Waknitz, J. Itskovitz-Eldor, and J. A. Thomson. 2000. *Dev. Biol.* 227: 271–278) and may therefore provide a cell source for cell therapies. hES cells were maintained for over 6 months *in vitro* (over 100 population doublings) before their ability to differentiate into the neural lineage was evaluated. Differentiation was induced by the formation of embryoid bodies that were subsequently plated onto appropriate substrates in defined medium containing mitogens. These populations contained cells that showed positive immunoreactivity to nestin, polysialylated neural cell adhesion molecule (PS-NCAM) and A2B5. After further maturation, these cells expressed additional neuron-specific antigens (such as MAP-2, synaptophysin, and various neurotransmitters). Calcium imaging demonstrated that these cells responded to neurotransmitter application. Electrophysiological analyses showed that cell membranes contained voltage-dependent channels and that action potentials were triggered by current injection. PS-NCAM and A2B5 immunoselection or culture conditions could be used to produce enriched populations (60–90%) which could be further differentiated into mature neurons. The properties of the hES-derived progenitors and neurons were found to be similar to those of cells derived from primary tissue. These data indicate that hES cells could provide a cell source for the neural progenitor cells and mature neurons for therapeutic and toxicological uses. © 2001 Elsevier Science

Key Words: embryonic stem cells; NRPs; GRPs; differentiation; development; progenitor cells; stem cells.

INTRODUCTION

Neural development involves sequential and progressive restriction in cell fate. As development progresses, neural stem cells generate more restricted neuronal and glial precursors that ultimately generate differentiated neurons, astrocytes, and oligodendrocytes (reviewed in 13, 20, 26). Multiple classes of murine precursor cells have been identified, characterized, and maintained in culture (15, 28, 29). Human versions of these cells have been isolated and shown to be similar, though not identical, to their rodent counterparts (6, 30, 32).

One of the significant challenges in this work is the acquisition of sufficient quantities of human neural cells for both basic and applied research. Primary cells can be propagated by serially passaging dividing human precursors (6, 30, 32), and while little is known about the long-term effects of cell culture, at least some data suggest that after prolonged culture the differentiation potential is limited (12, 25).

An alternative to using fetal tissue or progenitor cells is to use a naturally immortal stem cell, the embryonic stem (ES) cell. In addition to being immortal, murine ES cell lines have been shown to be totipotent (9, 18). Several recent reports (27, 31) have described the generation of human ES (hES) cell lines. The hES cells express telomerase (2), an enzyme demonstrated to immortalize cells in culture without inducing malignant transformation (4, 14). These hES cell lines have been maintained in continuous culture for over a year (over 250 population doublings) and retain their diploid status and the ability to differentiate into cells of the ectodermal, endodermal, and mesodermal lineages (2). hES cells, therefore, may provide a potentially unlimited source of precursor cells for transplantation applications.

Several groups have devised paradigms to bias differentiation of mouse ES cells by manipulating culture conditions. Bain *et al.* (3) for example described a method of aggregation and retinoic acid treatment

[1] To whom correspondence and reprint requests should be addressed. Fax: 650-473-7750. E-mail: mcarpenter@geron.com.
[2] Present address: Laboratory of Neuroscience, National Institute of Aging, 5600 Nathan Shock Drive, Baltimore, MD 21224.

0014-4886/01 $35.00

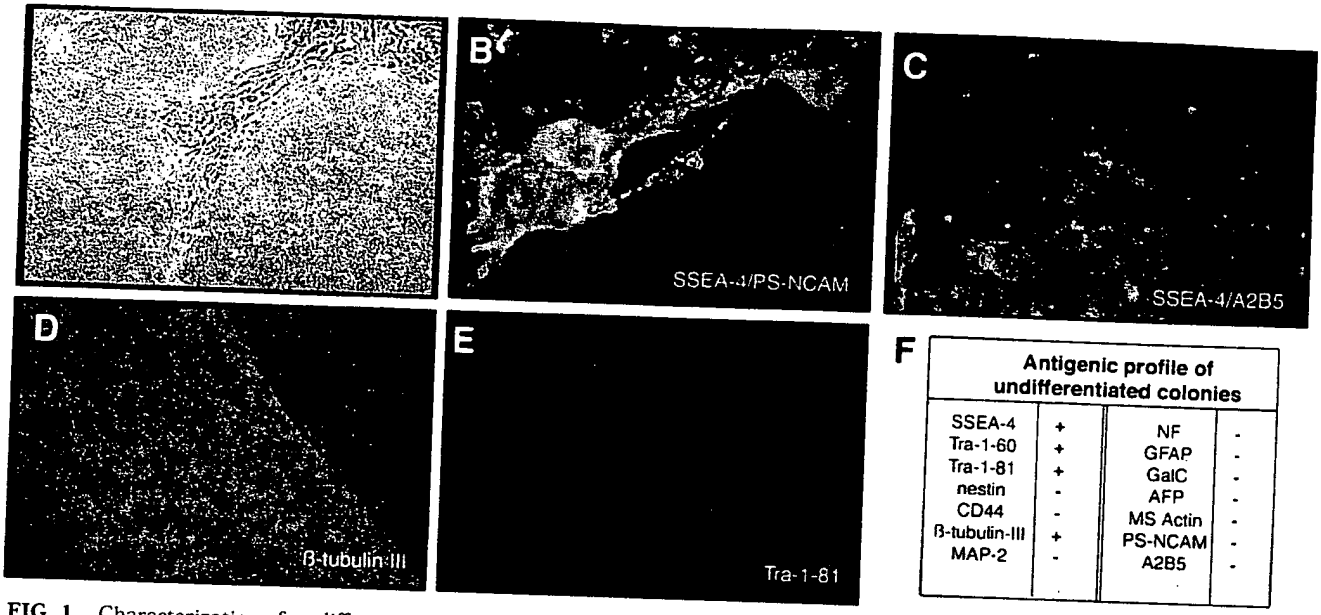

F

Antigenic profile of undifferentiated colonies			
SSEA-4	+	NF	-
Tra-1-60	+	GFAP	-
Tra-1-81	+	GalC	-
nestin	-	AFP	-
CD44	-	MS Actin	-
β-tubulin-III	+	PS-NCAM	-
MAP-2	-	A2B5	-

FIG. 1. Characterization of undifferentiated hES cultures. (A) Phase micrograph of H1 p47 undifferentiated cells maintained under feeder-free conditions. (B and C) SSEA-4 (green) and PS-NCAM (B) and A2B5 (C) (red) immunoreactivity in an undifferentiated colony of H7 p38 hES cells. (D and E) β-Tubulin III (D) and Tra 1-81 (E) immunoreactivity are colocalized in an undifferentiated H7 p26 colony. (F) Table of marker expression in undifferentiated colonies.

where as many as 40% of the total differentiated population consisted of neurons. Okabe *et al.* (22) used specific culture conditions to isolate a relatively homogenous population of nestin-immunoreactive neural stem cells, while Mujtaba *et al.* (21) used cell surface markers A2B5 and polysialylated neural cell adhesion molecule (PS-NCAM) to isolate neural and glial precursors from differentiating ES cell cultures.

In this report we describe a protocol for biasing human ES cell differentiation to generate neural derivatives. We show that neurons obtained in culture can mature, synthesize neurotransmitters, respond to neurotransmitters and are electrically active. We show that differentiation is preceded by the generation of neural precursors that can be selectively purified from other cells by magnetic bead sorting. Furthermore, the hES-derived neural precursors and neurons appear to have similar characteristics to cells derived from primary fetal spinal cord tissues.

MATERIALS AND METHODS

Substrate Preparation

Fibronectin (Sigma) was diluted to a concentration of 20 μg/ml in distilled water (Sigma). The fibronectin solution was applied to tissue culture dishes for a minimum of 4 h. Laminin (Sigma), used at a concentration of 20 μg/ml, was dissolved in DPBS (Dulbecco's phosphate-buffered saline, Gibco-BRL). In some case plates were precoated with poly-L-lysine (30–70 kDa) (Sigma Inc.). Poly-L-lysine was dissolved in distilled water (13.3 μg/ml) and applied to tissue culture plates for an hour. Excess poly-L-lysine was withdrawn and the plates were washed once with sterile water and allowed to air dry. Poly-L-lysine plates were then coated with FN solution and/or laminin as described above. Matrigel (Becton–Dickinson, Bedford, MA) was diluted 1:30 in cold Knockout DMEM (KO-DMEM) (Gibco) and coating was performed according to manufacturer's instructions. Plates were incubated at 4°C for at least overnight or at room temperature for 1 h.

Human ES Cell Culture

Male (H1) and female (H7 and H9) hES cell lines (31) were maintained as previously described (33). Briefly, cultures were maintained on Matrigel in MEF-conditioned medium (CM). CM was generated from hES cell medium (ESM) composed of 80% Knockout DMEM (Gibco), 20% Knockout Serum Replacement (Gibco), 0.1 mM β-mercaptoethanol, 1 mM glutamine, and 1% nonessential amino acids, supplemented with 4 ng/ml hbFGF (Gibco). Cultures were passaged by incubation in 200 units/ml collagenase IV (Gibco) for about 5–10 min at 37°C and then gently dissociated into small clusters in CM. Cells were passaged about once every week. Conditioned medium was generated from MEF (primary mouse embryonic fibroblasts), collected daily, and used immediately for feeding hES cultures. Before addition to the hES cultures this conditioned medium was supplemented with an additional 4 ng/ml of hbFGF (Gibco). Cells for generating CM were refed with ESM daily and used for 7–10 days.

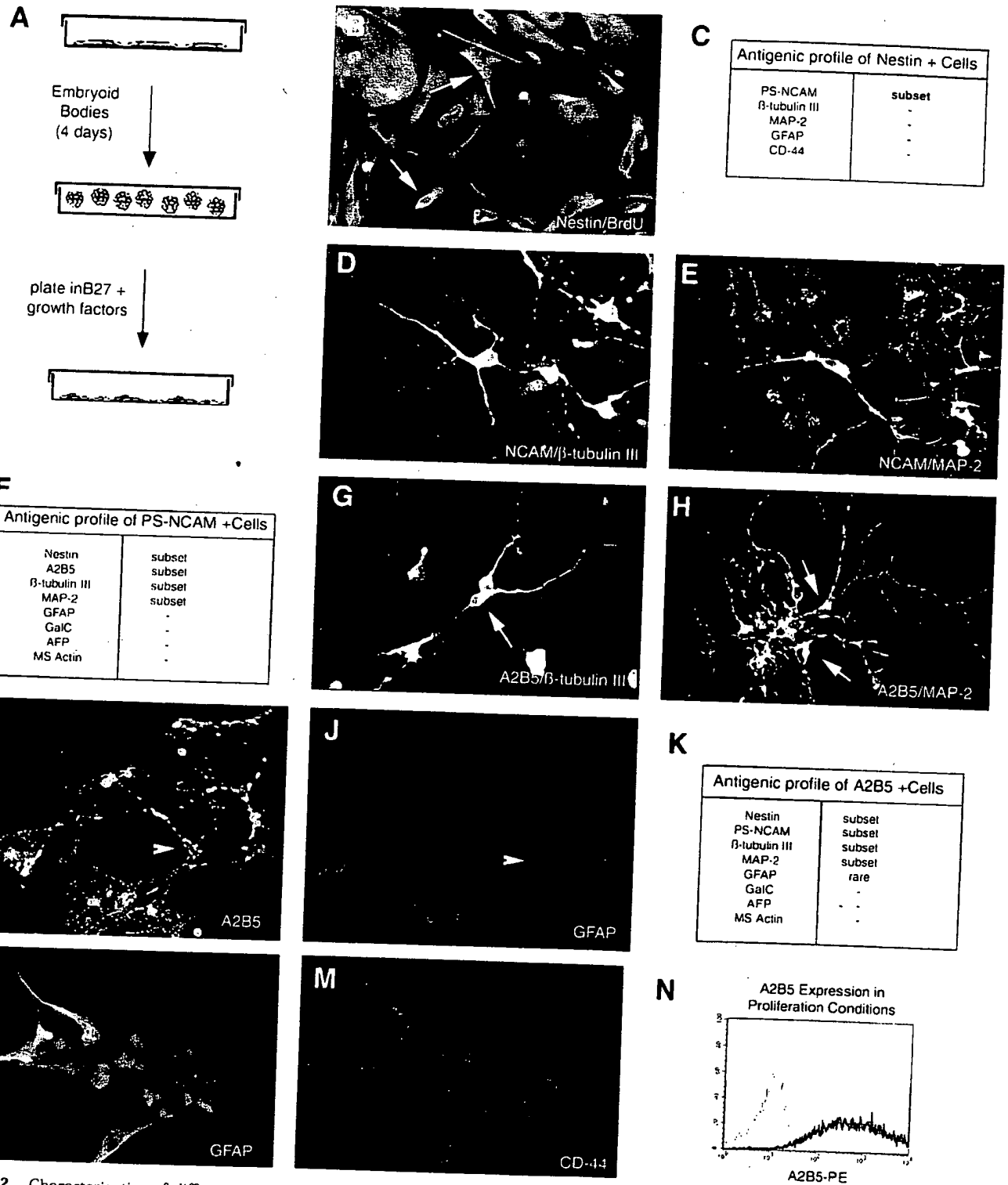

FIG. 2. Characterization of differentiated hES cells. (A) Schematic of differentiation of hES cells. EBs are generated from hES cells and maintained in serum-containing medium supplemented with 10 μM RA for 4 days. The EBs are then plated onto fibronectin-coated plates in DMEM/F-12 medium supplemented with B27, 10 ng/ml hEGF, 10 ng/ml hbFGF, 1 ng/ml hPDGF-AA, and 1 ng/ml hIGF-1 for 3–4 days before immunocytochemical evaluation. (B) Three days after plating, many cells express Nestin (green) and many of these cells incorporate BrdU (red). (C) Table of marker expression in nestin-positive cells in mitogens. (D–N) H9 p27, H9 p23, and H7 p52 hES cells differentiated as described in A. (D and E) PS-NCAM (red) and β-tubulin III (D) or MAP-2 (E) immunoreactivities (green) are colocalized in cells with a neuronal morphology. (F) Table of marker expression in PS-NCAM-positive cells. (G and H) A2B5 (red) and β-tubulin III (G) or MAP-2 (H) immunoreactivities (green) are colocalized in cells with a neuronal morphology. (I and J) A subpopulation of A2B5-positive cells colocalize GFAP. (K) Table of marker expression in A2B5-positive cells. (L and M) GFAP colocalizes with CD-44. (N) FACS analysis of A2B5 expression in H9 p26 cells differentiated by EB incubation in 10 μM RA and plated under proliferation conditions for 3 days. Ninety-six percent of the cells are expressing A2B5.

Differentiation of hES Cells

Embryoid bodies (EBs) were formed by harvesting undifferentiated ES cultures by incubation with 200 U/ml collagenase at 37°C for 5–10 min. Cells were gently scraped from the dish and resuspended in ultralow attachment polystyrene plates (Corning) in medium composed of KO-DMEM, 20% FBS, 1% nonessential amino acids, 1 mM glutamine, and 0.1 mM β-mercaptoethanol. In some experiments, 10 μM all-*trans* retinoic acid (RA) was added to the EBs in suspension. After 4 days in suspension, EBs were plated onto poly-L-lysine/fibronectin-coated plates in proliferation medium composed of DMEM/F-12 with B27 and N2 supplements (Gibco) and 10 ng/ml human epidermal growth factor (hEGF), 10 ng/ml human basic fibroblast growth factor (hbFGF) (Gibco), 1 ng/ml human platelet-derived growth factor-AA (hPDGF-AA) (R & D Systems), and 1 ng/ml human insulin-like growth factor-1 (hIGF-1) (R & D Systems). After 3 days under these conditions, the cells were harvested with trypsin and replated in differentiation medium composed of Neurobasal medium (Gibco) supplemented with B27, 10 ng/ml human neurotrophin-3 (hNT-3) (R & D Systems), and 10 ng/ml human brain-derived neurotrophic factor (hBDNF) (R & D Systems). These cultures were fed three times per week and fixed after 14–16 days.

Primary Cell Culture

Human cells (12–20 weeks gestation) obtained from Clonetics were trypsinized for 3 min, neutralized with 10% serum-containing medium, centrifuged, and resuspended in NEP basal medium containing hbFGF. Cells were gently triturated with a fire-polished pipet to a single-cell suspension. The dissociated cells were plated at a density of 2000–5000 cells per 12- or 18-mm poly-L-lysine/laminin-coated glass coverslip or 35-mm poly-L-lysine/laminin-coated tissue culture dish. The NEP basal medium (15) used in all experiments consisted of DMEM/F-12(GIBCO) supplemented with N2, hbFGF (25 ng/ml), and 10 ng/ml NT-3. Differentiation was induced by reducing concentrations of hbFGF to 10 ng/ml and adding 1 μM RA and 10 ng/ml bone morphogenic protein. Cells kept under these conditions for over 14 days were considered differentiated.

Flow Cytometry

Cells were dissociated in 0.5 mM EDTA in PBS and resuspended to about 5×10^5 cells in 50 μl diluent containing 0.1% BSA in PBS. For analyzing surface marker expression, cells were incubated with mouse primary antibodies (PS-NCAM) (1:1) and A2B5 (1:1) (Developmental Studies Hybridoma Bank, University of Iowa, Iowa City, IA) diluted in the diluent at 37°C for 30 min. After washing with the diluent, cells were incubated with PE-conjugated rat anti-mouse κ-chain antibodies (Becton–Dickinson, San Jose, CA) at 4°C for 30 min. Cells were washed and analyzed on FACS Calibur flow cytometer (Becton–Dickinson, San Jose, CA) using CellQuest software.

Immunocytochemistry

For surface markers, cells were incubated with primary antibodies [stage-specific embryonic antigen-4 (SSEA-4) (1:20), A2B5 (1:1), PS-NCAM (1:1) (Developmental Hybridoma Bank), and Tra 1-81 (1:80) (a gift from Dr. Peter Andrews)] diluted in KO-DMEM supplemented with 1% goat serum at 37°C for 30 min. After washing with PBS, cells were incubated with the FITC-conjugated goat anti-mouse IgG (1:150) (Pharmingen) or Texas Red-conjugated goat anti-mouse IgM (1:150) (Jackson) at 37°C for 30 min. Cells were then washed with warm KO-DMEM and fixed in 4% paraformaldehyde for 15 min, washed, stained with DAPI, and mounted.

For other immunocytochemistry, cells were fixed in 4% paraformaldehyde at RT for 20 min followed by permeabilization for 2 min in 100% ethanol. After fixation, cells were washed 2× with PBS, blocked with 10% normal goat serum in PBS at RT for 2 h or at 4°C overnight, followed by incubation at RT for 2 h with a primary antibody in PBS. After washing, cells were incubated with appropriate secondary antibodies in PBS containing 1% normal goat serum at RT for 30 min. Cells were then washed in PBS, stained with DAPI, and mounted. Antibodies included β-tubulin III (1:1000, Sigma), GABA (1:200, Sigma), glial fibrillary acidic protein (GFAP) (1:500, DAKO), microtubule-associated protein-2 (MAP-2) (1:500, Boehringer), CD-44 (1:100, Accurate), muscle-specific actin (1:50, Dako), neurofilament (1:1000, Sternberger), synaptophysin (1:10, Boehringer), tyrosine hydroxylase (1:200, Chemicon), human-specific NCAM (1:200, Chemicon), Texas Red- or FITC-conjugated goat anti-rabbit (1:150, Jackson), and Texas Red- or FITC-conjugated goat anti-mouse (1:150, Pharmingen). Antibodies to glutamate and glycine were obtained from Signature Immunologicals and used according to manufacturer's recommendations.

BrdU Incorporation

To assess proliferation of neuronal precursor cells, 5-bromo-2′deoxyuridine (BrdU, Sigma) at a concentration of 10 μM was added to the cells for 24 h. Cells were then fixed with 2% paraformaldehyde for 15 min at room temperature followed by 95% methanol for 30 min at −20°C. Cells were then washed 3× with PBS and 5% goat serum and permeabilized with 2 N HCl for 10 min. Acid was removed by washing 3× with PBS and 5% goat serum and the residual HCl was neutralized with 0.1 M sodium borate (Sigma) for 10 min. After rinsing with PBS, cells were incubated with anti-BrdU antibody (Caltag, 1:200) for 30 min at room tem-

perature in PBS with 5% goat serum and 0.5% Triton X-100. Cells were then incubated with Texas Red- or FITC-conjugated goat anti-mouse antibody (Jackson, 1:150) for 30 min, washed, and counterstained with DAPI before mounting.

Magnetic Bead Sorting

Cells were harvested by incubation with trypsin/EDTA, resuspended in PBS with 0.5% BSA and 2 mM EDTA (MACs buffer), and incubated with primary antibody for 6–8 min at 10°C. Cells were then washed twice in MACs buffer, incubated with MACs rat anti-mouse IgG microbeads, and washed again with MACs buffer. Labeled cells were then loaded into the MACs column and placed into the magnetic field. After allowing the negative cells to elute, the magnetic field was removed and the labeled cells were eluted from the column using MACs buffer.

Quantitation of Immunocytochemistry

Quantitation was accomplished by counting immunolabeled cells. Three to six wells were evaluated under each condition. Cell counts were performed by randomly selecting and counting four fields per well using a 40× objective. The number of nuclei was counted using DAPI (between 200 and 400 cells were counted per condition) and then the number of immunolabeled cells was evaluated using a FITC or TRITC filter. These numbers were then summed to give a total value for each well and subsequently averaged to give a mean ± SEM for each condition. When evaluating neurons, cells were only scored positive if they showed positive immunoreactivity for the specific marker and had at least one process that was 2× the diameter of the cell body.

Calcium Imaging

Standard Fura-2 imaging and whole-cell patch-clamp techniques were used as previously described (16, 23). Response profiles of the cells were determined using Fura-2 imaging to assay increases in cytosolic calcium ($[Ca^{2+}]_i$) following application of neurotransmitters or elevated potassium. Neurotransmitters studied were used at 0.5 mM, except ATP which was 10 μM, and included GABA, glutamate (E), glycine (G), elevated potassium (50 mM K^+ instead of 5 mM K^+), ascorbic acid (control), dopamine, acetylcholine (ACh), and norepinephrine. All neurotransmitter solutions were made with rat Ringers (RR) which consisted of (in mM): 140 NaCl, 3 KCl, 1 $MgCl_2$, 2 $CaCl_2$, 10 Hepes, and 10 glucose. External solutions were set to pH 7.4 with NaOH. Cells were perfused in the recording chamber at 1.2–1.8 ml/min and solutions were applied by bath application using a 0.2-ml loop injector located approximately 0.2 ml upstream of the bath inport. Transient increases in calcium were considered a response if the calcium levels rose to above 10% of the baseline value within 60 s from application and returned to baseline within 1–2 min.

Electrophysiology

Standard whole-cell patch-clamp techniques were used to record ionic currents from ES-derived NRP cells in the voltage-clamp mode and to examine action potential generation in the current-clamp mode. External bath solution was rat Ringers. Internal solution was a K-aspartate solution which consisted of (in mM): 50 KF, 75 K-aspartate, 15 NaCl, 11 EGTA, and 10 Hepes. Internal solution was set to pH 7.2 using KOH.

RESULTS

ES Cells Differentiate into Neural Derivatives

In these experiments, two female (H7 and H9) and one male (H1) undifferentiated hES cell lines were maintained under feeder-free conditions and grew as compact colonies surrounded by differentiated cells (Fig. 1A). Under these conditions, hES cells can be maintained for over 6 months (over 120 population doublings) and remain karyotypically and phenotypically stable. The undifferentiated cells express the POU transcription factor OCT-4, the catalytic component of telomerase hTERT, and continue to show telomerase activity. In addition, the undifferentiated colonies express surface markers associated with undifferentiated hES and embryonic carcinoma cells such as SSEA-4, Tra-160, and Tra-1-81 (33). To establish the baseline expression profile in hES cells, we evaluated the expression of markers for undifferentiated and differentiated cells in the undifferentiated hES cultures. In all three cell lines examined (H1, H7, and H9), the colonies of undifferentiated hES cells expressed characteristic markers such as SSEA-4 (Figs. 1B and 1C), Tra-1-60, and Tra-1-81 (Fig. 1E), but did not express most markers of differentiated cells such as MAP-2, GFAP, galactocerebroside (GalC), α-feto protein (AFP), and muscle-specific actin (summarized in the table in Fig. 1F). Differentiated cells outside the colonies did not show immunoreactivity to the undifferentiated markers (SSEA-4, Tra-1-60, and Tra-1-81), but were occasionally immunoreactive for markers associated with neural progenitor cells, such as PS-NCAM and A2B5 (Figs. 1B and 1C), as well as markers for more mature cells, such as MAP-2. In addition, cells from other germ layers were observed within the differentiated cell mass such as muscle cells or AFP-positive cells. Unexpectedly, we found that morphologically undifferentiated human ES cells showed positive immunoreactivity for β-tubulin III, which has been previously reported to be neuron-specific (10, 11). This im-

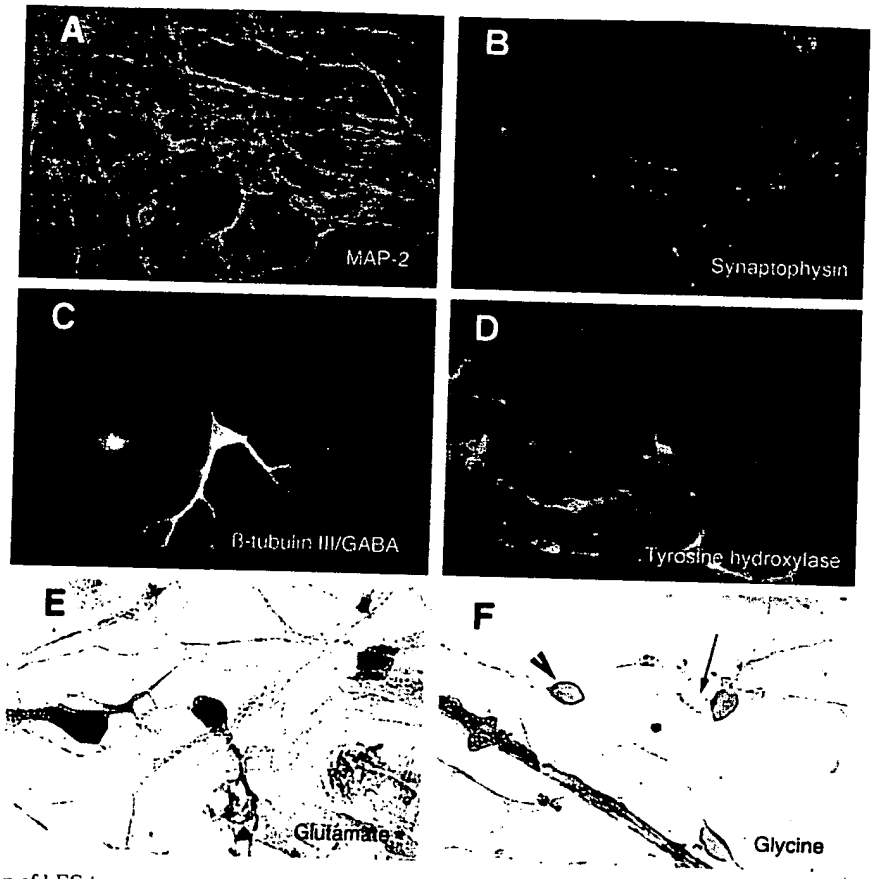

FIG. 3. Differentiation of hES into mature neurons. huEBs were maintained in 10 μM RA for 4 days and then plated onto fibronectin-coated plates in DMEM/F-12 medium supplemented with hEGF, hbFGF, hPDGF-AA, and hIGF for 3 days. These cultures were then passaged onto laminin in medium supplemented with 10 ng/ml hNT-3 and 10 ng/ml hBDNF and allowed to further differentiate for 14–16 days. MAP-2 (A) and synaptophysin (B) immunoreactivities in cultures of H9 p25. Blue staining indicated DAPI. (C) GABA immunoreactivity (red) and β-tubulin III immunoreactivity (green) in cultures of H7 hES cells (p61). (D) Tyrosine hydroxylase immunoreactivity in cultures of H9 (p23). Glutamate (E) and glycine (F) immunoreactivities in differentiated H1 cells.

munoreactivity colocalized with ES-specific markers such as Tra-1-81 (Figs. 1D and 1E) and appears as a filamentous stain within the cytoplasm. Upon differentiation into neurons, β-tubulin III immunoreactivity was also detected in cells with neuronal morphology (see below).

Murine ES cells have been shown to be capable of differentiating into neural precursors (21), neurons, astrocytes, and oligodendrocytes (3, 5, 19). To determine if hES cell lines could be used as a source of precursor cells, we evaluated several differentiation protocols and optimized a sequential procedure that allowed a significant fraction of cells to differentiate into neurons (summarized in Fig. 2A). The first stage of differentiation was induced by the formation of EBs in FBS medium with or without 10 μM RA. After 4 days in suspension, EBs were plated onto fibronectin-coated plates in defined proliferation medium supplemented with 10 ng/ml hEGF, 10 ng/ml hbFGF, 1 ng/ml hPDGF-AA, and 1 ng/ml hIGF-1. Under these conditions, the EBs adhered to the plates and cells began to migrate and proliferate on the plastic, forming a monolayer. After 3 days under these conditions, many cells with neuronal morphology were present. The cultures were then examined for the presence of ectoderm, mesoderm, and endoderm derivatives. In these experiments, we used three hES cell lines: H1, H7, and H9 (31). Similar results were found with each line.

Immunocytochemical analysis 3 days after plating EBs in proliferation medium showed that dividing nestin-immunoreactive neural precursor cells, as assessed by BrdU incorporation, were identified in H1 cultures (Fig. 2B). A subset of the nestin-positive cells coexpressed neural progenitor markers such as PS-NCAM and A2B5 but did not express markers for more mature cells (see table in Fig. 2C). In all three lines, putative neuronal and glial progenitor cells were also identified in cultures maintained in proliferation medium by the presence of PS-NCAM and A2B5 immunoreactivity. In initial experiments, EBs were cultured in the absence of RA. After plating these cells in proliferation medium, 56 $\pm$ 14% (four separate experiments, two cell

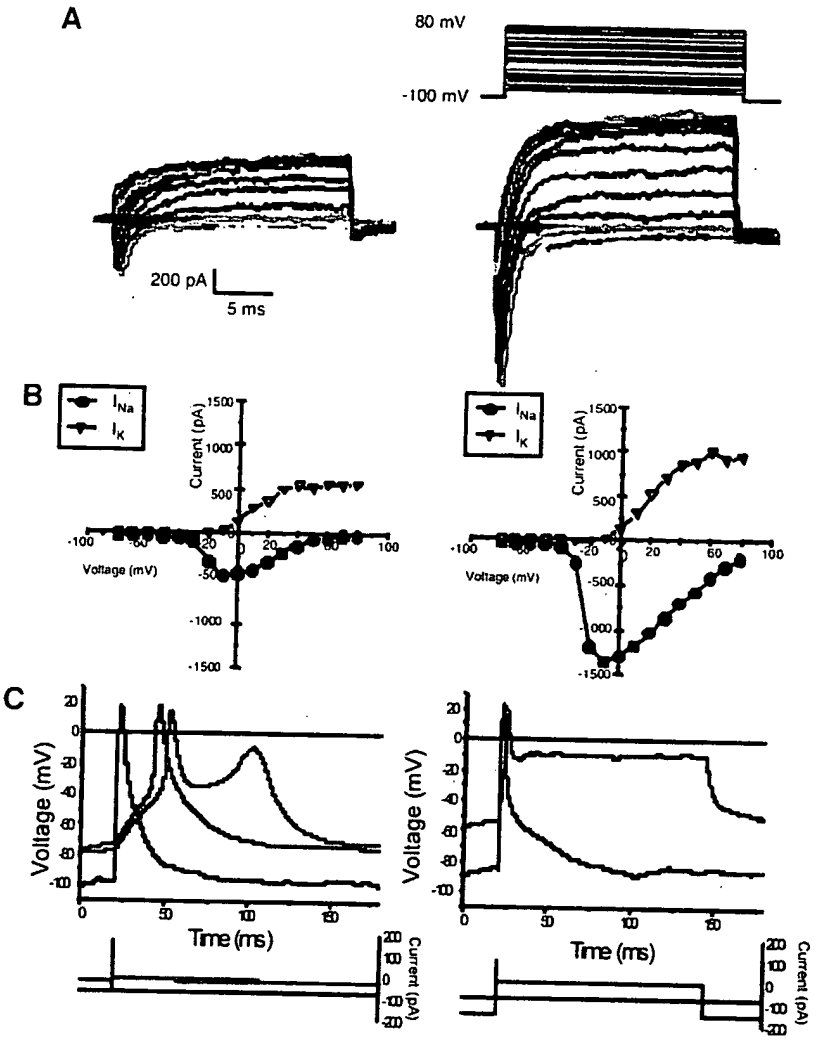

FIG. 5. Human ES-derived NRP cells express voltage-gated ionic currents and fire action potentials. (A) Ionic currents expressed by human ES-derived NRP cells. Two cells are shown in A which express typical sodium and potassium currents when depolarized to test potentials between −80 and 80 mV from a holding potential of −100 mV. Voltage protocol shown in top inset. (B) Current–voltage relationships. The peak current–voltage relationships of the inward (Na^+, filled circles) and outward (K^+, open triangles) potassium currents in A. Sodium current activates between −30 and 0 mV, reaching a peak at −10 or 0 mV. Potassium current activates at voltages above −10 mV and becomes equal to or larger in magnitude than the sodium current at voltages between 20 and 40 mV. (C) Action potentials. The same cells (A) generated action potentials in response to depolarizing stimuli. Cell membranes were held at voltages between −60 and −100 mV by injecting −80 or −150 pA of current. Cell membranes were depolarized for short durations (0.5 ms) by depolarizing current injections of 160 or 80 pA or for longer durations (37–125 ms) by simply removing the holding current injection. Brief depolarizing pulses (0.5 ms) generated action potentials with thresholds above −30 mV. Longer depolarizations also generated action potentials as the cell membranes slowly depolarized to rest; in some cases, a second, abortive action potential fired (left). Current injection protocols shown in bottom insets, color coded to corresponding voltage waveforms elicited above them.

lines) of the cells expressed PS-NCAM and 65 ± 9% (four separate experiments, two cell lines) expressed A2B5 as measured by flow cytometry. However, when EBs were maintained in 10 μM RA before plating in proliferation medium, 87 ± 9% of the cells were positive for A2B5 or PS-NCAM using flow cytometry (Fig. 2N).

Using immunocytochemistry, the morphology of the PS-NCAM-positive cells appeared mostly neuronal and a subpopulation of the PS-NCAM-positive cells also expressed β-tubulin III or MAP-2 (Figs. 2D and 2E). However, colocalization with glial markers such as GFAP and GalC was not identified. Occasional clusters of cells expressing muscle-specific actin or AFP were identified; however, these markers did not colocalize with any neuronal or glial markers tested (summarized in the table in Fig. 2F).

Examination of the A2B5-immunoreactive population showed two different phenotypes: flat cells and

A

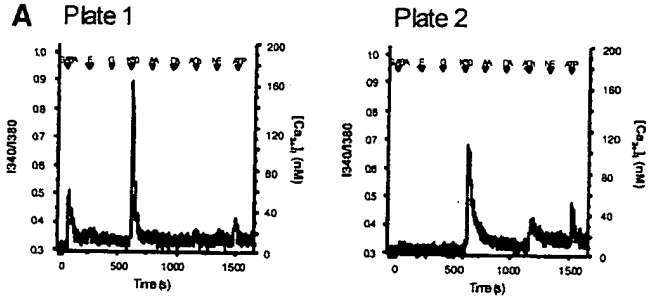

B

Neurotransmitter	% of NCAM+ Cells Responding
50 mM K+	94.3 ± 3.2
GABA	81.1 ± 5.4
Glutamate	15.1 ± 5.0
Glycine	13.2 ± 4.7
Dopamine	3.8 ± 2.6
Acetylcholine	79.2 ± 5.6
ATP	94.2 ± 3.2

FIG. 4. Human ES-derived NRP cells responded to neurotransmitters with increases in cytosolic calcium. (A) Individual cells responded to a subset of neurotransmitters. Ratioed emission data from single cells from two different coverslips. Approximate $[Ca^{2+}]_i$ is estimated by the right *y*-axis. Both cells responded to GABA, elevated potassium, acetylcholine, and ATP. The cell from plate 1 responded with a larger $[Ca^{2+}]_i$ increase to GABA than to ACh, while the opposite was true for the cell from plate 2. Neurotransmitter applications are shown by labeled triangles. (B) Table indicating frequency of cells responding to specific neurotransmitters ($n = 53$).

neuronal-like cells (see below). A subpopulation of the neuronal-like cells showed colocalization with neuronal markers such as β-tubulin III (Fig. 2G) and MAP-2 (Fig. 2H). Using a human-specific NCAM antibody we found that A2B5 and NCAM are coexpressed in a population of cells which have neuronal morphology. A subpopulation of the A2B5-positive flat cells expressed GFAP (Figs. 2I and 2J); however, the flat cells were not seen to express neuronal markers. It is unclear whether the remaining flat cells represent progenitor cells or an unidentified differentiated cell type.

Astrocyte formation was considerably less abundant than neuronal formation in these cultures. In addition, GFAP-positive cells were found in patches associated with neurons and were not colocalized with more mature neuronal markers, such as MAP-2 and neurofilament. A subpopulation of GFAP-positive cells was also found to coexpress CD-44 (Figs. 2M and 2N). GalC-positive cells were also identified in these cultures; most of these cells showed a flat, polygonal morphology and only a few cells had a process characteristic of oligodendrocytes. Because of the low abundance of GFAP and appropriate GalC-positive cells, we were unable to obtain accurate cell counts for these populations.

Similar data were collected from all three lines at various passages (26 to 31 passages or 125–150 population doublings) tested. Thus, hES cells can be induced to differentiate into neural derivatives that express nonoverlapping lineage-specific markers under appropriate differentiation conditions.

hES Differentiate into Mature Neurons

To determine if hES cell-derived neurons could mature in culture, we assessed their ability to synthesize neurotransmitters, respond to neurotransmitters, make synapses, and generate electrical activity. In these experiments, EBs treated with RA and placed into proliferation medium were replated into differentiation medium. Under these conditions, neurons with extensive processes could be seen after approximately 7 days. After 8–16 days these cultures were immunostained for the presence of neuronal and glial markers. For neuronal quantitation, MAP-2 immunoreactivity was used rather than β-tubulin III because of the β-tubulin III expression identified in the undifferentiated cultures. Cultures differentiated for 14 days contained 20–30% MAP-2-positive cells (Fig. 3A) and express synaptophysin (Fig. 3B). Although the cultures in proliferation medium contain high percentages of PS-NCAM and A2B5 cells, we obtained 30% MAP-2-positive cells upon differentiation. Although there are a small number of astrocytes present under these conditions, the remainder of the population requires further evaluation. It is likely that the remaining cells include neuronal and glial progenitors, but exact quantification will require further experimentation.

The above experiments include RA during the formation of EBs. We also evaluated whether the presence of RA was necessary for the formation of neurons. Using the H9 line at p25, we found that EBs maintained in 10 μM RA and further differentiated as described above generated considerably more neurons. In these experiments, cultures exposed to RA contained 26.5 ± 5.4% ($n = 6$ wells) MAP-2-positive cells while cultures derived from EBs maintained without RA contained only 5.7 ± 2.4% ($n = 6$ wells) MAP-2-positive cells. As seen previously, GFAP-immunoreactive cells were observed in patches. These data indicate that while RA is not necessary for the formation of neurons, the presence of high concentrations of RA appears to enhance the formation of neurons.

The presence of neurotransmitters was also assessed. After differentiation of the H7 or H9 lines GABA-immunoreactive cells were identified which coexpressed β-tubulin III or MAP-2 in three separate experiments (Fig. 3C). Most of these cells had a neuronal morphology but occasional GABA-positive cells were identified that did not coexpress neuronal markers; these cells had an astrocytic morphology. TH-positive cells which coexpressed MAP-2 were identified in all experiments (five experiments) (Fig. 3D). In these experiments, approximately 3% of the MAP-2 cells expressed TH (three experiments). In addition, expres-

sion of glutamate and glycine was identified (Figs. 3E and 3F) after differentiation of the H1 line.

Functional Activity of Neurons Derived from hES Cells

Calcium imaging. To assess the capacity of hES-derived neurons to respond to neurotransmitters, EBs were generated from the H1 cell line, plated in mitogens, and then replated in NT-3 and BDNF for 7 days as described above. Calcium levels were examined in PS-NCAM-positive cells after perfusion with various neurotransmitters or 50 mM potassium using Fura-2 imaging. Of the 53 cells tested, 94.3 ± 3.2% responded to elevated potassium, and most of the cells responded to GABA, acetylcholine, and ATP while only 3.9% failed to respond to any of the agonists applied (Fig. 4A). These data are summarized in the table in Fig. 4B.

Electrophysiology

In addition to the presence of neurotransmitter receptors, we evaluated the presence of voltage-operated channels using patch and voltage clamping. H1 cultures carried in parallel to the cultures used for calcium imaging were used in these experiments. Of the six PS-NCAM-positive cells tested, all six expressed sodium and potassium currents (Figs. 5A and 5B) and all six fired action potentials when held at hyperpolarized potentials and injected with varying amplitudes and durations of depolarizing currents (Fig. 5C). Passive membrane properties were determined with voltage steps from −70 to −80 mV and we calculated the average capacitance (Cm) to be 8.97 ± 1.17 pF, membrane resistance (Rm) to be 487.8 ± 42.0 MΩ, and access resistance (Ra) to be 23.4 ± 3.62 MΩ of the six cells. Ionic currents were examined by holding the cells at −100 mV and stepping to test voltages between −80 and 80 mV in 10-mV increments. Peak sodium and potassium currents were extracted from these data. We calculated the average sodium current (I_{Na}) to be −531.8 ± 136.4 pA, the average potassium current (I_K) to be 441.7 ± 113.1 pA, the average sodium current density [I_{Na}(density)] to be −57.7 ± 7.78 pA/pF, and the average potassium current density [I_K(density)] to be 48.2 ± 10.4 pA/pF (Figs. 5A and 5B). These data indicate that neurons generated from hES cells have voltage-operated channels which can generate action potential at appropriate voltages.

Enrichment of Neural Progenitor Cells

Neural progenitor cells are likely to be a good source of cells for cell transplantation in neurodegenerative diseases. It has been previously demonstrated that neuronal-restricted and glial-restricted precursors can be isolated using the surface antigens PS-NCAM and A2B5 (15, 21). Therefore, we examined whether this population showed proliferative capacity and could be enriched using immunoselection.

Under our proliferation conditions we identified neural progenitor populations expressing PS-NCAM and A2B5. To determine if these cells could proliferate, EB cultures plated in proliferation medium were pulsed with BrdU for 24 h. Both PS-NCAM- and A2B5-positive cells showed BrdU incorporation (Figs. 6A and 6B). In addition, our costaining data described above indicate that both of these populations have the capacity to form neurons (Figs. 2D–2H). As seen in rodent cultures, PS-NCAM cells appeared to be restricted to neuronal formation. As mentioned previously, A2B5-positive cells showed two separate morphologies: flat cells and cells with neuronal morphology (Fig. 6C). A2B5-positive cells with neuronal morphology colocalized neuronal markers such as β-tubulin III and MAP-2. In addition, A2B5 and PS-NCAM had overlapping expression, which was restricted to cells with neuronal morphology (Fig. 6D and data not shown). A small number of the flat A2B5 cells also expressed GFAP. However, GFAP expression was not restricted to A2B5 cells.

It has previously been demonstrated that these cell populations can be enriched using immunoselection techniques (15, 21). Therefore, we used magnetic bead sorting or immunopanning to enrich A2B5-positive and PS-NCAM-positive cells. In these experiments, the EBs were maintained in the absence of RA before plating in proliferation medium. At the time of selection, cultures contained approximately 56 ± 14% PS-NCAM-immunoreactive cells and 65 ± 9% A2B5-immunoreactive cells. After selection, these populations could be enriched to 86 ± 6% PS-NCAM-positive cells or 91 ± 2% A2B5-positive cells (four separate experiments using two cell lines). An example of this type of enrichment is shown in Fig. 6E, in which the starting population of H1 p47 hES cells contained 53% PS-NCAM-positive cells. After immunoselection, the negative population contained 27% PS-NCAM-positive cells and the positive population contained 91% PS-NCAM-positive cells.

Immunoselected cells were maintained in defined medium supplemented with 10 ng/ml NT-3 and 10 ng/ml BDNF. Using H7 p30 cells immunoselected for PS-NCAM, we found that after 14 days of differentiation in NT-3 and BDNF, a subpopulation of the NCAM-positive cells colocalized β-tubulin III or MAP-2 (Figs. 7A and 7B). Cell counts showed that 25 ± 4% of the cells were MAP-2 immunoreactive and 3 ± 1% of the MAP-2-positive cells were TH positive (Fig. 7E) while only 1.9 ± 0.8% of the MAP-2-positive cells were GABA positive (Fig. 7D). GFAP-immunoreactive cells were also identified in these cultures (3.2 ± 0.6%), but GFAP did not colocalize with PS-NCAM (Fig. 7C) or the other neuronal markers. GalC immunoreactivity was not identified in these cultures.

A2B5-enriched cells, on the other hand, have the capacity to generate both neurons and astrocytes.

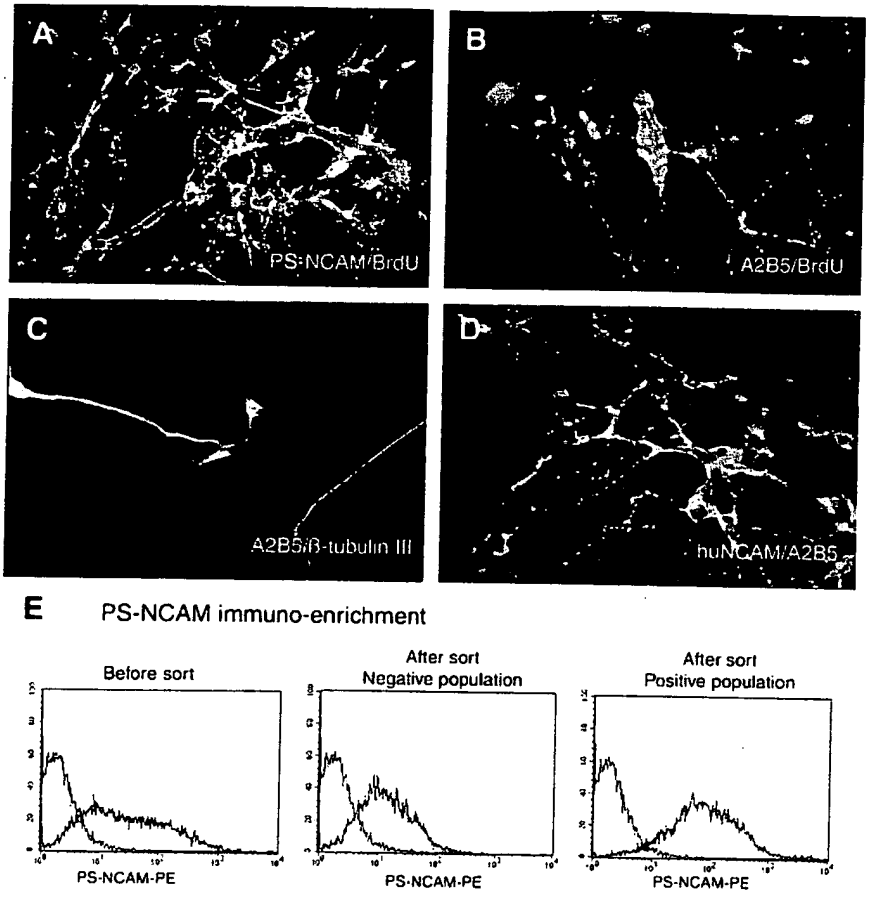

FIG. 6. Enrichment of neural progenitor cells using immunoselection. huEBs were maintained in 10 μM RA for 4 days and then plated onto fibronectin-coated plates in DMEM/F-12 medium supplemented with hEGF, bFGF, hPDGF-AA, and hIGF-1 for 3 days. PS-NCAM (A) and A2B5 (B) (green) immunoreactivity in H9 (p27) under these culture conditions. A subpopulation of both cell types incorporate BrdU (red nuclei). (C) Two different morphologies are identified with A2B5 immunoreactivity (red). β-Tubulin III is colocalized in some cells with a neuronal morphology. Cells under these conditions were harvested and immunoselected using the MACs magnetic cell sorter. The percentage of cells expressing PS-NCAM or A2B5 before and after immunoselection was assessed using flow cytometry as described under Materials and Methods. After sorting, cells were plated at 5×10^5 cells/well in differentiation medium containing 10 ng/ml hNT-3 and 10 ng/ml hBDNF. (E) Quantitation of a representative sort using the PS-NCAM antibody. In this experiment EBs were generated from H1 p49 without RA and plated for 3 days in proliferation medium. Cells were harvested and samples were collected for flow cytometry. During the magnetic sort, samples of the flowthrough and of the enriched populations were collected for flow cytometry before the remaining cells were plated in differentiation medium. The samples were stained for PS-NCAM and quantified using flow cytometry. Before the sort, 50% of the population expressed PS-NCAM; after the sort, only 28% of the flowthrough (negative population) expressed PS-NCAM, whereas 86% of the positive population expressed PS-NCAM.

A2B5-immunoselected cells were subjected to the same differentiation protocol as PS-NCAM cells. As seen in the parent population, A2B5-immunoreactive cells were either flat cells or cells with neuronal morphology. After 2 weeks under differentiation conditions, A2B5 cells showed colocalization with β-tubulin III or MAP-2 (Figs. 7F and 7G). Cultures of H9 p26 A2B5 cells had 32 $\pm$ 3% MAP-2-positive cells. In addition, 3 $\pm$ 1% of the MAP-2 cells were TH positive (Fig. 7J) while only 0.6 $\pm$ 0.3% were GABA immunoreactive (Fig. 7I). A very small percentage of the cells (0.73 $\pm$ 0.6%) expressed GFAP. Some of the A2B5 flat cells colocalized GFAP (Fig. 7H). There was also a population of GFAP cells that did not express A2B5.

Human Fetal Cells Differentiate into Neural Derivatives

The differentiation of ES cells is believed to recapitulate normal development. The results described above indicate that hES cell lines generate PS-NCAM- and A2B5-immunoreactive cells that can generate multiple neuronal phenotypes. To determine if similar cells were present in fetal neural tube cultures, we obtained first-passage fetal cells (12–20 weeks gestation, from Clonetics) and examined them for the presence of PS-NCAM-immunoreactive cells. Fetal cultures were a mixed population of cells with a substantial fraction expressing nestin, A2B5, or GFAP immunoreactivity

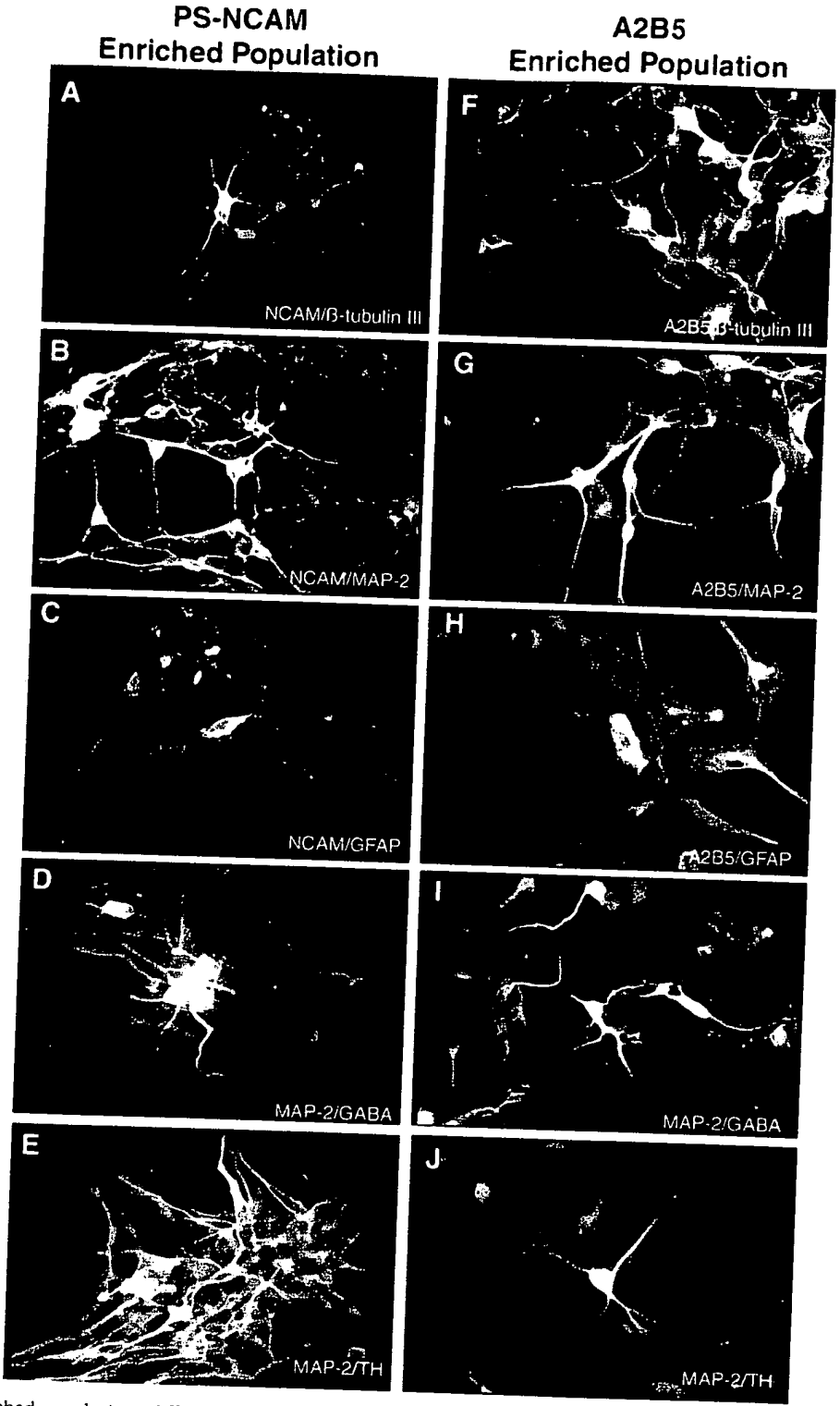

FIG. 7. Immunoenriched populations differentiate into mature neurons. After immunoselection, the cells were plated into N2 medium supplemented with 10 ng/ml hNT-3 and 10 ng/ml hBDNF for 14 days. (A–E) H7 p30 PS-NCAM sorted cells differentiated in NT-3 and BDNF for 14 days. A subpopulation of the PS-NCAM cells (red) colocalize β-tubulin III (A) and MAP-2 (B) (green). (C) PS-NCAM-positive cells (red) did not colocalize GFAP (green). These cultures contained MAP-2-positive cells (green) which also expressed GABA (D) or TH (E) (red). (F–J) Characterization of H9 p29 hES cells that were differentiated and immunoselected using the A2B5 antibody. A subpopulation of the A2B5 cells (red) expressed β-tubulin II (F) or MAP-2 (G) (green). (H) A few A2B5 cells (red) were identified that also expressed GFAP (green). These cultures contained MAP-2-positive cells (green) which also expressed GABA (I) or TH (H) (red).

(23) (Figs. 8A and 8C). A subset of cells (40–50%) expressed PS-NCAM immunoreactivity (Fig. 8D). PS-NCAM-immunoreactive cells coexpressed other neuronal markers (Fig. 8C and table in Fig. 8B). A subset of the PS-NCAM-immunoreactive and β tubulin III cells were dividing cells indicating the existence of a dividing NRP population (Fig. 8C). As in differentiated ES cell cultures, expression of A2B5 was limited to a small proportion of the neuronal population and was also expressed by nonneuronal cells (Fig. 8J). Thus, ES cell differentiation generates cells similar in morphology and phenotype as those present in fetal cultures. To test the differentiation of PS-NCAM-immunoreactive cells, these cells were grown under differentiation conditions and their ability to generate differentiated neurons was tested. As described for ES cell cultures, PS-NCAM-immunoreactive cells differentiated into cells that became postmitotic and expressed different kinds of neurotransmitters/synthesizing enzymes [Figs. 8E–8H and (23)]. PS-NCAM immunoreactivity did not colocalize with markers for astrocytes or oligodendrocytes (data not shown).

DISCUSSION

We have shown that multiple human ES cell lines maintained in an undifferentiated state for 26–31 passages or 125–150 population doublings express characteristic markers and are capable of differentiating into multiple neural derivatives. Neuronal cells that differentiate from hES cell cultures express PS-NCAM and mature in culture to synthesize different classes of neurotransmitters. PS-NCAM-immunoreactive cells can be immunoenriched and the PS-NCAM-expressing cells do not appear to generate astrocytes or oligodendrocytes, but retain the ability to generate multiple neuronal phenotypes.

In contrast, ES cell-derived A2B5-immunoreactive cells appear to be a mixed population of cells that can generate both neurons and astrocytes. These cells can also be immunoenriched and the resulting population retains the ability to generate neurons and astrocytes. Thus, human ES cells can be induced to differentiate into neural derivatives that express lineage-specific markers under appropriate differentiation conditions and neuronal derivatives can be isolated using cell surface labels.

Comparison of human ES cell cultures with their rodent counterparts revealed some important differences. As shown previously, undifferentiated hES cells expressed SSEA-4 immunoreactivity, an antigen that is not expressed in undifferentiated mouse ES cells. In addition, the undifferentiated hES cells do not appear to require LIF (27, 31). Of particular importance is our observation of β-III tubulin expression in colonies of undifferentiated hES cells. These β-III tubulin-immunoreactive cells did not appear neuronal either by morphology or by coexpression of other neuronal markers. These cells were not included in our analysis of neuronal differentiation and only β-III tubulin-immunoreactive cells that showed neuronal morphology and coexpressed other neuronal markers were considered neurons.

A further difference between the mouse and human cells is the response to retinoic acid. Using the standard neural induction protocol for mouse ES cells (3) with 4 days of EB culture without RA and 4 days with 1 μM RA and then plating the EBs in defined medium did not result in enhancement of neuronal formation. However, increasing the RA concentration 10-fold, as has been demonstrated in human EC lines (8, 24), resulted in a 5-fold increase in the number of MAP-2-positive neurons formed after terminal differentiation. Furthermore, we found that EBs maintained in 10 μM RA and then plated in mitogens resulted in cultures that contained as much as 90% A2B5- or PS-NCAM-positive cells.

PS-NCAM- and A2B5-positive cells were very abundant in our differentiated hES cultures maintained in mitogens. Immunocytochemistry shows the presence of various neurotransmitters after further differentiation. In addition, we found that hES cells can differentiate into mature neurons that generate action potentials. However, spontaneous action potentials were not detected, even though synaptophysin immunoreactivity indicates the presence of synapses. This finding may be due to the fact that cells selected for electrophysiological examination were somewhat isolated from the other cells in the culture (for ease of detection). Alternatively, there may be a relatively low number of excitatory neurons or the synapses may be immature. Ninety-four percent of the neurons assayed responded to depolarization (50 mM potassium). Neurons derived from human cell populations expressed voltage-gated sodium and potassium channels, responded to ligands such as glutamate and acetylcholine, but did not fire action potentials (23). Ligand-gated currents evoked by GABA, glutamate, and kainate developed slowly *in vitro*, requiring up to 70 days in differentiation culture before expressing maximal responses (7). Of particular importance is our finding that hES-derived neurons respond to dopamine and produce TH. At the time of these experiments, the hES cells had undergone as many as 150 population doublings. In each experiment we found that about 3% of the neurons expressed TH.

Similar to PS-NCAM-expressing cells, A2B5-immunoreactive cells were very abundant under our culture conditions. These cells generated both neurons and astrocytes suggesting that A2B5 immunoreactivity is not exclusive to either neuronal or glial precursors. This may indicate that the A2B5 epitope is expressed by at least two populations of cells in cultures. A subset of the A2B5-immunoreactive cells appear neuronal and

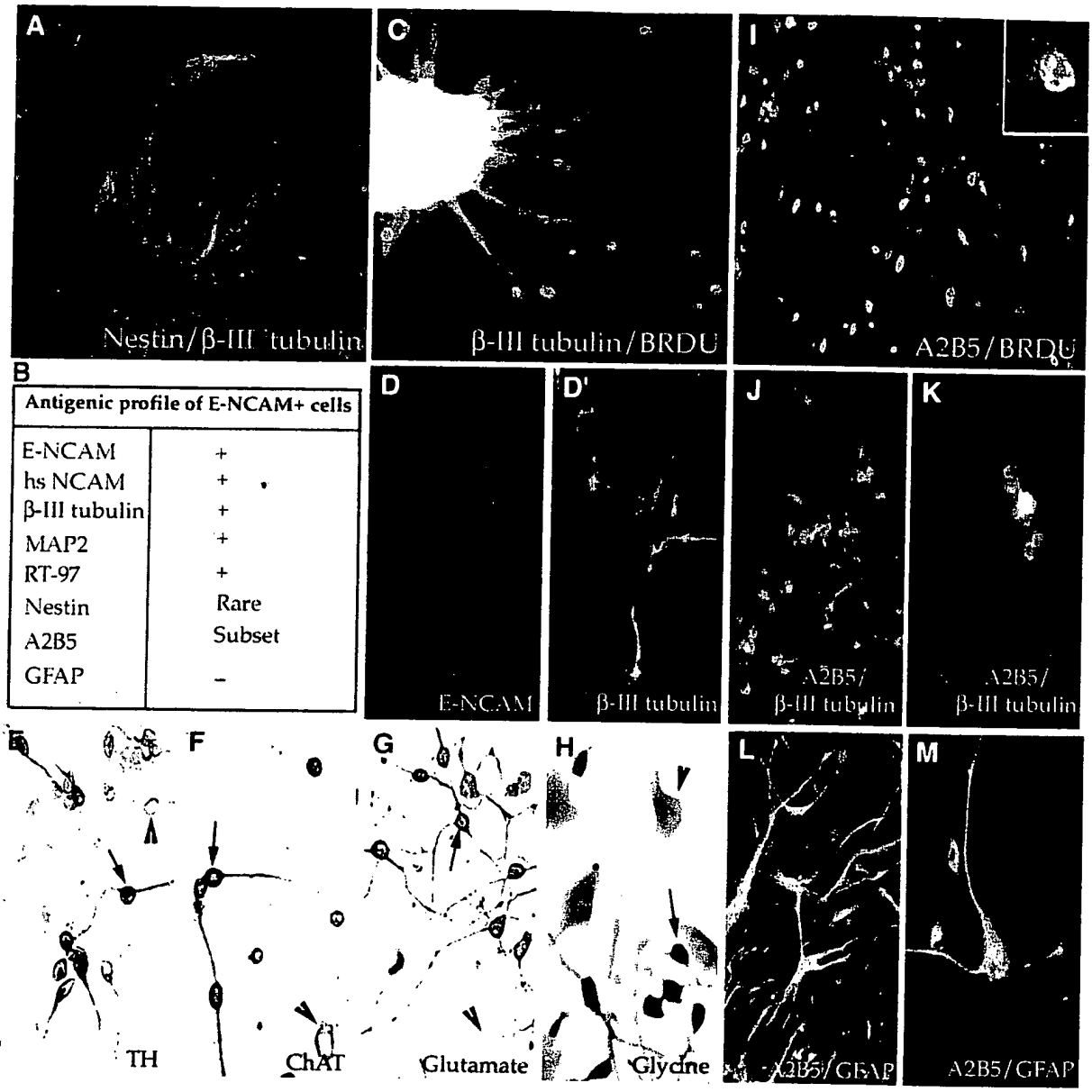

FIG. 8. PS-NCAM-immunoreactive cells express neuronal properties while A2B5-immunoreactive cells express neuronal and glial properties. Fetal cells obtained from Clonetics were plated in culture and processed after 48 h (A), 5 days (C, D, D', I–M), or 2 weeks (E–H). Cells were stained for nestin (green, A), BRDU (red, C; green, I, inset to I), β-III tubulin (green C, D', J, K), A2B5 (red, I–M), TH (brown, E), ChAT (brown, F), glutamate (brown, G), and glycine (brown, H). A shows that Clonetics cells are a mixed population with a subset expressing PS-NCAM immunoreactivity. PS-NCAM-immunoreactive cells have a characteristic antigenic profile (summarized in B). PS-NCAM-immunoreactive cells coexpress β-III tubulin (D, D') and E-NCAM/β-III tubulin cells divide in culture (C). When maintained in culture for 2 weeks, PS-NCAM-immunoreactive cells mature and subsets of cells express different neurotransmitters (G, H) or neurotransmitter-synthesizing enzymes (E, F). In contrast A2B5-immunoreactive cells comprise a small proportion of cells at this stage (I and data not shown), a subset of which incorporate BRDU (I and inset to I). A majority of A2B5-immunoreactive cells (>95%) do not coexpress β-III tubulin immunoreactivity (J), though occasional A2B5/β-III tubulin-immunoreactive cells are seen (K). While most A2B5-immunoreactive cells do not express GFAP, A2B5-expressing cells can differentiate into A2B5−/GFAP+ astrocytes (L) and into A2B5+/GFAP+ astrocytes (M).

double labeling shows that these cells coexpress PS-NCAM and MAP-2 immunoreactivity. In addition, we noted a more fibroblastic-appearing cell that did not express neuronal markers and resembled the A2B5-immunoreactive cells identified in rodent ES cell cultures (21). A small subpopulation of these fibroblastic-like cells also expressed GFAP, but it is unclear what cell type the remaining population represents. In contrast to the rapid and robust maturation of neurons, few astrocytes were detected. A subpopulation of the

astrocytes expressed CD-44, a cell surface glycoprotein that is the predominant receptor for hyaluronate and is expressed by astrocytes in the adult brain. Recent studies in the chick embryo have suggested that CD-44 may recognize astrocyte precursors (1, 17). We therefore examined differentiating ES cell cultures for CD-44 expression. Coexpression of CD-44 and GFAP was seen in a substantial number of astrocytes. Since the antibody we have used recognizes an extracellular epitope, this antibody can be used to label and sort astrocyte and astrocyte precursor populations.

Our data show that hES-derived progenitors have similar characteristics to progenitors derived from primary human spinal cord. We found that the hES-derived PS-NCAM neuronal progenitors had the same characteristics as cells from primary tissue. One of the advantages of the hES-derived cells is the abundance of starting material, which allows the generation of large quantities of neurons.

In summary, our results demonstrate that hES cells have the capacity to generate mature, functional neurons *in vitro*. In addition, hES cells can generate more restricted precursor cells that can be enriched by the addition of RA or by immunoselection, or both. These data indicate that human ES cells provide an abundant and scalable source of cells for the isolation of these cell types for therapeutic and drug discovery applications.

ACKNOWLEDGMENTS

The authors thank Drs. Calvin Harley and Jane Lebkowski for insightful discussions and critical review of the manuscript. The authors also thank Dr. Kamb for permission to use space and equipment for these experiments and Drs. Lucero and Piper for their help with electrophysiology. This work was funded by Geron Corporation.

REFERENCES

1. Alfei, L., M. Aita, B. Caronti, R. De Vita, V. Margotta, L. Medolago Albani, and A. M. Valente. 1999. Hyaluronate receptor CD44 is expressed by astrocytes in the adult chicken and in astrocyte precursor cells in early development of the chick spinal cord. *Eur. J. Histochem.* **43:** 29–38.
2. Amit, M., M. K. Carpenter, M. S. Inokuma, C. P. Chiu, C. P. Harris, M. A. Waknitz, J. Itskovitz-Eldor, and J. A. Thomson. 2000. Clonally derived human embryonic stem cell lines maintain pluripotency and proliferative potential for prolonged periods of culture. *Dev. Biol.* **227:** 271–278.
3. Bain, G., D. Kitchens, M. Yao, J. E. Huettner, and D. I. Gottlieb. 1995. Embryonic stem cells express neuronal properties *in vitro*. *Dev. Biol.* **168:** 342–357.
4. Bodnar, A. G., M. Ouellette, M. Frolkis, S. E. Holt, C. P. Chiu, G. B. Morin, C. B. Harley, J. W. Shay, S. Lichtsteiner, and W. E. Wright. 1998. Extension of life-span by introduction of telomerase into normal human cells. *Science* **279:** 349–352.
5. Brüstle, O., K. Choudary, K. Karram, A. Huttner, K. Murray, M. Dubois-Dalcq, and R. McKay. 1998. Chimeric brains generated by intraventricular transplantation of fetal human brain cells into embryonic rats. *Nat. Biotechnol.* **16:** 1040–1044.
6. Carpenter, M., X. Cui, Z. Hu, J. Jackson, S. Sherman, A. Seiger, and L. Wahlberg. 1999. *In vitro* expansion of a multipotent population of human neural progenitor cells. *Exp. Neurol.* **158:** 265–278.
7. Chalmers-Redman, R. M., T. Priestley, J. A. Kemp, and A. Fine. 1997. *In vitro* propagation and inducible differentiation of multipotential progenitor cells from human fetal brain. *Neuroscience* **76:** 1121–1128.
8. Cheung, W., W. Fu, W. Wing, and N. Ip. 1999. Production of human CNS neurons from embryonal carcinoma cells using a cell aggregation method. *BioTechniques* **26:** 946–954.
9. Evans, M. J., and M. H. Kaufman. 1981. Establishment in culture of pluripotential cells from mouse embryos. *Nature* **292:** 154–156.
10. Fanarraga, M. L., J. Avila, and J. C. Zabala. 1999. Expression of unphosphorylated class III β-tubulin isotype in neuroepithelial cells demonstrates neuroblast commitment and differentiation. *Eur. J. Neurosci.* **11:** 517–527.
11. Ferreira, A., and A. Caceres. 1992. Expression of the class III β-tubulin isotype in developing neurons in culture. *J. Neurosci. Res.* **32:** 516–529.
12. Fricker, R. A., M. K. Carpenter, C. Winkler, C. Greco, M. A. Gates, and A. Bjorklund. 1999. Site-specific migration and neuronal differentiation of human neural progenitor cells after transplantation into the adult rat brain. *J. Neurosci.* **19:** 5990–6005.
13. Gage, F. H., J. Ray, and L. J. Fisher. 1995. Isolation, characterization, and use of stem cells from the CNS. *Annu. Rev. Neurosci.* **18:** 159–192.
14. Jiang, X., G. Jimenez, E. Chang, M. Frolkis, B. Kusler, M. Sage, M. Beeche, A. G. Bodnar, G. M. Wahl, T. D. Tlsty, and C. P. Chiu. 1999. Telomerase expression in human somatic cells does not induce changes associated with a transformed phenotype. *Nat. Genet.* **21:** 111–114.
15. Kalyani, A., K. Hobson, and M. S. Rao. 1997. Neuroepithelial stem cells from the embryonic spinal cord: Isolation, characterization, and clonal analysis. *Dev. Biol.* **186:** 202–223.
16. Kalyani, A. J., D. Piper, T. Mujtaba, M. Lucero, and M. S. Rao. 1998. Spinal cord neuronal precursors generate multiple neuronal phenotypes in culture. *J. Neurosci.* **18:** 7856–7868.
17. Marret, S., B. Delpech, A. Delpech, H. Asou, N. Girard, M. N. Courel, C. Chauzy, C. Maingonnat, and C. Fessard. 1994. Expression and effects of hyaluronan and of the hyaluronan-binding protein hyaluronectin in newborn rat brain glial cell cultures. *J. Neurochem.* **62:** 1285–1295.
18. Martin, G. R. 1981. Isolation of a pluripotent cell line from early mouse embryos cultured in medium conditioned by teratocarcinoma stem cells. *Proc. Natl. Acad. Sci. USA* **78:** 7634–7638.
19. McDonald, J., X. Liu, Y. Qu, S. Liu, S. Mickey, D. Turetsky, D. Gottlieb, and D. Choi. 1999. Transplanted embryonic stem cells survive, differentiate and promote recovery in injured rat spinal cord. *Nat. Med.* **5:** 1410–1412.
20. McKay, R. 1997. Stem cells in the central nervous system. *Science* **276:** 66–71.
21. Mujtaba, T., D. R. Piper, A. Kalyani, A. K. Groves, M. T. Lucero, and M. S. Rao. 1999. Lineage-restricted neural precursors can be isolated from both the mouse neural tube and cultured ES cells. *Dev. Biol.* **214:** 113–127.
22. Okabe, S., K. Forsberg-Nilsson, A. Spiro, M. Segal, and R. McKay. 1996. Development of neuronal precursor cells and functional postmitotic neurons from embryonic stem cells *in vitro*. *Mech. Dev.* **59:** 89–102.
23. Piper, D., T. Mujtaba, M. Rao, and M. Lucero. 2000. Immunocytochemical and physiological characterization of a population of cultured human neural precursors. *J. Neurophysiol.* **84:** 534–548.

24. Pleasure, S., C. Page, and V. Lee. 1992. Pure, postmitotic, polarized human neurons derived from NTera 2 cells provide a system for expressing exogenous proteins in terminally differentiated neurons. *J. Neurosci.* **12:** 1802–1815.

25. Quinn, S., W. Walters, A. Vescovi, and S. Whittemore. 1999. Lineage restriction of neuroepithelial precursor cells from fetal human spinal cord. *J. Neurosci. Res.* **57:** 590–602.

26. Rao, M. 1999. Multipotent and restricted precursors in the central nervous system. *Anat. Rec.* **257:** 137–148.

27. Reubinoff, B. E., M. F. Pera, C. Y. Fong, A. Trounson, and A. Bongso. 2000. Embryonic stem cell lines from human blastocysts: Somatic differentiation *in vitro*. *Nat. Biotechnol.* **18:** 399–404.

28. Reynolds, B. A., and S. Weiss. 1996. Clonal and population analyses demonstrate that an EGF-responsive mammalian embryonic precursor is a stem cell. *Dev. Biol.* **175:** 1–13.

29. Reynolds, B. S., and S. Weiss. 1992. A multipotent EGF-responsive striatal embryonic progenitor cell produces neurons and astrocytes. *J. Neurosci.* **12:** 4565–4574.

30. Svendsen, C. N., M. A. Caldwell, J. Shen, M. G. ter Borg, A. Rosser, P. Tyers, S. Karimol, and S. B. Dunnett. 1997. Long-term survival of human central nervous system progenitor cells transplanted into a rat model of Parkinson's disease. *Exp. Neurol.* **148:** 135–146.

31. Thomson, J. A., J. Itskovitz-Eldor, S. S. Shapiro, M. A. Waknitz, J. J. Swiergiel, V. S. Marshall, and J. M. Jones. 1998. Embryonic stem cell lines derived from human blastocysts. *Science* **282:** 1145–1147.

32. Vescovi, A., E. Parati, A. Gritti, P. Poulin, M. Ferrario, E. Wanke, P. Frolichsthal-Schoeller, L. Cova, M. Arcellana-Panlilio, A. Colombo, and R. Galli. 1999. Isolation and cloning of multipotential stem cells from the embryonic human CNS and establishment of transplantable human neural stem cells lines by epigenetic stimulation. *Exp. Neurol.* **156:** 71–83.

33. Xu, C., M. S. Inokuma, J. Denham, K. Golds, P. Kundu, J. D. Gold, and M. K. Carpenter. 2001. Feeder-free growth of undifferentiated human embryonic stem cells. *Nat. Biotechnol.* **19:** 971–974.

Human embryonic stem cells can differentiate into myocytes with structural and functional properties of cardiomyocytes

See related Commentary on pages 363–364.

Izhak Kehat,[1] Dorit Kenyagin-Karsenti,[2] Mirit Snir,[1] Hana Segev,[2] Michal Amit,[2] Amira Gepstein,[1,3] Erella Livne,[3] Ofer Binah,[4] Joseph Itskovitz-Eldor,[2] and Lior Gepstein[1]

[1]Cardiovascular Research Laboratory, Department of Physiology and Biophysics,
[2]Department of Obstetrics and Gynecology, Rambam Medical Center,
[3]Department of Anatomy, and
[4]Bernard Katz Center for Cell Biophysics, The Bruce Rappaport Faculty of Medicine, Technion-Israel Institute of Technology, Haifa, Israel

Address correspondence to: Lior Gepstein, Cardiovascular Research Laboratory, The Bruce Rappaport Faculty of Medicine, Technion-Israel Institute of Technology, 2 Efron Street, PO Box 9649, 31096 Haifa, Israel.
Phone: 972-4-829-5303; Fax: 972-4-829-5333; E-mail: mdlior@tx.technion.ac.il.
Or to: Joseph Itskovitz-Eldor, Department of Obstetrics and Gynecology, Rambam Medical Center and the Bruce Rappaport Faculty of Medicine, Technion, Haifa, Israel.
Phone: 972-4-8542536; Fax: 972-4-8542503; E-mail: Itskovitz@rambam.health.gov.il.

Izhak Kehat and Dorit Kenyagin-Karsenti contributed equally to this work.

Received for publication January 5, 2001, and accepted in revised form May 31, 2001.

The study of human cardiac tissue development is hampered by the lack of a suitable in vitro model. We describe the phenotypic properties of cardiomyocytes derived from human embryonic stem (ES) cells. Human ES cells were cultivated in suspension and plated to form aggregates termed embryoid bodies (EBs). Spontaneously contracting areas appeared in 8.1% of the EBs. Cells from the spontaneously contracting areas within EBs were stained positively with anti–cardiac myosin heavy chain, anti–α-actinin, anti-desmin, anti–cardiac troponin I (anti-cTnI), and anti-ANP antibodies. Electron microscopy revealed varying degrees of myofibrillar organization, consistent with early-stage cardiomyocytes. RT-PCR studies demonstrated the expression of several cardiac-specific genes and transcription factors. Extracellular electrograms were characterized by a sharp component lasting 30 ± 25 milliseconds, followed by a slow component of 347 ± 120 milliseconds. Intracellular Ca^{2+} transients displayed a sharp rise lasting 130 ± 27 milliseconds and a relaxation component lasting 200–300 milliseconds. Positive and negative chronotropic effects were induced by application of isoproterenol and carbamylcholine, respectively. In conclusion, the human ES cell–derived cardiomyocytes displayed structural and functional properties of early-stage cardiomyocytes. Establishment of this unique differentiation system may have significant impact on the study of early human cardiac differentiation, functional genomics, pharmacological testing, cell therapy, and tissue engineering.

J. Clin. Invest. **108**:407–414 (2001). DOI:10.1172/JCI200112131.

Introduction

The study of early human cardiomyocyte development is hampered by the lack of a suitable model. Hence, valuable information regarding the differentiation of early human cardiac precursor cells, the development of excitability, excitation-contraction coupling, and the molecular signals involved in these processes is largely lacking. In addition, adult cardiomyocytes permanently withdraw from the cell cycle and therefore cannot regenerate. Hence, significant loss of cardiomyocytes is irreversible and leads to the development of progressive heart failure. A potential novel therapeutic approach for this situation is to increase the number of functional myocytes within the depressed region by implantation of myogenic cells. Recent studies demonstrated that fetal cardiomyocytes could survive in infarcted tissue, differentiate, and possibly improve cardiac performance (1, 2). Given that human fetal tissue cannot be obtained in sufficient quantities in the clinical setting, a new source of human cardiomyocytes is sorely needed.

Embryonic stem (ES) cells are continuously growing stem cell lines of embryonic origin, first isolated from the inner cell mass of mouse blastocysts (3). These unique cells are characterized by their capacity to proliferate in an undifferentiated state for a prolonged period in culture, and by their ability to differentiate into every tissue type in the body. The advent of murine ES cells has provided important insights into the early steps of development of excitability in the mammalian heart, including patterns of gene expression, myofibrillogenesis, ion channel development and function, receptor development, and calcium handling (4–9).

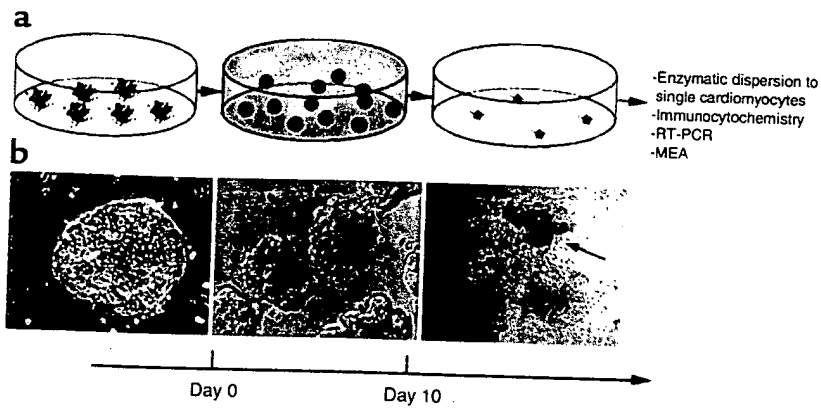

Figure 1
Stages in EB production and differentiation. (a) Schematic of the three stages in human ES cell differentiation. Initially, the ES colonies are grown on top of the MEF feeder layer (left). To induce differentiation, cells are transferred to suspension, where they aggregate to form EBs (middle). After 10 days in suspension, EBs are plated on gelatin-coated culture dishes, where they are observed for the appearance of spontaneous contractions (right). (b) Photomicrographs depicting the just-mentioned three stages: ES colony (left), EBs in suspension (middle), and a contracting area in the outgrowth on an EB (right, arrow).

Given the outstanding potential demonstrated by mouse ES cells, it is not surprising that much effort has been spent on the development of human ES cell lines. This quest ended recently when two groups described the generation of human blastocyst-derived ES cell lines (10, 11). The human ES cells were demonstrated to fulfill all the criteria defining ES cells, namely, derivation from the pre- or peri-implantation embryo, prolonged undifferentiated proliferation under special conditions, and the capacity to form derivatives of all three germ layers. Hence, when cultured with mitotically inactivated mouse embryonic fibroblast (MEF) feeder layer, they could be maintained in the undifferentiated state for prolonged periods. Further studies revealed that when human ES cells were allowed to spontaneously differentiate, they formed embryoid bodies (EBs) containing derivatives of all three germ layers (12). More recently, the effects of different growth factors on differentiation into various lineages were tested in this system (13).

In this report, we describe the use of human ES cells as a reproducible differentiation system for human cardiomyocytes. Using this system, spontaneously contracting foci were, for the first time to our knowledge, demonstrated to have ultrastructural and functional properties consistent with a cardiomyocytic phenotype.

Methods

ES cell preparation and production of EBs. Human undifferentiated ES cells of the single-cell clone H9.2 (14) were grown on mitotically inactivated (mitomycin C) MEF feeder layer in culture medium as described previously (10). The culture medium consisted of 80% knockout DMEM (no-pyruvate, high-glucose formulation; Life Technologies Inc., Rockville, Maryland, USA) supplemented with 20% FBS (HyClone, Logan, Utah, USA), 1 mM L-glutamine, 0.1 mM mercaptoethanol, and 1% nonessential amino acid stock (all from Life Technologies Inc.).

To induce differentiation, ES cells were dispersed to small clumps (three to 20 cells) using collagenase IV (Life Technologies Inc.; 1 mg/ml for 20 minutes). The cells were then transferred to plastic Petri dishes (Miniplast, Ein Shemer, Israel), at a cell density of about 5×10^6 cells in a 58-mm dish, where they were cultured in suspension for 7–10 days. During this stage, the cells aggregated to form EBs, which were then plated on 0.1% gelatin-coated culture dishes, at a density of one to five EBs in a 1.91-cm^2 well, and observed microscopically for the appearance of spontaneous contractions. Figure 1a is a schematic summarizing the different stages in EB generation.

To assess the efficacy of the cardiomyocytic differentiating system, 1,884 EBs were plated on gelatin-coated dishes and monitored microscopically daily for the presence of contractions for up to 30 days after plating. The percentage of EBs displaying contracting areas, as well as the distribution of the timing of onset of spontaneous beating, was evaluated. In a preliminary study, we noted that varying ES cell density input in the suspension phase, although modifying the number of EBs produced, did not affect the percentage of beating EBs. Similarly, screening of two different lots of serum also did not modify the cardiomyocytic yield significantly. In addition, the effect of DMSO, a known stimulant, on differentiation into cardiomyocytic lineage was assessed by adding DMSO (Sigma Chemical Co., St. Louis, Missouri, USA) at a concentration of 0.75% (vol/vol) to the culture medium during the 10 days of growth in suspension. The percentage of contracting EBs and the timing of onset of spontaneous contractions were examined microscopically in 454 EBs.

Immunostaining. Contracting areas were mechanically dissected using a pulled-glass micropipette. These areas were then enzymatically dispersed using trypsin-EDTA (0.5% trypsin, 0.53 mM EDTA; Life Technologies Inc.) for 15 minutes at 37°C. Cells were plated on laminin-coated glass coverslips at a low density to allow visualization of individual cells, incubated for 48 hours, fixed using 4% paraformaldehyde with sucrose, and permeated using 0.5% Triton X-100 (Sigma Chemical Co.). Cells were blocked with 10% BSA and incubated with primary antibodies overnight at 4°C. Primary antibodies used were mAb's for myosin cardiac heavy chain α/β at a dilution of 1:50, mAb's for cardiac muscle troponin I at a dilution of 1:5,000, mAb's for desmin at a dilution of 1:100, and polyclonal antibodies for atrial natriuretic peptide (ANP) at a dilution of

1:250 (all from Chemicon International Inc., Temecula, California, USA). Staining of sarcomeric α-actinin and nebulin was performed using anti-sarcomeric α-actinin mAb's at a dilution of 1:800 and anti-nebulin mAb's at a dilution of 1:200 (both from Sigma Chemical Co.), respectively. After three washes with PBS, cells were incubated with secondary donkey anti-mouse, FITC-conjugated IgG antibodies, absorbed against human tissue for myosin heavy chain, desmin, and troponin I staining, or rhodamine-conjugated anti-rabbit IgG antibodies for α-actinin, ANP, and nebulin staining (both from Chemicon International) at a dilution of 1:100 for 1 hour at room temperature. Preparations were examined using fluorescence microscopy. Dispersed cells isolated from noncontracting EBs served as controls.

RT-PCR. Total RNA from undifferentiated ES cells and contracting EBs was extracted using TRI reagent kit (Sigma Chemical Co.) according to the manufacturer's instructions. cDNA was synthesized from 1 μg total RNA using SuperScript II reverse transcriptase (Life Technologies Inc.). cDNA samples were subjected to PCR amplification with primers selective for human cardiac genes. The PCR primers and the reaction conditions used are described in Table 1. The PCR products were size fractionated by 2% agarose gel electrophoresis.

Electron microscopy. For transmission electron microscopy, the spontaneously contracting areas were mechanically dissected. The tissues were fixed in 3% glutaraldehyde in 0.1 M cacodylate buffer (pH 7.4) at 4°C for 24 hours, postfixed in 1% OsO_4 in the same buffer for 1 hour, dehydrated in graded ethanols, and embedded in Epon 812. Thin (60–90 nm) sections were used for ultrastructural evaluation using a JEOL USA Inc. 100 SX transmission electron microscope (Peabody, Massachusetts, USA) operating at 80 kV.

Extracellular electrophysiological recording and pharmacological studies. Intact contracting areas within the EBs were mechanically dissected using a pulled-glass micropipette and plated on gelatin-coated multielectrode arrays (MEA; Multi Channel Systems MCS GmbH, Reutlingen, Germany) (18). The MEA consists of 60 titanium nitride electrodes with gold contacts 30 μm in diameter with an interelectrode distance of 200 μm. The contracting areas were plated on top of the MEAs, and cells were confluent over the electrodes. However, in some EBs with relatively small contracting areas, the contracting area did not cover all electrodes; hence, recordings were performed from fewer than 60 electrodes. Extracellular signals were recorded simultaneously from all 60 electrodes at 25 kHz and were band-pass filtered from 1 to 3,000 Hz. Recordings were performed in culture medium at 37°C. A pH of 7.4 was maintained using perfusion with air containing 5% CO_2. Chronotropic responses were assessed by extracellular recordings for 10 minutes before and after the culture medium was replaced by a medium containing 10^{-6} M isoproterenol, 10^{-6} M carbamylcholine, 10^{-5} M 3-isobutyl-1-methylxanthine (IBMX), or 10^{-6} M forskolin (all from Sigma Chemical Co.).

Intracellular calcium ($[Ca^{2+}]_i$) transients. The EBs were loaded with fura 2-AM (Molecular Probes Inc., Eugene, Oregon, USA) for 25 minutes at room temperature (24–25°C) at a final concentration of 5 μM, in a 1:1 mixture of Tyrode's solution. EBs were then transferred to a nonfluorescent chamber mounted on the stage of an inverted microscope (Diaphot 300; Nikon Inc., Tokyo, Japan). The chamber was perfused with Tyrode's solution at a rate of 1 ml/min. Experiments were performed at 37°C. Fura 2 fluorescence was measured using a dual-wavelength system (Deltascan; Photon Technology International, Lawrenceville, New Jer-

Table 1
PCR primers used in this study

Gene product	Primer	reaction condition	Product size (bp)
hANP	GAACCAGAGGGGAGAGACAGAG CCCTCAGCTTGCTTTTTAGGAG	35 cycles at 61°C in 1 mM $MgCl_2$	406
MLC-2A	ACAGAGTTTATTGAGGTGCCCC AAGGTGAAGTGTCCCAGAGG	35 cycles at 61°C in 1 mM $MgCl_2$	381
MLC-2V	TATTGGAACATGGCCTCTGGAT GGTGCTGAAGGCTGATTACGTT	35 cycles at 61°C in 1 mM $MgCl_2$	382
GATA4	AGACATCGCACTGACTGAGAAC GACGGGTCACTATCTGTGCAAC	30 cycles at 60°C in 1 mM $MgCl_2$	475
α-Myosin heavy chain	GTCATTGCTGAAACCGAGAATG GCAAAGTACTGGATGACACGCT	40 cycles at 61°C in 2 mM $MgCl_2$	413
Oct-4	GAGAACAATGAGAACCTTCAGGAGA TTCTGGCGCCGGTTACAGAACCA[A]	35 cycles at 55°C in 1.5 mM $MgCl_2$	219
Nkx2.5	CTTCAAGCCAGAGGCCTACG CCGCCTCTGTCTTCTTCAGC[B]	35 cycles at 55°C in 1.5 mM $MgCl_2$	233
cTnT	GGCAGCGGAAGAGGATGCTGAA GAGGCACCAAGTTGGGCATGAACGA[C]	35 cycles at 60°C in 1.5 mM $MgCl_2$	150
cTnI	CCCTGCACCAGCCCCAATCAGA CGAAGCCCAGCCCGGTCAACT[C]	35 cycles at 60°C in 1.5 mM $MgCl_2$	250
GAPDH	AGCCACATCGCTCAGACACC GTACTCAGCGGCCAGCATCG[D]	25 cycles at 61°C in 1.5 mM $MgCl_2$	302

hANP, human ANP; Oct-4, octamer-binding protein 4. [A]Ref. 15. [B]Ref. 16. [C]Ref. 17. [D]Ref. 12.

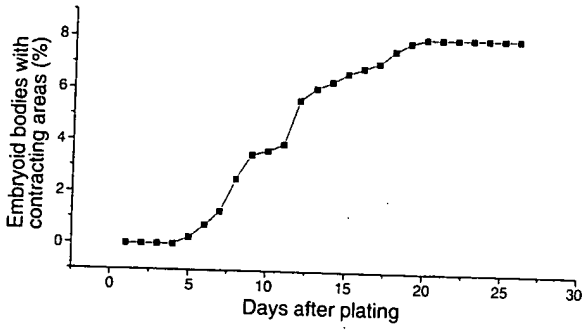

Figure 2
Cumulative percentage of EBs containing spontaneously contracting areas as a function of the number of days after plating of the EB.

sey, USA) as described previously (19). Briefly, two different wavelengths (340 and 380 nm) were used for excitation, and the emitted fluorescence (510 nm) was collected and detected by a photomultiplier tube (710 PMT, photomultiplier detection system; Photon Technology International). Raw data were stored for off-line analysis by the FeliX software (Photon Technology International) as 340 and 380 nm counts and as the ratio $R = F_{340}/F_{380}$. The Savitzky-Golay smoothing algorithm was used to reduce noise level.

Statistical analysis. Data are expressed as mean ± SD. To assess possible chronotropic effects, the average spontaneous beating rate was compared before and after drug application using two-tailed paired Student's *t* test. *P* values less than 0.05 were considered significant.

Results

Human ES cell–derived cardiomyocytes form spontaneously contracting areas. Figure 1b depicts typical examples of ES colonies grown on top of the MEF feeder layer, the formation of EBs during the suspension phase, and an EB containing a contracting area after plating. Rhythmically contracting areas appeared at 4–22 days after plating. Figure 2 illustrates the cumulative percentage of EBs containing contracting areas as a function of the time after plating. Such contracting areas appeared in 153 (8.1%) of the 1,884 EBs studied. At 11–12 days after plating, 50% of the plateau value was reached. The contracting areas usually appeared in the outgrowth of the EB, with a diameter range of 0.2–2 mm, and continued to beat vigorously for up to 5 weeks (the longest period studied). DMSO at a concentration of 0.75% did not cause a major change in the percentage of beating EBs, with 46 of 454 (10.1%) of the EBs demonstrating contracting areas.

Structural analysis. Light microscopy revealed that the contracting areas were composed mainly of relatively small mononuclear cells, 10–30 μm in diameter, with round or rod-shaped morphology. Transmission electron microscopy of these cells revealed mononuclear cells, with parallel arrays of myofibrillar bundles oriented in an irregular manner in some cells (Figure 3a), whereas more mature sarcomeric organization was apparent in others (Figure 3, b and c). The degree of myofibrillar organization varied within different areas of the same cell, among different cells in the same EB, and among different EBs. Nevertheless, in general, a shift from an immature phenotype manifested by disorganized myofibrillar stacks in early stage EBs (Figure 3a) to a more organized sarcomeric structure in later stage EBs (Figure 3, b and c) was noted. In some foci, the formation of early and more developed Z bands could be observed (Figure 3, b and c). The intercalated disc, another cellular structure that characteristically appears during in vivo cardiomyocyte differentiation, was observed in many of the differentiating

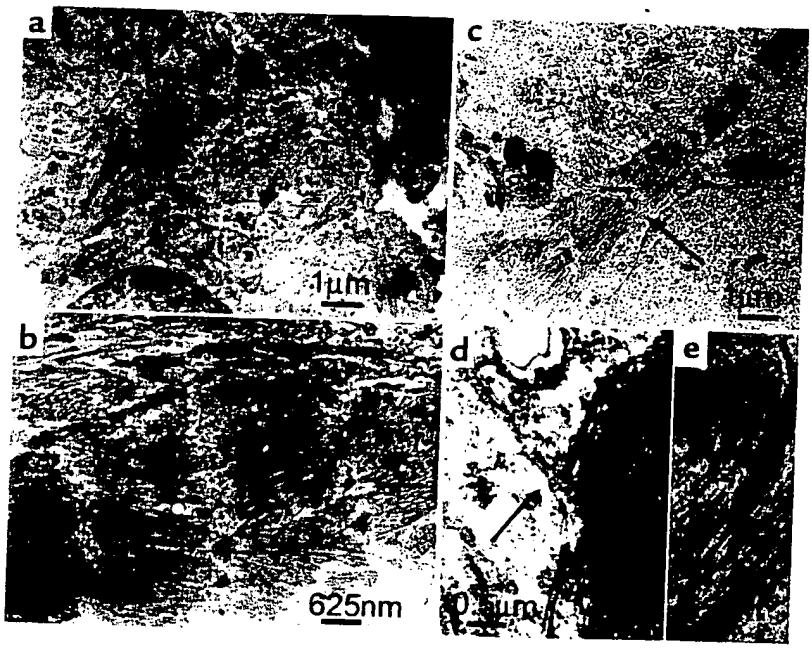

Figure 3
Ultrastructural analysis of ES-derived cardiomyocytes. (**a**) Transmission electron micrograph of sectioned beating EB 10 days after plating. Relatively unorganized myofibrillar bundles can be seen in some myocytes. (**b**) A cell 27 days after plating, displaying a more mature sarcomeric organization. (**c**) A different cell from the same EB as in **b**, demonstrating more organized sarcomeres and Z-bands (arrow). (**d**) High-power electron micrograph showing the presence of a gap junction (arrow) from a cell 16 days after plating. (**e**) High-power electron micrograph showing the presence of desmosomes (arrow) from a cell 16 days after plating.

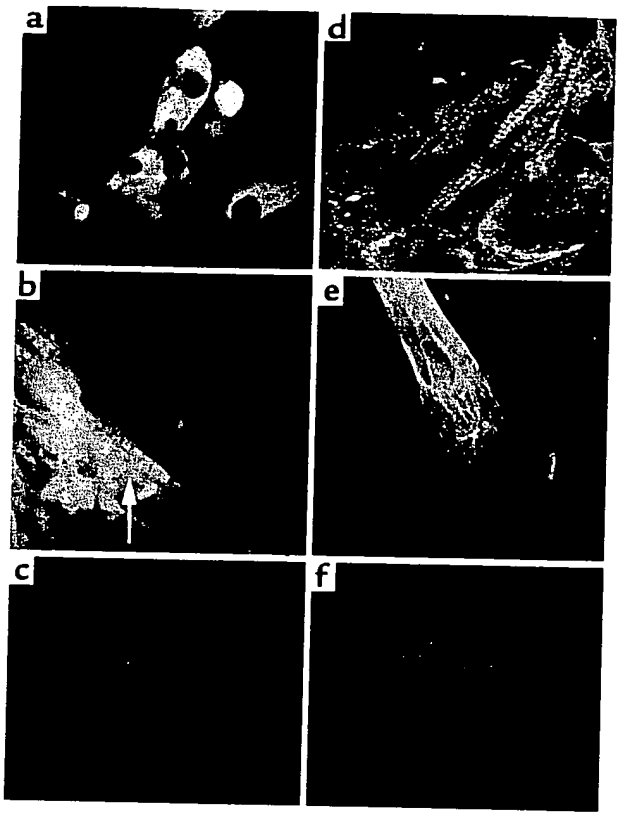

Figure 4
Immunostaining of ES cell–derived cardiomyocytes. (**a**) Immunostaining of dispersed cells from a beating EB (day 16 after plating) with anti-cardiac α/β-myosin heavy chain mAb's. Several cells stained positively. ×40. (**b**) Higher magnification of a cardiomyocyte in a more developed stage (day 16 after plating). Note the appearance of early striation pattern (arrow). ×63. (**c**) Positive staining with anti-sarcomeric α-actinin mAb's (day 17 after plating). ×63. (**d**) Positive staining with cTnI mAb's (day 30 after plating). ×63. (**e**) Positive staining with anti-desmin mAb's (day 18 after plating). ×63. (**f**) Positive staining with anti-ANP antibodies (day 16 after plating). ×63.

EBs. Hence, intercalated discs composed of gap junctions and desmosomes were observed to connect adjacent cells (Figure 3, d and e).

Using immunocytochemistry, the presence of cardiac-specific proteins and their spatial organization were studied in dispersed cells forming contracting EBs. Figure 4a shows positive immunostaining of dispersed myocytes with anti-cardiac α/β-myosin heavy chain mAb's. Varying degrees of myofibrillar organization were noted among the cells. The staining patterns ranged from cytoplasmic clumps in some cells to nonparallel bundles of elongated fibrillar structures in others. Some of these bundles displayed an early striated pattern (Figure 4b). The contracting myocytes also stained positively with anti-α-actinin mAb's (Figure 4c), anti-cTnI mAb's (Figure 4d), and anti-desmin mAb's (Figure 4e), with different cells demonstrating varying degrees of sarcomeric organization. In addition, the positive staining by anti-ANP (Figure 4f) suggested the presence of cytoplasmic ANP granules. In contrast to the positive staining with cardiac-specific proteins, cells from the contracting areas did not demonstrate nebulin immunoreactivity, confirming the cardiomyocytic, rather than skeletal, nature of the cells.

To determine the percentage of cardiomyocytes in the contracting areas, the regions exhibiting spontaneous contracting activity were microdissected, enzymatically dispersed, and plated at low density to allow identification of individual cells by immunocytochemistry. Using cTnI mAb's, the percentage of positively stained cells was 29.4%.

Gene expression studies. The expression of several cardiac-specific genes was assessed in the human ES cell–derived cardiomyocytes and in undifferentiated ES cells using RT-PCR. As shown in Figure 5, myocytes from contracting EBs expressed the cardiac transcription factors GATA4 and Nkx2.5 as well as the cardiac-specific genes cTnI, cardiac troponin T (cTnT), atrial myosin light chain (MLC-2A), ventricular myosin light chain (MLC-2V), and α-myosin heavy chain. MLC-2A expression was also noted in the undifferentiated ES cells, but was markedly increased in the contracting EBs. Octamer-binding protein 4, a marker of undifferentiated cells, was expressed in the ES cells. This expression significantly declined in the contracting EBs. The housekeeping gene *GAPDH* served as an internal control.

Measurements of $[Ca^{2+}]_i$ transients. $[Ca^{2+}]_i$ transients were measured from spontaneously contracting EBs using fura-2AM (n = 7). The average spontaneous beating rate was 0.9 ± 0.11 Hz. Figure 6a displays typical recordings with an initial rise in systolic $[Ca^{2+}]_i$ and a slower decay. The time to peak systolic $[Ca^{2+}]_i$

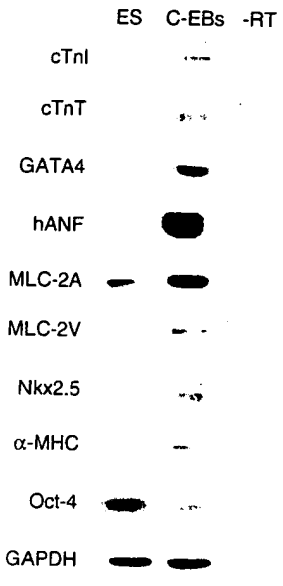

Figure 5
Expression of specific markers in the contracting EBs. Negative images of ethidium-stained gels are shown. RNA samples from undifferentiated ES cells and contracting EBs (C-EBs) were analyzed by RT-PCR for the expression of cardiac-specific markers: cTnI, cTnT, GATA4, human ANP, MLC-2A, MLC-2V, Nkx2.5, and α-myosin heavy chain. Octamer-binding protein 4 (Oct-4) is an ES-cell marker. GAPDH served as internal standard. "-RT" indicates no cDNA.

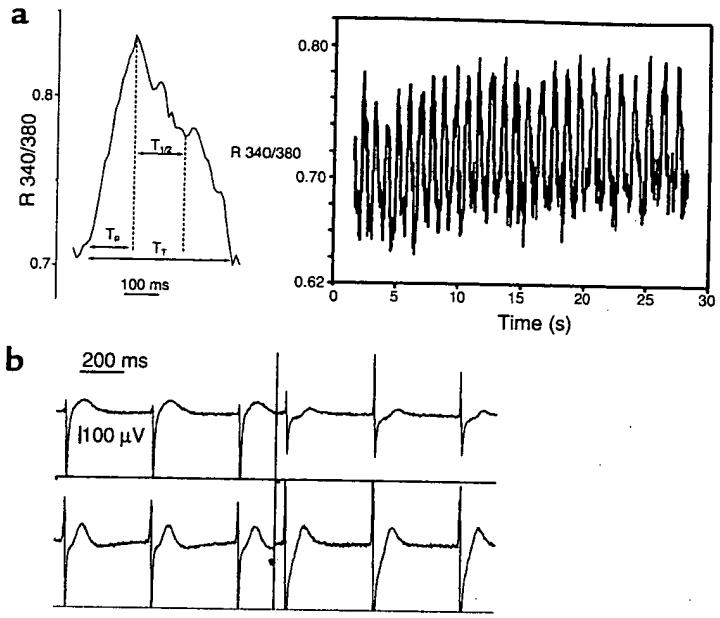

Figure 6

Functional analysis of contracting area within the EBs. (**a**) Calcium transients of human ES cell-derived cardiomyocytes as determined by fura-2 fluorescence. A typical calcium transient is shown on the left, and continuous recording is shown on the right. T_p, time to peak; T_t, total transient time; $T_{1/2}$, time to half-peak relaxation. (**b**) Typical extracellular electrophysiological recordings from different areas of the EB. Note the presence of a sharp and slow component. R, ratio.

averaged 130 ± 27 milliseconds, the time to half-peak relaxation was 143 ± 94 milliseconds, and total transient length was 465 ± 180 milliseconds. In all cases, the $[Ca^{2+}]_i$ signals were synchronous with the contraction rate observed microscopically.

Extracellular electrophysiological recordings and chronotropic studies. Extracellular recordings from the contracting areas displayed electrograms consisting of a sharp component with a peak-to-peak amplitude of 630 ± 33 µV lasting 30 ± 25 milliseconds, followed by a slow component of 347 ± 120 milliseconds, representing the depolarization and repolarization processes, respectively (Figure 6b). The average spontaneous beating rate was 94 ± 33 beats per minute (n = 8) and was stable (mean frequency SD of 1.55 beats per minute) during a recording period of 20 minutes in all EBs studied.

Positive and negative chronotropic responses were observed after administration of the β-agonist isoproterenol and the muscarinic agonist carbamylcholine, respectively. Isoproterenol at 10^{-6} M significantly increased spontaneous contraction rate to 146% ± 43% of its baseline value (n = 8; P < 0.01). Similarly, the direct adenylate cyclase activator forskolin and the phosphodiesterase inhibitor IBMX increased spontaneous contraction rate to 182% ± 48% (n = 6; P < 0.01) and 152% ± 77% (n = 6; P < 0.05) of its initial value. In contrast, the muscarinic agonist carbamylcholine at 10^{-6} M decreased the rate to 78% ± 20% of its initial value (n = 6; P < 0.05). The latter effect was reversed by application of the muscarinic antagonist atropine. All of these responses were prompt, occurring within 90 seconds of drug application.

Discussion

ES cells provide a unique cellular system to study commitment and differentiation of embryonic tissue under in vitro conditions. Cultured as EBs, murine ES cells recapitulate the development of cardiomyocytes from very early cardiac precursor cells to terminally differentiated cells (7). The advent of the murine ES model has thus provided important insights into the early steps of cardiomyogenesis, including the origin, commitment, and differentiation of cardiac cells, patterns of gene expression, myofibrillogenesis, ion channel development and function, and calcium handling (4–9). Nevertheless, there are significant differences between human and murine development, and, for ethical reasons, it is essentially impossible to study the postimplantation human embryo directly.

In this report, we have described a reproducible novel system in which human ES cells differentiate into cardiomyocytic tissue. Our results demonstrate that the spontaneously contracting tissue within the developing EBs contain myocytes portraying structural and functional properties consistent with early-stage cardiac tissue.

Several lines of evidence confirm the cardiomyocytic nature of these cells. Ultrastructural analysis of the differentiating cardiomyocytes showed that these cells were mainly mononuclear and round or rod-shaped, contained different degrees of myofibrillar bundle organization, and exhibited nascent intercalated discs. These myofibrillar structures stained positively with anti-human cardiac myosin heavy chain, anti-α-actinin, anti-desmin, and anti-cTnI mAb's. The cells, however, did not exhibit immunoreactivity with anti-nebulin mAb's, a specific skeletal muscle sarcomeric protein shown to be expressed early in skeletal myoblast differentiation (20).

These results are consistent with ultrastructural properties of early-stage cardiomyocytes and with the developmental process of myofibrillar assembly. Previous studies demonstrated that during in vivo cardiomyogenesis, myofibrils are initially distributed in sparse, irregular myofibrillar arrays, which gradually mature into parallel arrays of myofibrils and ultimately align into densely packed sarcomeres (21, 22).

ES-derived cardiomyocytes express a number of cardiomyocyte-specific genes, including the transcription factors GATA4 and Nkx2.5, which play a significant role in heart formation in vertebrates (23). In addition, in this study the cardiac proteins ANP, cTnI, cTnT,

MLC-2A, MLC-2V, and α-myosin heavy chain were also found to be expressed. MLC-2A expression was also noted in the undifferentiated ES cells, but was markedly increased in the contracting EBs. This expression probably reflects some background differentiation of the ES cells on the feeder layer. The presence of both MLC-2A and MLC-2V might suggest the presence of a number of cardiomyocytic cell types within the contracting areas.

The extracellular recordings, the $[Ca^{2+}]_i$ transients, and the pharmacological studies clearly demonstrate that the contracting areas within the EBs displayed physiological properties consistent with cardiomyocytic tissue and significantly differed from noncardiac (skeletal or smooth) muscle. All components of normal cardiac excitation-contraction coupling were demonstrated within this tissue, namely electrical activation, increase in $[Ca^{2+}]_i$ and the resulting contraction.

Little is known about calcium handling in the normal developing human heart. $[Ca^{2+}]_i$ transients in adult human atrial tissue, studied using fura-2 (24), were similar to the ones recorded in the present study with respect to total duration of the $[Ca^{2+}]_i$ transient and to time of half-peak calcium relaxation. However, the time to peak transient in the EBs (130 ± 27 milliseconds) was longer than the one obtained in human atrial myocytes (52.5 ± 3.1 milliseconds). This difference may have been the result of a number of causes. In the murine ES model, the contracting areas within EBs were shown to be a mixture of atrial, ventricular, and sinus nodal cells (25). Given that different cardiomyocyte types display different calcium characteristics (26), it is possible that the $[Ca^{2+}]_i$ transients measured in whole beating EBs, in the current study, represent a superposition of a mixed population of myocytes with fast and slow cell characteristics. Alternatively, the lower rate in $[Ca^{2+}]_i$ rise may have been due to lower efficiency and immaturity of the calcium machinery in early developing cardiac cells.

The extracellular recordings demonstrated a sharp and a slow component most probably consistent with a relatively long action potential duration characteristic of cardiomyocytes. Fetal and neonatal human skeletal muscle cells in culture, on the other hand, display a much shorter action potential, with mean action potential duration at 50% of depolarization (APD_{50}) of only 7.5 milliseconds (27). The positive and negative chronotropic responses to isoproterenol and carbamylcholine demonstrated the presence of functional adrenergic and cholinergic receptors, respectively, in pacemaker cells. A major pathway of the β-adrenoreceptor–dependent chronotropic response is the activation of adenylate cyclase and the consequent rise in cytosolic cAMP and stimulation of protein kinase. The positive chronotropic effect exerted by forskolin, a direct activator of adenylate cyclase, and by IBMX, a phosphodiesterase inhibitor, suggests that this signaling pathway is already present early in human cardiomyocytic differentiation.

Differences between the murine and human models. Several differences distinguish human and mouse ES cells. Human ES cells have a slightly different morphology and form flatter colonies. The stage-specific embryonic antigen-3 and antigen-4, as well as TRA-1-60 and TRA-1-81, have been shown to be expressed by human but not by mouse ES cells (10). In contrast to the mouse, human ES cells differentiate when cultured in the absence of MEF feeder layer, even in the presence of leukemia inhibitory factor.

The differences between the human and mouse cell lines are not limited to the stem cells. In the normal embryo, heart formation begins with the initiation of differentiation by myocardial and endocardial precursors and leads up to the formation of the cardiac valves. These events cover the first 12 days in the life of a mouse embryo and the first 35 days in the life of a human embryo (23). It is not surprising, therefore, that differentiation of human ES cells into cardiomyocytes proceeds at a slower rate than in mouse ES cells. In the mouse model, ES cells are cultivated in hanging drops for 2 days and are further cultivated as EBs in suspension for 5 days. Spontaneously contracting areas appear 1 day after plating, and, within 2–10 days, 80–90% of EBs reveal pulsating areas (28). In the human ES cell differentiation system described here, cells were grown in suspension for 10 days, and spontaneous contractions did not commence before day 4 after plating, with the median value being 11 days. Furthermore, only 8.1% of EBs revealed pulsating areas. These variations may represent differences between the species, differences between the cell lines, or some yet undetermined factor required in the in vitro differentiation of human ES cells. Several factors that may be optimized in the future to increase cardiomyocytic yield include different serum content, length of suspension period, the use of growth factors, or the use of supporting stroma.

Morphologically, in vitro differentiation of human and mouse ES cells appears to follow parallel pathways. The assembly of the Z-line from periodically aligned Z-bodies and the transition from disorganized myofibrils to the more organized sarcomeric pattern described here have also been noted in the mouse model (7). In the two models, different degrees of myofibrillar assembly coexist within adjacent cardiomyocytes in the same EB and within the same cell. Nevertheless, in the human model, ultrastructural maturation proceeded much more slowly, seemed more heterogeneous, and did not reach the fully mature adult phenotype during the observation period.

Possible research and clinical applications. Establishment of a cardiomyocyte differentiating system from human ES cells may become a powerful tool for understanding cardiac development and function, as human cardiomyocytes are not accessible in adequate quantities for research, especially at this early stage of differentiation. Specifically, important insights may be gathered with regard to the mechanisms involved in cardiac lineage commitment, the process of sarcomeric organization,

action potential and ion channel development, pacemaker organization, calcium handling, and establishment of the adrenergic and cholinergic receptors, as well as the molecular signals involved in these processes.

Another attractive application of these cells is in cell replacement therapy. Adult cardiomyocytes withdraw permanently from the cell cycle during differentiation; hence, any significant loss of cardiomyocytes (as occurs, for example, during myocardial infarction) is irreversible and leads to diminished cardiac function and to the development of progressive heart failure. A potential novel approach for this situation may be the implantation of myogenic cells within the infarcted tissue (1, 2, 29, 30). Although a number of myocyte preparations have been suggested, the inherent electrophysiological, structural, and contractile properties of cardiomyocytes strongly suggest that they may be the ideal donor cell type. Because human fetal cardiomyocytes cannot be obtained in sufficient numbers for clinical purposes, the use of cardiomyocytes derived from ES cell lines may become an attractive option. Nevertheless, several obstacles must be overcome in order to achieve this goal, including the generation of enriched and relatively pure cardiomyocyte cultures and the establishment of different strategies to counter immune rejection.

In summary, this study described the generation of a reproducible cardiomyocyte differentiation system from human ES cells. The generated myocytes were shown to display functional and structural properties consistent with early-stage cardiomyocytes. The establishment of this unique system may have an important impact on the understanding of human cardiac development and function, and may provide a powerful research and clinical tool in several fields such as pharmacological and toxicological testing, functional genomics, early cardiomyogenesis, cell therapy, and tissue engineering.

Acknowledgments

This research was supported in part by the Israel Science Foundation; by the Technion V.P.R. Fund–Malat Family, Loewengart, and Hirshenstrauss-Gutman Medical Research Fund (L. Gepstein); and by the fund for Medical Research and Development of Infrastructure and Health Services, Rambam Medical Center (J. Itskovitz-Eldor). We thank Pesisa Shentzere for technical support, and Ruth Singer for editing of the manuscript.

1. Soonpaa, M.H., Koh, G.Y., Klug, M.G., and Field, L.J. 1994. Formation of nascent intercalated disks between grafted fetal cardiomyocytes and host myocardium. *Science.* **264**:98–101.
2. Leor, J., Patterson, M., Quinones, M.J., Kedes, L.H., and Kloner, R.A. 1996. Transplantation of fetal myocardial tissue into the infarcted myocardium of rat. A potential method for repair of infarcted myocardium? *Circulation.* **94**(Suppl. 9):II332–II336.
3. Evans, M.J., and Kaufman, M.H. 1981. Establishment in culture of pluripotential cells from mouse embryos. *Nature.* **292**:154–156.
4. Sánchez, A., Jones, W.K., Gulick, J., Doetschman, T., and Robbins, J. 1991. Myosin heavy chain gene expression in mouse embryoid bodies. An in vitro developmental study. *J. Biol. Chem.* **266**:22419–22426.
5. Metzger, J.M., Lin, W.-I., Johnston, R.A., Westfall, M.V., and Samuelson, L.C. 1995. Myosin heavy chain expression in contracting myocytes isolated during embryonic stem cell cardiogenesis. *Circ. Res.* **76**:710–719.
6. Maltsev, V.A., Wobus, A.M., Rohwedel, J., Bader, M., and Hescheler, J. 1994. Cardiomyocytes differentiated in vitro from embryonic stem cells developmentally express cardiac-specific genes and ionic currents. *Circ. Res.* **75**:233–244.
7. Hescheler, J., et al. 1997. Embryonic stem cells: a model to study structural and functional properties in cardiomyogenesis. *Cardiovasc. Res.* **36**:149–162.
8. Maltsev, V.A., Ji, G.J., Wobus, A.M., Fleischmann, B.K., and Hescheler, J. 1999. Establishment of β-adrenergic modulation of L-type Ca^{2+} current in the early stages of cardiomyocyte development. *Circ. Res.* **84**:136–145.
9. Viatchenko-Karpinski, S., et al. 1999. Intracellular Ca^{2+} oscillations drive spontaneous contractions in cardiomyocytes during early development. *Proc. Natl. Acad. Sci. USA.* **96**:8259–8264.
10. Thomson, J.A., et al. 1998. Embryonic stem cell lines derived from human blastocysts. *Science.* **282**:1145–1147.
11. Reubinoff, B.E., Pera, M.F., Fong, C.-Y., Trounson, A., and Bongso, A. 2000. Embryonic stem cell lines from human blastocysts: somatic differentiation in vitro. *Nat. Biotech.* **18**:399–404.
12. Itskovitz-Eldor, J., et al. 2000. Differentiation of human embryonic stem cells into embryoid bodies compromising the three embryonic germ layers. *Mol. Med.* **6**:88–95.
13. Schuldiner, M., Yanuka, O., Itskovitz-Eldor, J., Melton, D.A., and Benvenisty, N. 2000. Effects of eight growth factors on the differentiation of cells derived from human embryonic stem cells. *Proc. Natl. Acad. Sci. USA.* **97**:11307–11312.
14. Amit, M., et al. 2000. Clonally derived human embryonic stem cell lines maintain pluripotency and proliferative potential for prolonged periods of culture. *Dev. Biol.* **227**:271–278.
15. Abdel-Rahman, B., Fiddler, M., Rappolee, D., and Pergament, E. 1995. Expression of transcription regulating genes in human preimplantation embryos. *Hum. Reprod.* **10**:2787–2792.
16. Shiojima, I., et al. 1996. Molecular cloning and characterization of human cardiac homeobox gene *CSX1*. *Circ. Res.* **79**:920–929.
17. Ricchiuti, V., Apple, F.S. 1999. RNA expression of cardiac troponin T isoforms in diseased human skeletal muscle. *Clin. Chem.* **45**:2129–2135.
18. Igelmund, P., et al. 1999. Action potential propagation failures in long-term recordings from embryonic stem cell-derived cardiomyocytes in tissue culture. *Pflugers Arch.* **437**:669–679.
19. Felzen, B., et al. 1998. Fas (CD95/Apo-1)-mediated damage to ventricular myocytes induced by cytotoxic T lymphocytes from perforin-deficient mice. A major role for inositol 1,4,5-triphosphate. *Circ. Res.* **82**:438–450.
20. Begum, S., et al. 1998. Differentiation of muscle-specific proteins in chicken somites as studied by immunofluorescence microscopy. *Cell Tissue Res.* **293**:305–311.
21. Manasek, F.J. 1970. Histogenesis of the embryonic myocardium. *Am. J. Cardiol.* **25**:149–168.
22. Chacko, K.J. 1976. Observations on the ultrastructure of developing myocardium of rat embryos. *J. Morphol.* **150**:681–709.
23. Stainier, D.Y. 2001. Zebrafish genetics and vertebrate heart formation. *Nat. Rev. Genet.* **2**:39–48.
24. Brixius, K., Pietsch, M., Hoischen, S., Müller-Ehmsen, J., and Schwinger, R.H.G. 1997. Effect of inotropic interventions on contraction and Ca^{2+} transients in the human heart. *J. Appl. Physiol.* **83**:652–660.
25. Maltsev, V.A., Rohwedel, J., Hescheler, J., and Wobus, A.M. 1993. Embryonic stem cells differentiate in vitro into cardiomyocytes representing sinusnodal, atrial and ventricular cell types. *Mech. Dev.* **44**:41–50.
26. Kolossov, E., et al. 1998. Functional characteristics of ES cell-derived cardiac precursor cells identified by tissue-specific expression of the green fluorescent protein. *J. Cell Biol.* **143**:2045–2056.
27. Iannaccone, S.T., Li, K., and Sperelakis, N. 1987. Transmembrane electrical characteristics of cultured human skeletal muscle cells. *J. Cell. Physiol.* **133**:409–413.
28. Wobus, A.M., Wallukat, G., and Hescheler, J. 1991. Pluripotent mouse embryonic stem cells are able to differentiate into cardiomyocytes expressing chronotropic responses to adrenergic and cholinergic agents and Ca^{2+} channel blockers. *Differentiation.* **48**:173–182.
29. Taylor, D.A., et al. 1998. Regenerating functional myocardium: improved performance after skeletal myoblast transplantation. *Nat. Med.* **4**:929–933.
30. Klug, M.G., Soonpaa, M.H., Koh, G.Y., and Field, L.J. 1996. Genetically selected cardiomyocytes from differentiating embryonic stem cells form stable intracardiac grafts. *J. Clin. Invest.* **98**:216–224.

nature biotechnology

Electromechanical integration of cardiomyocytes derived from human embryonic stem cells

Izhak Kehat[1,3], Leonid Khimovich[1], Oren Caspi[1], Amira Gepstein[1], Rona Shofti[1], Gil Arbel[1], Irit Huber[1], Jonathan Satin[5], Joseph Itskovitz-Eldor[4] & Lior Gepstein[1,2,3]

Cell therapy is emerging as a promising strategy for myocardial repair. This approach is hampered, however, by the lack of sources for human cardiac tissue and by the absence of direct evidence for functional integration of donor cells into host tissues. Here we investigate whether cells derived from human embryonic stem (hES) cells can restore myocardial electromechanical properties. Cardiomyocyte cell grafts were generated from hES cells *in vitro* using the embryoid body differentiating system. This tissue formed structural and electromechanical connections with cultured rat cardiomyocytes. *In vivo* integration was shown in a large-animal model of slow heart rate. The transplanted hES cell–derived cardiomyocytes paced the hearts of swine with complete atrioventricular block, as assessed by detailed three-dimensional electrophysiological mapping and histopathological examination. These results demonstrate the potential of hES-cell cardiomyocytes to act as a rate-responsive biological pacemaker and for future myocardial regeneration strategies.

Because the regenerative capacity of adult heart tissue is limited, any substantial cell loss or dysfunction, such as occurs during myocardial infarction, is mostly irreversible[1] and may lead to progressive heart failure, a leading cause of morbidity and mortality[2]. Similarly, tissue loss or dysfunction at critical sites in the cardiac electrical conduction system may result in inefficient rhythm initiation or impulse conduction, requiring the implantation of a permanent electronic pacemaker[3].

Transplantation of excitable myogenic cells within the dysfunctional zone is a possible therapeutic approach to restoring cardiac electromechanical functions. Although several cell types have been proposed[4–13], the inherent structural, electrophysiological and contractile properties of cardiomyocytes strongly suggest that they may be the ideal donor cell type. However, clinical application of this strategy is hampered by the paucity of cell sources for human cardiomyocytes and by the limited evidence of direct functional integration between host and donor cells[14].

Human ES cells represent a promising source of donor cardiomyocytes. These unique cell lines, isolated from human blastocysts[15,16], can be propagated in the undifferentiated state in culture and coaxed to differentiate into derivatives of all three germ layers[17]. Recently, a reproducible cardiomyocyte differentiating system was established by culturing hES cells as three-dimensional differentiating cell aggregates termed embryoid bodies[18–21]. Cells isolated from spontaneously beating areas of the cultures displayed structural, molecular and functional properties of early-stage cardiomyocytes[18–21]. More recently, we have demonstrated that this differentiating system generates *in vitro* a functional cardiomyocyte syncytium with spontaneous pacemaker activity and action-potential propagation[22].

Here we explore the utility of this unique tissue in cell therapy procedures aimed at restoring myocardial electromechanical functions. We show that excitable cardiac tissue generated from hES cells integrates structurally and functionally *in vitro* over the long term with rat cardiomyocyte cultures. Human ES cell–derived cardiomyocytes were also tested in a large animal model of complete atrioventricular block.

The cardiac conduction system consists of specialized cells that generate and conduct the electrical impulse in the heart. If this specialized conduction system is damaged at the atrioventricular junction, complete block of the electrical propagation between the atria and the ventricles ensues. This results in slow heart rate and circulatory compromise, currently one of the major indications for treatment with a permanent electronic pacemaker.

We found that hES cell–derived cardiomyocytes successfully pace the ventricle in swine with complete heart block. This result shows that the transplanted cells survive, function, and integrate with host cells following *in vivo* grafting and also provides proof-of-concept evidence for the ability of these cells to function as a biological alternative to the electronic pacemaker.

RESULTS

Functional integration in hybrid cultures

The spontaneously contracting areas identified in some of the differentiating embryoid bodies comprised mainly small cells that stained positively for cardiac-specific markers (**Fig. 1a**). The myocytes were arranged in an isotropic pattern and were connected electrically through gap junctions. Interestingly, the hES cell–derived

[1]The Sohnis Family Research Laboratory for the Regeneration of Functional Myocardium, Department of Biophysics and Physiology, the Bruce Rappaport Faculty of Medicine, Technion-Israel Institute of Technology, P.O. Box 9649, Haifa, Israel. [2]The Rappaport Family Institute for Research in the Medical Sciences. [3]Departments of Cardiology and [4]Obstetrics and Gynecology, Rambam Medical Center, Haifa, 31096 Israel. [5]Department of Physiology, University of Kentucky College of Medicine, Lexington, Kentucky, 40536-0298, USA. Correspondence should be addressed to L.G. (mdlior@tx.technion.ac.il).

Published online 26 September 2004; doi:10.1038/nbt1014

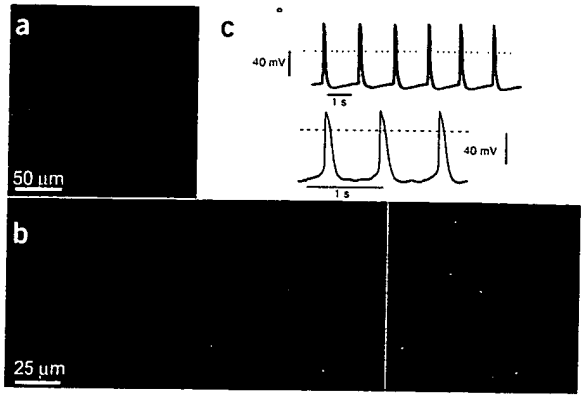

Figure 1 Morphological and functional characterization of the hES cardiomyocytes. (**a**) Immunostaining with anti-cardiac troponin I antibodies (red). Note that the contracting areas consist of positively stained early-stage cardiomyocytes distributed in an isotropic pattern within the embryoid body. Nuclei were counterstained with ToPro3 (blue). (**b**) Positive immunostaining of the beating embryoid bodies with anti-Cx43 (red immunosignal, left panel) and anti-Cx45 (green, middle panel). Note the colocalization of the Cx43 and Cx45 immunosignals to the same gap junctions (yellow dotted staining, right panel). (**c**) Examples of patch-clamp recordings from the hES cardiomyocytes (20–30 d after plating) showing spontaneous action-potential generation. The action potentials recorded from the spontaneously beating cells, either from small clusters of cells (top tracing) or isolated cells (bottom tracing), were characterized by an embryonic-like phenotype.

cardiomyocytes expressed both connexin-43 (Cx43) and Cx45, which in many cases colocalized to the same gap junctions (**Fig. 1b**), a phenomenon common to embryonic cardiomyocytes[23].

The beating embryoid bodies displayed stable and continuous activity for several weeks in culture. Whole-cell patch-clamp recordings from isolated beating hES cardiomyocytes demonstrated uniform embryonic-like action-potential morphology and confirmed the presence of an inherent pacemaking activity in these cells (**Fig. 1c**). Detailed electrophysiological investigation revealed that the biophysical basis for this spontaneous automaticity is a high-input resistance (generated by a low Kir current density) coupled with a relatively high sodium channel density[24].

We next assessed the ability of the hES cardiomyocytes to integrate *in vitro* with primary cultures of neonatal rat ventricular myocytes. The contracting areas within the embryoid bodies were dissected and added to the cardiomyocyte cultures (**Fig. 2a**). Within 24 h after grafting we could already detect microscopically, in all 22 cocultures studied, synchronous mechanical activity (**Supplementary Movie** online).

To further characterize the functional interactions within the cocultures, we mapped their electrical activity with a high-resolution microelectrode array (MEA) mapping technique[22,25] (**Fig. 2a**). By recording extracellular potentials simultaneously from 60 electrodes, we were able to generate high-resolution activation maps that characterize impulse initiation and conduction within the cocultures. A typical MEA map generated during spontaneous rhythm is shown in **Fig. 2b**. In this case, electrical activation was initiated within the rat tissue (red) and then propagated to the rest of the coculture. Electrograms recorded simultaneously from the human and rat tissues (**Fig. 2b**) demonstrated tight temporal coupling continuously for up to 21 d, the longest period studied.

We next carried out pacing studies in which either the rat (**Fig. 2c**) or human (**Fig. 2d**) tissues were stimulated through one of the MEA electrodes. Synchronous activity was maintained in the cocultures during both conditions. To assess electromechanical coupling between the two tissues, we correlated the mechanical contractions in the hES cardiomyocytes, as detected by a photodiode, with the electrical activity. As can be seen in **Fig. 3a**, the mechanical contractions of the embryoid bodies were time-locked with the electrical activity in both human and rat tissues.

The degree of electrical coupling in the cocultures was assessed during long-term recordings and after adrenergic stimulation and partial gap-junction uncoupling. A histogram depicting the ratio between the activation cycle-lengths in the human and rat tissues is shown in **Fig. 3b**. The narrow peak at a ratio of 1 represents equal cycle lengths and confirms that electrical activity in the embryoid bodies was synchronous with that of the rat tissue. Isoproterenol (10 μM) caused a significant increase in the spontaneous beating rate (from 1.5 ± 0.6 to 1.9 ± 0.8 Hz, $P < 0.05$), but electrical coupling between the two cell types was not hindered (**Fig. 3c**). Similarly, mild gap-junction uncoupling using 1-heptanol (0.5 mM) did not alter this

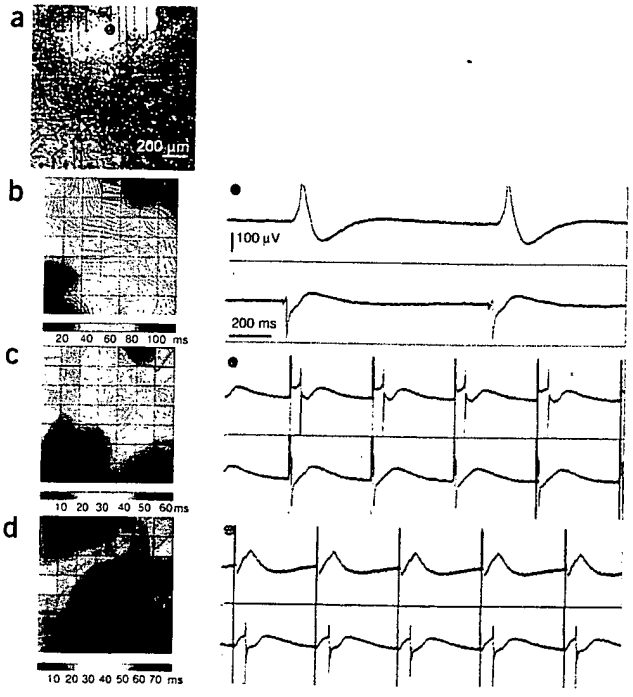

Figure 2 Functional integration in the cocultures. (**a**) Phase-contrast micrograph of coculture grown on top of the MEA, showing the hES cardiomyocytes as a white cluster and the rat ventricular myocyte monolayer in black. (**b**) Left; detailed activation map during spontaneous activity showing the electrical activation originating (red area in the map) in the rat tissue and then propagating to the rest of the coculture, activating also the human tissue. Right; simultaneous recordings from the hES cell–derived (red electrode in **Figure 1a**) and rat (green electrode) cardiac tissues demonstrating synchronous electrical activity between the two tissue types. (**c**,**d**) Activation maps (left) and simultaneous recordings (right) from the rat and human tissues during pacing of either the rat (**c**) or human (**d**) tissue.

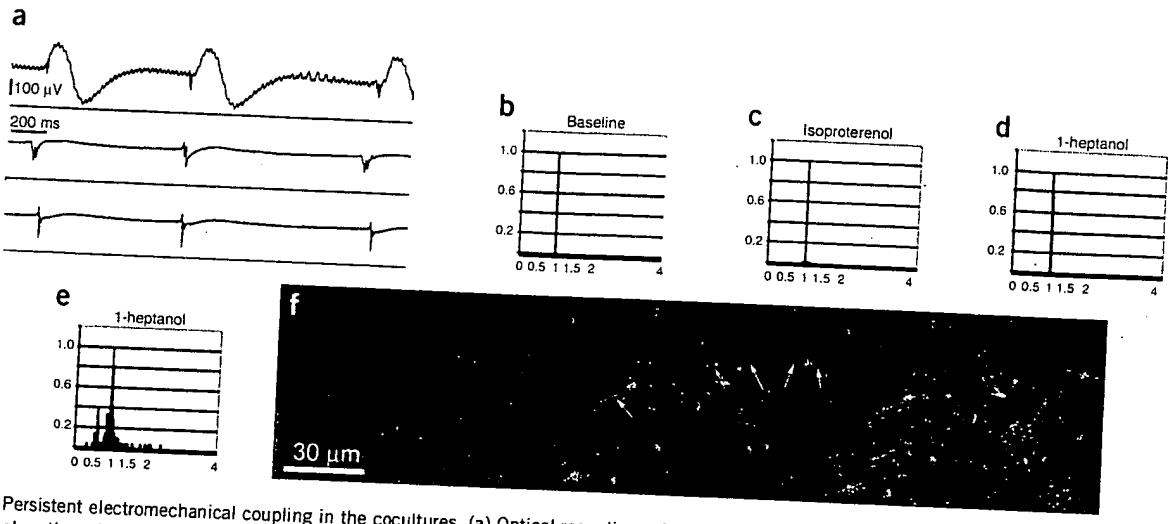

Figure 3 Persistent electromechanical coupling in the cocultures. (**a**) Optical recordings of the contractions in the embryoid body (top) showing synchronous mechanical motion with the electrical activity in the human (middle) and rat (bottom) tissues. (**b–e**) Histograms of the electrical activation cycle-length ratios between the rat and human tissues. The narrow peak at a ratio of 1 represents synchronous activity during long-term recordings at baseline (**b**), after isoproterenol administration (**c**) and in the majority of cultures after heptanol application (**d**). In the minority of cocultures, mild gap junction uncoupling with heptanol caused episodes of 2:1 conduction blocks (**e**). (**f**) Representative confocal images showing the spatial distribution of gap junction (positive Cx43 staining, green) at the interphase between the hES cardiomyocytes and rat cardiomyocytes. Left; spatial distribution of the human cells (stained red by anti-human mitochondrial antibodies) and rat cardiomyocytes (identified by ToPro3 staining of cell nuclei and lack of red cytoplasmic staining). Middle; spatial distribution of gap junctions (positive punctuate Cx43 green staining) in the hybrid cultures. Arrows mark the presence of gap junctions at the tissues' junction. Right; spatial distribution of the hES cardiomyocytes, rat cells and gap junctions.

tight coupling in the majority (five of the eight) of the cocultures (**Fig. 3d**), whereas in three cocultures occasional episodes of 2:1 conduction block were noted (**Fig. 3e**). Higher doses of heptanol (5 mM, causing total gap-junction uncoupling) totally abolished conduction in the hybrid cultures, indicating the significance of the generated gap junctions in electromechanical synchronization.

For electromechanical coupling to occur, specific structural interactions must develop at the interface between donor and host cells. Immunofluorescent staining for Cx43 (the major gap-junction protein) in conjunction with confocal microscopy demonstrated positive Cx43 immunostaining within the contracting embryoid bodies (**Fig. 1b**), between the neonatal rat ventricular myocytes, and at the border between the human and rat cardiomyocytes in the coculture experiments (**Fig. 3f**).

Generation of an *in vivo* biological pacemaker

To assess graft survival and functional integration *in vivo*, we measured the ability of hES cardiomyocytes to pace the heart of pigs with complete heart block. Complete block was induced by ablating the His bundle (the major electrical conduction pathway between the

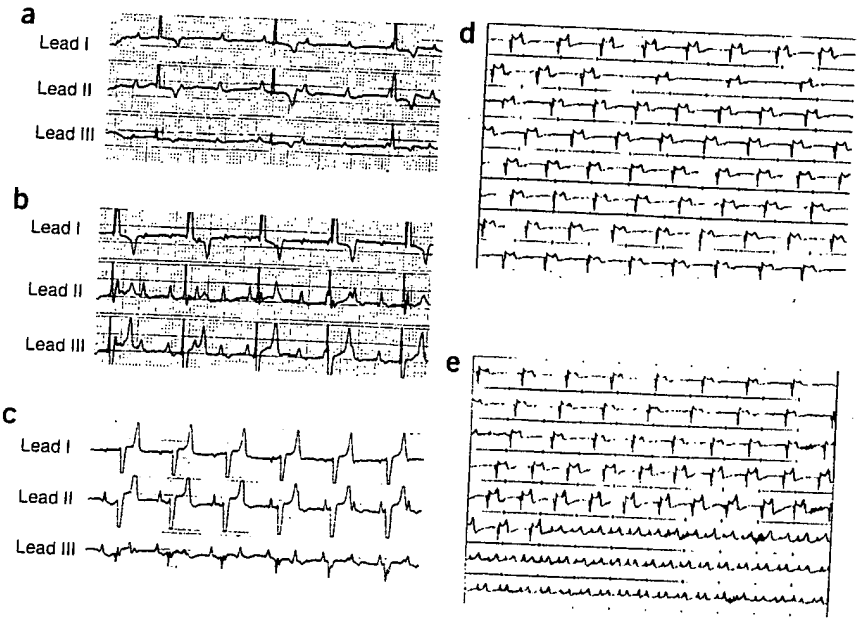

Figure 4 ECG recordings in one of the animals with complete atrioventricular block. (**a–c**) Typical ECG recordings (leads I, II and III) after the creation of complete atrioventricular block. During follow-up, episodes of the junctional escape rhythm (**a**), ventricular paced rhythm (**b**) and the new ventricular ectopic rhythm (**c**) were identified. (**d,e**) Long-term ECG recordings using an implantable loop-recorder. In each animal we could observe three different morphologies that correlate with the three different ECG patterns described in **Figure 4a–c**. Note in this example the presence of a stable and sustained ectopic rhythm after cell transplantation (**d**). Episodes of the sustained ectopic activity were interspersed with periods of the junctional escape rhythm (e, bottom) because of their similar rates. The first rhythm (e, top) was correlated, during electroanatomical mapping, with the new ventricular ectopic rhythm (electrical activation originating from the transplantation site in the posterolateral wall), whereas the second ECG pattern (e, bottom) was correlated with the junctional escape rhythm.

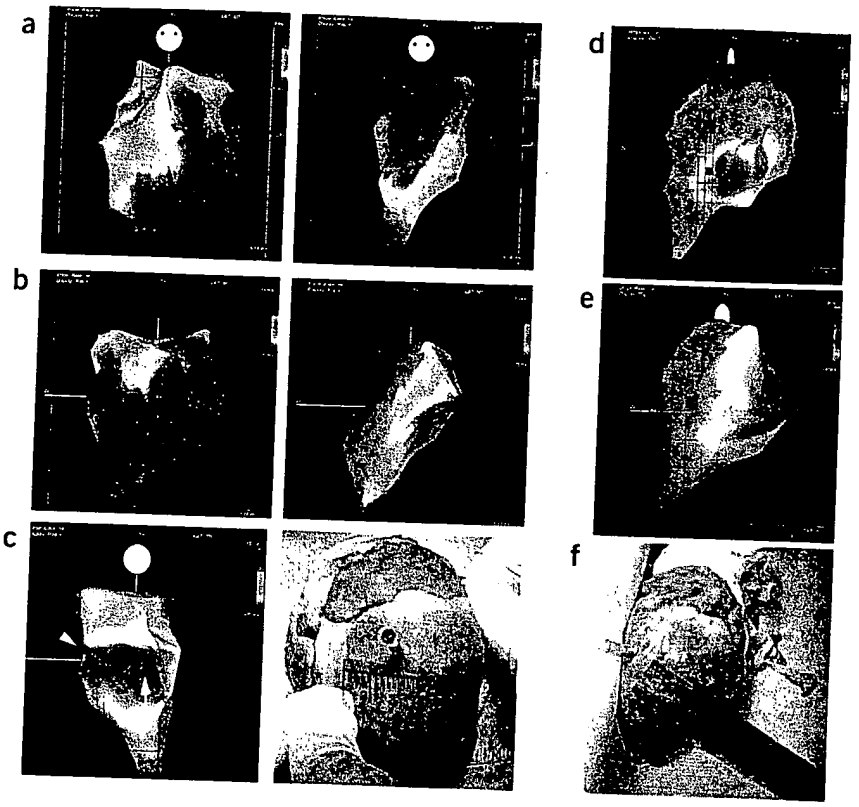

Figure 5 Electroanatomical mapping and pathological correlation of the new ectopic rhythm. (**a**,**b**) Electroanatomical mapping of the junctional (left) and the new ventricular ectopic (right) rhythms. Maps are shown from anteroposterior (**a**) and left lateral (**b**) views. Note that the earliest activation (red) during the junctional rhythm (left) originated from the superior septum, with the posterolateral wall being activated last (blue-purple). In contrast, earliest activation during the new ventricular ectopic rhythm (right) was detected at the posterolateral wall (red area) with the septum being activated last. (**c**) Spatial correlation between the electroanatomical map (left) and the pathological findings (right). During mapping, a focal ablation (arrowhead) was done 2 cm away from the earliest activation site (arrow). Excellent spatial correlation was noted in pathology, with the ablation site (marked by the pink needle) being exactly 2 cm away from the cell injection site (blue suture). (**d**–**f**) Reproducibility of the electrophysiological findings. The same animal was mapped during two separate occasions and the corresponding reproducible electroanatomical maps are presented in a left posterior oblique view (**d**,**e**). A focal ablation was delivered during each mapping procedure on opposite sides of the earliest activation site. Note the excellent correlation in pathology (**f**) with the cell injection site (blue suture) located exactly between the two ablation sites (marked by the two green needles).

atria and the ventricles) with an electrophysiological ablation catheter. Complete atrioventricular block was immediately identified by the appearance of the typical dissociation between atrial (p waves) and ventricular (QRS deflections) activities (**Fig. 4a**). To prevent an extremely slow heart rate in the animals immediately following the creation of atrioventricular block, we also implanted an electronic pacemaker and positioned its electrode at the right ventricular apex.

Electrocardiogram (ECG) recordings after complete atrioventricular block demonstrated the presence of a typical junctional escape rhythm (**Fig. 4a**). The source of this slow escape rhythm, which is characteristic of atrioventricular block, are cardiac cells with inherent pacemaking properties located distal to the site of conduction block. This pacemaking function is usually dormant during normal cardiac function but may become active when the ventricular beating rate slows substantially, as occurs during complete heart block. The ECG recordings also showed intermittent episodes of ventricular pacing (**Fig. 4b**) resulting from the programmed activity of the implanted electronic pacemaker when the spontaneous heart rate fell below a predetermined threshold.

After creation of atrioventricular block, we injected spontaneously contracting clusters of hES cardiomyocytes (40–150 beating embryoid bodies) into the posterolateral region of the left ventricle and marked the epicardial injection site with a suture. We also performed control injections of medium or nonmyocyte hES cell–derivatives into a completely different location in the anterior wall of each animal. A few days after cell transplantation, we could detect episodes of a new ventricular ectopic rhythm (**Fig. 4c**) that had a substantially different morphology (negative axis in leads I, II and III) compared with the junctional (**Fig. 4a**) or paced (**Fig. 4b**) rhythms.

The new ectopic rhythm was detected in 11 out of the 13 animals studied. In five animals this ectopic activity was limited to isolated beats or short runs of activity. In the remaining six animals, the ectopic activity was manifested by the presence of a regular, sustained and hemodynamically stable rhythm (**Fig. 4d**). The average rate of this new rhythm was 59 $\pm$ 11 beats/min, which was similar to the junctional escape rhythm (61 $\pm$ 6 beats/min), explaining the competition between the two rhythms observed in all animals (**Fig. 4e**). Interestingly, this new rhythm was sensitive to adrenergic stimulation, with the rate increasing to 94 $\pm$ 18 beats/min after administration of isoproterenol (10–20 μg/min, $P < 0.05$).

We next subjected the animals to an electrophysiological mapping procedure 1–3 weeks after cell transplantation. Mapping was done with a nonfluoroscopic mapping technique that uses special locatable catheters to generate detailed three-dimensional electroanatomical maps of the heart[26,27]. We initially mapped the junctional escape rhythm (**Fig. 5a,b**; left panels). Not surprisingly, electrical activation was initiated at the superior septum (red), with the posterolateral wall being activated last (blue-purple). The average left ventricle activation time was 50 $\pm$ 6 ms. In contrast, the new ventricular ectopic rhythm was characterized by a shift in the earliest electrical activation to the area of cell transplantation at the posterolateral wall (red area in **Fig. 5a,b**; right panels). Activation then propagated to the rest of the ventricle, with the septum being activated last. Total activation time of this new rhythm was 65 $\pm$ 12 ms. In contrast, we did not note any ectopic activity from control sites (in which medium or noncardiomyocytes were injected) in the anterior wall, nor did we note any substantial ectopic activity in three control animals in which nonmyocyte cells were grafted.

To verify that the origin of the new ventricular ectopic activity was the site of cell grafting, we navigated the catheter to the earliest

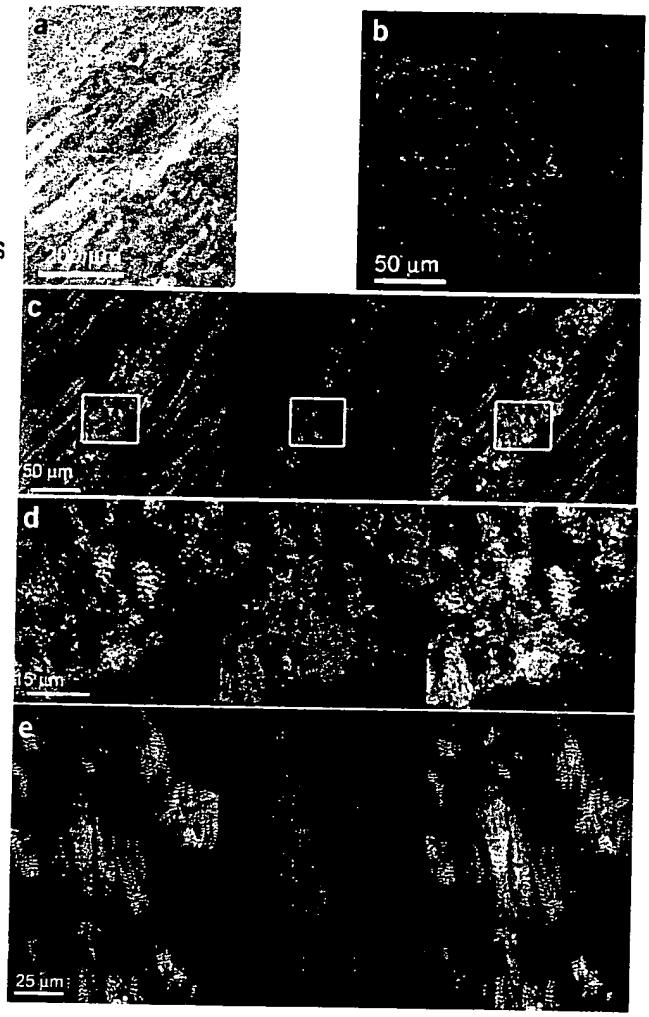

Figure 6 Histological examination of the site of earliest electrical activation. (a) Hematoxylin & eosin staining showing the transplanted cells within the myocardial tissue. (b) High-magnification immunostaining of the area of cell transplantation with anti-human mitochondria antibodies (red) verifying the human phenotype of the transplanted cells. Nuclei were counterstained with ToPro3 (blue). Note the clustering of human cells in the grafted embryoid bodies. (c) Identification of the transplanted cells and their cardiac phenotype. The left and middle panel show the results of immunostaining with anti-α cardiac actinin antibodies (cardiomyocyte phenotype, green) and anti-human mitochondria antibodies (identifying the grafted human cells, red) respectively, whereas the right panel presents the superposition of both images. (d) High-magnification of the area marked by the box in **Figure 6c** showing that the grafted hES cardiomyocytes are small myocytes with an early-striated pattern. (e) High-resolution confocal image of the transplanted cells in a different animal. Note that in rare cases, the grafted cells matured to form elongated cardiomyocytes. The left and middle panel shows the results of immunostaining with anti-α cardiac actinin and anti-human mitochondria antibodies respectively, whereas the right panel shows the superposition of both images.

activation site (arrow in **Fig. 5c**) and did a focal ablation at a nearby location (arrowhead). After harvesting the hearts, we noted an excellent spatial correlation between the electrophysiological and pathological findings (n = 8). Thus, the distances between the locations of earliest activation and ablation in the maps (19 ± 5 mm) highly correlated (r^2 = 0.93) with the measured distances between the ablation and injection sites (20 ± 5 mm) in pathology (**Fig. 5c**, right). To verify the reproducibility of the source of the new ectopic activity, we repeated the mapping procedure in some animals. The acquired maps (**Fig. 5d,e**) were highly reproducible, and focal ablations delivered during each of these mapping procedures on opposite sides of the earliest activation were later identified with excellent spatial correlation in pathology (**Fig. 5f**).

We next validated the presence of the grafted cells at the site of earliest electrical activity. Histological sections from this area identified the transplanted cells, which were organized as cell clusters and were aligned in the appropriate juxtaposition with host cardiomyocytes (**Fig. 6a–c**). The grafted cells were identified and their human nature was established by positive immunostaining with anti-human mitochondrial antibodies (**Fig. 6b–e**). The cardiomyocyte phenotype of many (but not all) of the grafted cells was confirmed using anti-cardiac α-actinin antibodies (**Fig. 6c–e**). The morphology of the grafted hES cardiomyocytes (small cells with early-striated staining pattern, typical of embryonic-like cardiomyocytes) closely resembled their *in vitro* structure (**Fig. 1a**) and thus had not matured substantially after *in vivo* transplantation. In a minority of cases, we noted a more advanced maturation stage of the grafted cells (**Fig. 6e**). In contrast, we did not detect any transplanted cells in sections taken from remote myocardial areas.

DISCUSSION

Cell therapy is a promising therapeutic approach to myocardial repair[28]. In this report, we generated spontaneously excitable cardiomyocyte tissue from hES cells and showed that it integrates structurally, electrically and mechanically with rat cardiac cells *in vitro*. We then demonstrated that the transplanted hES cardiomyocytes survive, integrate and function *in vivo* by showing that they pace the ventricle in pigs with complete heart block.

Recent reports suggest that myocyte transplantation may improve cardiac function in animal models of myocardial infarction[4,12,29–32]. However, it is not clear whether this functional improvement is due to direct contribution to contractility by the transplanted myocytes, attenuation of the remodeling process, amplification of an endogenous repair process or induction of angiogenesis. For example, although transplantation of skeletal myoblasts was shown to improve myocardial performance, gap junctions were not observed between graft and host tissues[4,33]. Yet even the presence of such gap junctions between host and donor cardiomyocyte tissues, as observed in some studies[8,9], does not guarantee functional integration. For such integration to occur, currents generated in one cell passing through gap junctions must be sufficient to depolarize neighboring cells.

Our results demonstrate long-term electromechanical integration between host and donor tissues at several levels. Electromechanical coupling was initially demonstrated *in vitro* by the presence of positive Cx43 immunostaining at the interface between the hES and rat cardiomyocytes and by the appearance of synchronized electrical and mechanical activities in these cocultures. The high degree of coupling was evident by the lack of local conduction delay at the tissues' junction, by the continuous long-term coupling and by the persistent coupling during altered pacemaker position, adrenergic stimulation and partial (but not total) gap-junction uncoupling.

This study also provides evidence for the *in vivo* functional integration of donor cells by demonstrating the ability of hES-cell cardiomyocytes to pace the heart in swine with complete atrioventricular block. Electroanatomical mapping and subsequent

pathological examination confirmed that the source of the new ventricular ectopic rhythm was the site of cell transplantation. Nevertheless, because it is not possible in these whole-organ experiments to map the electrical activity at the cellular level, we could not rule out that this new activity resulted from an indirect effect of the transplanted cells on neighboring host cardiomyocytes. Potential mechanisms for such an effect include the secretion of certain factors from the grafted cardiomyocytes or the generation of electronic currents between grafted and neighboring cardiomyocytes. Similarly, we could not rule out cell fusion as a possible mechanism of the observed results.

Disturbances in the pacemaker function or impulse propagation through the cardiac conduction system may result in severe bradycardia, circulatory failure and even death, and usually require the implantation of a permanent electronic pacemaker. Our proof-of-concept study suggests the use of excitable cell grafts as a biological alternative to implantable devices. We chose to transplant spontaneously excitable cardiomyocyte cell clusters rather than single cardiomyocytes because we hypothesized that because of sink-source mismatches, isolated donor cells connected simultaneously to a number of neighboring cells will not be able to depolarize these cells to threshold and capture the ventricle.

The ability of hES-cell cardiomyocytes to generate stable spontaneous pacemaking activity was demonstrated at several levels. Patch-clamp studies of isolated cells confirmed that they generate repetitive, spontaneous action-potentials and that this automaticity stems from a high-input resistance (low Kir channel density) coupled with a prominent sodium current and the presence of the hyperpolarization-activated current[24]. Continuous pacemaking activity and stable conduction properties were also demonstrated at the multicellular level *in vitro* during long-term recordings of isolated embryoid bodies[22] and in the coculture experiments. Finally, studies in the complete atrioventricular block model also demonstrated the pacemaking capacity of the hES-cell cardiomyocytes *in vivo*.

The possible use of hES-cell cardiomyocytes for biological pacemaking is further strengthened by some of their unique properties. Besides the capability to screen the phenotypic properties of the cells *ex vivo*, they could be genetically engineered to enhance their function. Moreover, the observation that hES-cell cardiomyocytes possess functional adrenergic and cholinergic receptors that respond with appropriate chronotropic changes to specific agonists both *in vitro*[18,22] and *in vivo* suggests that a biological pacemaker could function in a physiological, rate-responsive manner.

The clinical application of such an approach, however, would require continuous fail-safe and long-term function of the grafted pacemaking cells, verification of which was beyond the scope of this study. We noted sustained ectopic activity in only half the animals, and these episodes were interspersed with episodes of junctional escape rhythm. These rhythm changes were probably due to similarities in the rates and therefore competition between the two rhythms, but we could not rule out pacing failure of the transplanted cells. It is also possible that early-stage embryonic myocytes would eventually mature into working ventricular myocytes and lose their propensity for spontaneous pacemaking. In this respect, one might be able to combine innovative gene therapy approaches[34–37] to biological pacing with a cell therapy strategy to create cell grafts with well-characterized, long-term pacemaking properties.

Human ES-cell cardiomyocytes may have advantages over other cell candidates for cardiac repair, such as the availability of potentially unlimited numbers of cardiomyocytes, the possibility of generating different cardiomyocyte cell types, the relative ease of genetic manipulation of these cells and their inherent structural and functional cardiomyocyte properties[19]. Nevertheless, several obstacles must be overcome before this strategy can reach the clinic, including the generation of large quantities of pure cardiomyocyte cultures, the prevention of immune rejection and the demonstration that the grafts survive, function and improve myocardial performance in diseased hearts. A major concern is the possible development of ES cell–related tumors such as teratomas, which were not observed in the current study. To minimize this risk, cells grafts must be free of undifferentiated ES cells.

In summary, this report provides evidence that transplanted hES-cell cardiomyocytes can integrate *in vitro* and *in vivo* with host cardiac tissue. These results suggest the potential utility of these cells to serve as a biological pacemaker and for cardiac regenerative medicine in general.

METHODS

hES cell culturing and generation of embryoid bodies. Human undifferentiated ES cells of the clone H9.2[38] were grown on a mitotically inactivated (mitomycin C) mouse embryonic fibroblast feeder layer (MEF) as previously described[18,38]. The culture medium consisted of 20% FBS (HyClone), 80% knockout DMEM supplemented with 1 mM L-glutamine, 0.1 mM mercaptoethanol and 1% nonessential amino acids (all from Life Technologies). To induce differentiation, hES cells were dispersed to small clamps (3–20 cells) using collagenase IV (1 mg/ml, Life Technologies). The cells were then transferred to plastic Petri dishes at a cell density of about 5×10^6 cells in a 58-mm dish, where they were cultured in suspension for 7–10 d. During this stage the cells aggregated to form embryoid bodies, which were then plated on 0.1% gelatin-coated culture dishes and observed for the appearance of spontaneous contractions. Intact contracting areas within the embryoid bodies were then mechanically dissected using a pulled glass micropipette for use in the different experiments.

Patch-clamp studies. For single-cell action-potential analysis, the whole-cell configuration of the patch-clamp technique was used. Cells were isolated from beating embryoid bodies by 1-h digestion at 37 °C with collagenase B (1 mg/ml, Roche Molecular Biochemical). After dissociation, cells were replated for 1–3 d on gelatin-coated glass coverslips. The patch pipette solution consisted of (in mM): 120 KCl, 1 $MgCl_2$, 3 Mg-ATP, 10 HEPES, 10 EGTA, pH 7.3. The bath recording solution consisted of (in mM): 140 NaCl, 5.4 KCl, 1.8 $CaCl_2$, 1 $MgCl_2$, 10 HEPES, 10 glucose, pH 7.4. Upon seal formation and after patch-break, analog capacitance compensation was used. Series resistance compensation was used up to 80%. Axopatch 200B, Digidata1322 and pClamp8 (Axon) were used for data amplification, acquisition and analysis.

Generation of primary neonatal rat ventricular myocyte cultures. Primary monolayer cultures of neonatal rat (Sprague-Dawley) ventricular myocytes were prepared as previously described[25]. Briefly, after excision, the ventricles were minced in Dulbecco's phosphate buffered saline (Biological industries) and later treated with RDB (IIBR). After centrifugation, the dispersed cells were suspended in culture medium (Ham's F10), 5% fetal calf serum, 5% horse serum, 100 U/ml penicillin, 100 mg/ml streptomycin (all from Biological industries), 1 mM $CaCl_2$ and 50 mg/100 ml bromodeoxyuridine (Sigma). Dispersed cells were then cultured on gelatin-coated (0.1%) microelectrode culture plates or on glass coverslips at a density of 1.5×10^6 cells/ml.

Electrophysiological and mechanical assessment of the hybrid cultures. Once a well-synchronized activity was established in the neonatal rat cardiomyocyte cultures, spontaneously contracting areas within the human embryoid bodies were mechanically dissected and added to the cultures. The electrophysiological properties of the hybrid cultures were examined using a microelectrode array (MEA) data acquisition system (Multi Channel Systems)[22,25]. The MEA plates consist of a matrix of 60 titanium nitride-gold contact (30 μm) electrodes with an interelectrode distance of 100 or 200 μm allowing simultaneous recording of the extracellular potentials at a sampling rate of 10 kHz. All recordings were made at 37 °C and a pH of 7.4.

Local activation time (LAT) at each electrode was determined by the timing of the maximal negative intrinsic deflection (dV/dt_{min}). This information was then used for the generation of color-coded activation maps by interpolating the LAT values between the electrodes using MATLAB standard two-dimensional plotting function (MATLAB 5.3.0, The MathWorks). Mechanical contractions were detected through a microscope (Axiovert 135, Zeiss) using a photodiode (UV100BG, EG&G).

Immunohistochemistry. In the *in vitro* studies isolated embryoid bodies or the cocultures were fixed in 4% paraformaldehyde. In the *in vivo* studies, the hearts were harvested, frozen in liquid nitrogen and cryosectioned. Immunostaining was done using anti-human mitochondria antibodies, anti-Cx43, anti-cardiac troponin I (all from Chemicon) and anti- sarcomeric α- actinin antibodies (Sigma). Secondary antibodies were FITC-conjugated anti-rabbit IgG and Cy3-conjugated anti-mouse IgG (Chemicon) or using the Zenon Labeling Kit (Molecular Probes). Nuclei were counterstained by ToPro3 (Molecular Probes). Confocal microscopy was done using a Nikon Eclipse E600 microscope and Bio-Rad Radiance 2000 scanning system.

Establishment of the swine complete atrioventricular block model and cell transplantation. The study involved 13 study pigs (30–50 kg) and 3 controls. All animal experimental protocols were approved by the Animal Use and Care Committee of the Technion Faculty of Medicine. Anesthesia was maintained after intubation and mechanical ventilation with isoflurane 1%. Vascular access was obtained using cutdown of the jugular veins and carotid arteries. A 7F electrophysiological catheter was introduced to the right atrium through the jugular vein. The catheter was then navigated to the His bundle position (the major electrical conduction pathway, connecting the atria with the ventricles). Complete atrioventricular block was then created by ablating this bundle using radio-frequency energy (using a 500-kHz RF generator; RFG-3C, Radionics in a temperature control mode, 60 °C). After the generation of complete atrioventricular block, we implanted a single chamber pacemaker (ELA Medical) and positioned its electrode at the right ventricular apex to allow ventricular pacing if the junctional escape rate was <50 beats/min.

Cell transplantation. Through a left thoracotomy, we injected the hES cardiomyocytes (40–150 contracting embryoid bodies) at a site in the posterolateral wall of the left ventricle. A suture was used to mark the exact locations where injections were made. In each animal, control injections using either medium or nonmyocyte ES derivatives were made at a different site in the anterior wall. Similar grafting experiments using nonmyocyte cell transplantation were done in the posterolateral wall in three control animals. After the procedure, the animals were treated by daily injections of cyclosporin A (10 mg/kg) and methylprednisolone (2 mg/kg) to prevent immune rejection. Body-surface electrocardiographic recordings were made daily to characterize the rate and configuration of the escape rhythm. In three animals we also implanted subcutaneously an implantable loop recorder (Reveal Plus, Medtronic) that allows continuous recording of body-surface ECGs.

Electroanatomical mapping. A nonfluoroscopic, catheter-based, electroanatomical mapping technique (Carto, Biosense-Webster) was used to assess the electrophysiological activation patterns of the different ventricular rhythms. This system, described in detail elsewhere[26,27], uses magnetic technology to accurately detect the location of a special locatable catheter while it is deployed within the heart. By sampling the location of the catheter together with the local electrogram recorded from its tip at a plurality of endocardial sites, detailed three-dimensional electroanatomical maps of the cardiac chambers can be generated. The LAT at each sampled site was determined as the time interval between a fiducial point on the body-surface ECG and the steepest negative intrinsic deflection from the unipolar recordings. The LATs were color coded (red being earliest activation site and purple the latest) and superimposed on the three-dimensional geometry of the map.

One to three weeks after cell injection, animals were subjected to an additional electrophysiological study. Detailed electroanatomical mapping of the left ventricle was done during the appearance of the new ectopic ventricular rhythm. In some animals we also mapped the junctional escape rhythm. After establishment of the origin of the new ectopic rhythm (earliest activation site), we navigated the catheter to a nearby site (usually 2 cm away) and created a focal radio frequency ablation (temperature, 60 °C; output, 10–40 W) to allow for pathological correlation.

Note: Supplementary information is available on the Nature Biotechnology website.

ACKNOWLEDGMENTS

We thank Asaf Zaretzki and Edith Cohen for their valuable help in the animal studies. We thank Ofer Shenker and the interdisciplinary unit for their technical assistance. This research was supported in part by the Israel Science Foundation (grant no. 520/01), by the Israel Health Ministry, by the Johnson & Johnson Focused Research Grant and by the Nahum Guzik Research Fund.

COMPETING INTERESTS STATEMENT

The authors declare that they have no competing financial interests.

Received 23 February; accepted 19 August 2004
Published online at http://www.nature.com/naturebiotechnology/

1. Pasumarthi, K.B. & Field, L.J. Cardiomyocyte cell cycle regulation. *Circ. Res.* **90**, 1044–1054 (2002).
2. Cohn, J.N. *et al.* Report of the National Heart, Lung, and Blood Institute Special Emphasis Panel on Heart Failure Research. *Circulation* **95**, 766–770 (1997).
3. Kusumoto, F.M. & Goldschlager, N. Cardiac pacing. *N. Engl. J. Med.* **334**, 89–97 (1996).
4. Taylor, D.A. *et al.* Regenerating functional myocardium: improved performance after skeletal myoblast transplantation. *Nat. Med.* **4**, 929–933 (1998).
5. Murry, C.E., Wiseman, R.W., Schwartz, S.M. & Hauschka, S.D. Skeletal myoblast transplantation for repair of myocardial necrosis. *J. Clin. Invest.* **98**, 2512–2523 (1996).
6. Menasche, P. *et al.* Autologous skeletal myoblast transplantation for severe postinfarction left ventricular dysfunction. *J. Am. Coll. Cardiol.* **41**, 1078–1083 (2003).
7. Muller-Ehmsen, J. *et al.* Rebuilding a damaged heart: long-term survival of transplanted neonatal rat cardiomyocytes after myocardial infarction and effect on cardiac function. *Circulation* **105**, 1720–1726 (2002).
8. Reinecke, H., Zhang, M., Bartosek, T. & Murry, C.E. Survival, integration, and differentiation of cardiomyocyte grafts: a study in normal and injured rat hearts. *Circulation* **100**, 193–202 (1999).
9. Soonpaa, M.H., Koh, G.Y., Klug, M.G. & Field, L.J. Formation of nascent intercalated disks between grafted fetal cardiomyocytes and host myocardium. *Science* **264**, 98–101 (1994).
10. Leor, J., Patterson, M., Quinones, M.J., Kedes, L.H. & Kloner, R.A. Transplantation of fetal myocardial tissue into the infarcted myocardium of rat. A potential method for repair of infarcted myocardium? *Circulation* **94**, II332–336 (1996).
11. Toma, C., Pittenger, M.F., Cahill, K.S., Byrne, B.J. & Kessler, P.D. Human mesenchymal stem cells differentiate to a cardiomyocyte phenotype in the adult murine heart. *Circulation* **105**, 93–98 (2002).
12. Orlic, D. *et al.* Bone marrow cells regenerate infarcted myocardium. *Nature* **410**, 701–705 (2001).
13. Klug, M.G., Soonpaa, M.H., Koh, G.Y. & Field, L.J. Genetically selected cardiomyocytes from differentiating embryonic stem cells form stable intracardiac grafts. *J. Clin. Invest.* **98**, 216–224 (1996).
14. Rubart, M. *et al.* Physiological coupling of donor and host cardiomyocytes after cellular transplantation. *Circ. Res.* **92**, 1217–1224 (2003).
15. Thomson, J.A. *et al.* Embryonic stem cell lines derived from human blastocysts. *Science* **282**, 1145–1147 (1998).
16. Reubinoff, B.E., Pera, M.F., Fong, C.Y., Trounson, A. & Bongso, A. Embryonic stem cell lines from human blastocysts: somatic differentiation *in vitro*. *Nat. Biotechnol.* **18**, 399–404 (2000).
17. Itskovitz-Eldor, J. *et al.* Differentiation of human embryonic stem cells into embryoid bodies compromising the three embryonic germ layers. *Mol. Med.* **6**, 88–95 (2000).
18. Kehat, I. *et al.* Human embryonic stem cells can differentiate into myocytes with structural and functional properties of cardiomyocytes. *J. Clin. Invest.* **108**, 407–414 (2001).
19. Gepstein, L. Derivation and potential applications of human embryonic stem cells. *Circ. Res.* **91**, 866–876 (2002).
20. Xu, C., Police, S., Rao, N. & Carpenter, M.K. Characterization and enrichment of cardiomyocytes derived from human embryonic stem cells. *Circ. Res.* **91**, 501–508 (2002).
21. Mummery, C. *et al.* Differentiation of human embryonic stem cells to cardiomyocytes: role of coculture with visceral endoderm-like cells. *Circulation* **107**, 2733–2740 (2003).
22. Kehat, I., Gepstein, A., Spira, A., Itskovitz-Eldor, J. & Gepstein, L. High-resolution electrophysiological assessment of human embryonic stem cell-derived cardiomyocytes: a novel *in vitro* model for the study of conduction. *Circ. Res.* **91**, 659–661 (2002).
23. Alcolea, S. *et al.* Downregulation of connexin 45 gene products during mouse heart development. *Circ. Res.* **84**, 1365–1379 (1999).
24. Satin, J. *et al.* Mechanism of spontaneous excitability in human embryonic stem cell derived cardiomyocytes. *J. Physiol.* (2004).
25. Feld, Y. *et al.* Electrophysiological modulation of cardiomyocytic tissue by transfected fibroblasts expressing potassium channels: a novel strategy to manipulate excitability. *Circulation* **105**, 522–529 (2002).
26. Ben-Haim, S.A. *et al.* Nonfluoroscopic, *in vivo* navigation and mapping technology. *Nat. Med.* **2**, 1393–1395 (1996).

27. Gepstein, L., Hayam, G. & Ben-Haim, S.A. A novel method for nonfluoroscopic catheter-based electroanatomical mapping of the heart. *In vitro* and *in vivo* accuracy results. *Circulation* **95**, 1611–1622 (1997).
28. Reinlib, L. & Field, L. Cell transplantation as future therapy for cardiovascular disease?: A workshop of the National Heart, Lung, and Blood Institute. *Circulation* **101**, E182–187 (2000).
29. Etzion, S. *et al.* Influence of embryonic cardiomyocyte transplantation on the progression of heart failure in a rat model of extensive myocardial infarction. *J. Mol. Cell. Cardiol.* **33**, 1321–1330 (2001).
30. Li, R.K. *et al.* Natural history of fetal rat cardiomyocytes transplanted into adult rat myocardial scar tissue. *Circulation* **96**, II 179–186, discussion 177–186 (1997).
31. Scorsin, M. *et al.* Does transplantation of cardiomyocytes improve function of infarcted myocardium? *Circulation* **96**, II–188–193 (1997).
32. Menasche, P. *et al.* Myoblast transplantation for heart failure. *Lancet* **357**, 279–280 (2001).
33. Reinecke, H., MacDonald, G.H., Hauschka, S.D. & Murry, C.E. Electromechanical coupling between skeletal and cardiac muscle. Implications for infarct repair. *J. Cell. Biol.* **149**, 731–740 (2000).
34. Edelberg, J.M., Aird, W.C. & Rosenberg, R.D. Enhancement of murine cardiac chronotropy by the molecular transfer of the human beta2 adrenergic receptor cDNA. *J. Clin. Invest.* **101**, 337–343 (1998).
35. Miake, J., Marban, E. & Nuss, H.B. Biological pacemaker created by gene transfer. *Nature* **419**, 132–133 (2002).
36. Qu, J. *et al.* Expression and function of a biological pacemaker in canine heart. *Circulation* **107**, 1106–1109 (2003).
37. Potapova, I. *et al.* Human mesenchymal stem cells as a gene delivery system to create cardiac pacemakers. *Circ. Res.* **94**, 952–959 (2004).
38. Amit, M. *et al.* Clonally derived human embryonic stem cell lines maintain pluripotency and proliferative potential for prolonged periods of culture. *Dev. Biol.* **227**, 271–278 (2000).

nature publishing group

home
search
help

INVOICE Nature Sales

Please print this form for your records.

Bill to:
barbara carter
41 perham street
west roxbury, ma 02132
US

Phone: 6173257856
E-mail: bcarter@bromsun.com

Order Date: 03/14/2005
Order No. : 68885

Item	Product No.	Description		Price
1	2NBTFTNBT1014RE	Article purchase from Nature Biotechnology.		$ 30.00
			SubTotal	$ 30.00
			Tax	$ 0.00
			Total	$ 30.00

You may now return to:
Nature Biotechnology Electromechanical integration of cardiomyocytes derived from human embryonic stem cells.

Rapid Publication

Insulin Production by Human Embryonic Stem Cells

Suheir Assady,[1] Gila Maor,[1] Michal Amit,[1] Joseph Itskovitz-Eldor,[1,2] Karl L. Skorecki,[1,2] and Maty Tzukerman[2]

Type 1 diabetes generally results from autoimmune destruction of pancreatic islet β-cells, with consequent absolute insulin deficiency and complete dependence on exogenous insulin treatment. The relative paucity of donations for pancreas or islet allograft transplantation has prompted the search for alternative sources for β-cell replacement therapy. In the current study, we used pluripotent undifferentiated human embryonic stem (hES) cells as a model system for lineage-specific differentiation. Using hES cells in both adherent and suspension culture conditions, we observed spontaneous in vitro differentiation that included the generation of cells with characteristics of insulin-producing β-cells. Immunohistochemical staining for insulin was observed in a surprisingly high percentage of cells. Secretion of insulin into the medium was observed in a differentiation-dependent manner and was associated with the appearance of other β-cell markers. These findings validate the hES cell model system as a potential basis for enrichment of human β-cells or their precursors, as a possible future source for cell replacement therapy in diabetes. *Diabetes* 50:1691–1697, 2001

Approximately 5–10% of all diabetic individuals suffer from type 1 diabetes. Recent studies have emphasized the importance of strict glycemic control in order to reduce ophthalmologic, neurological, and renal complications of the disease (1). Yet, pancreatic cell and islet cell replacement is currently considered the only curative therapy. Indeed, this approach was recently shown to reverse glomerular lesions in patients with diabetic nephropathy (2). The promise of this approach has recently been further strengthened by a report of the use of an improved, less hazardous glucocorticoid-free immunosuppresive regimen in islet allograft transplantation (3). However, the shortage of donations is a primary obstacle preventing this therapeutic modality from becoming a practical solution. Thus, attention has focused on the use of alternative sources such as xenografts, which have other disadvantages, including the potential risk of undetermined zoonotic infections (4). It has also been reported that β-cell lines derived from rodents might provide an unlimited source for cell replacement therapy (5–7). In addition to the problem inherent in xenobiotic sources, such cell lines have been shown to display phenotypic instability, with loss of insulin biosynthesis and regulated secretion while proliferating. Another more recently described approach involves extending the β-cell phenotype to other tissues using in vivo gene transfer (8,9), either by expressing the insulin gene or an insulin gene analogue under the control of a glucose sensitive promoter or by ectopic expression of insulin promoter factor-1 (IPF1)/pancreatic and duodenal homeobox gene-1 (PDX1) (10).

The establishment of pluripotent human embryonic stem (hES) cells (11,12) and embryonic germ (EG) cells (13) have introduced a new potential source for cell therapy in type 1 diabetic patients, especially in light of recent successes in producing glucose-sensitive insulin-secreting cells from mouse embryonic stem (ES) cells (14). hES cells grow as homogeneous and undifferentiated colonies when they are propagated on a feeder layer of mouse embryonic fibroblasts (MEFs) (11). As previously shown, they have a normal karyotype and express telomerase and embryonic cell-surface markers. Removal from the MEF feeder layer is associated with differentiation into derivatives of the three EG layers, as evident from teratomas formed after subcutaneous injection in nude mice (11). Endodermal markers, but not insulin expression, were reported in a previous general survey of different growth conditions and differentiation markers in EG cells (15). Using reverse transcriptase-polymerase chain reaction (RT-PCR) applied to RNA extracted from differentiated hES cells, detection of a variety of differentiated cell markers, including insulin, was reported (16). However, quantitative aspects, including elaboration of insulin into the medium and percentage of insulin-producing cells, were not determined. Such information is crucial to assess the feasibility of using hES cells as a potential source for β-cell replacement therapy. These questions were addressed in the current study, using the differentiation of the H9 line of hES cells as described by Thomson et al. (11). Using a variety of experimental approaches, we found abundant cells with β-cell features, most notably including insulin production and secretion.

From the [1]Bruce Rappaport Faculty of Medicine, Technion, Israel Institute of Technology, and [2]Rambam Medical Center, Bat-Galim, Haifa, Israel.

Address correspondence and reprint requests to Karl L. Skorecki, Rappaport Research Institute, P.O. Box 9649, Bat-Galim, Haifa 31096, Israel. E-mail: skorecki@techunix.technion.ac.il.

Received for publication 16 March 2001 and accepted in revised form 17 May 2001. Posted on the World Wide Web at www.diabetes.org/diabetes on 29 June 2001.

bFGF, basic fibroblast growth factor; dNTP, deoxyribonucleotide; EB, embryoid body; EG, embryonic germ; ES, embryonic stem; GK, glucokinase; hES, human ES; hIns, human insulin; IPF1, insulin promoter factor-1; MEF, mouse embryonic fibroblast; Ngn3, neurogenin-3; Oct4, octamer-binding transcription factor-4; PDX1, pancreatic and duodenal homeobox gene-1; PCR, polymerase chain reaction; RT, reverse transcriptase.

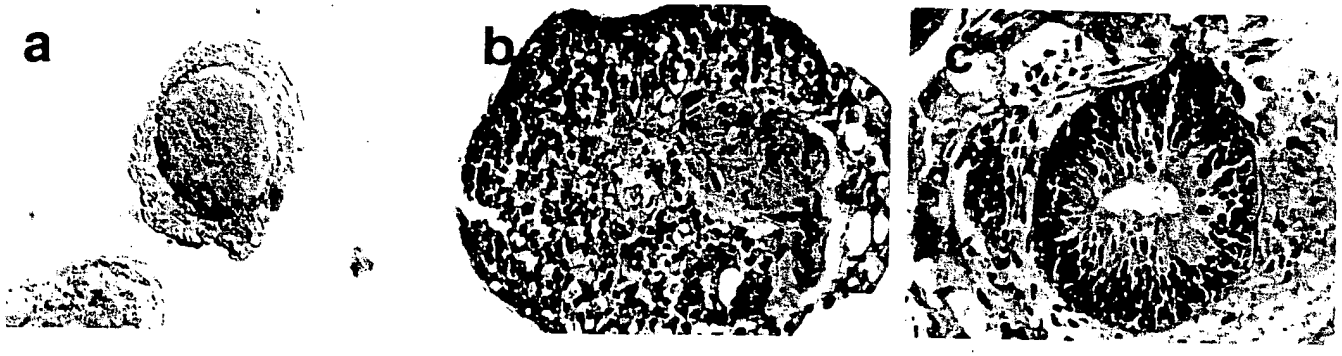

FIG. 1. Differentiation of hES cells in suspension culture. *A*: Simple EB 3 days after removal of MEF and growing in suspension culture. EBs were collected every 3 days, fixed in 10% neutral-buffered formalin, dehydrated in graduated alcohol, and embedded in paraffin. Then, 5-μm sections were stained with hematoxylin and eosin day 3 (*B*) and day 17 (*C*) after differentiation. Original magnification 20× (*A*) and 40× (*B* and *C*).

RESEARCH DESIGN AND METHODS

Tissue culture. Large stocks of primary MEFs were prepared as described by Robertson (17) and stored in liquid nitrogen. After each thaw, cells were used for only 3–5 passages.

The hES-H9 cells were maintained in the undifferentiated state by propagation in culture on a feeder layer of MEFs that had been mitotically inactivated by γ-irradiation with 35 Gy and plated on gelatin-coated six-well plates. Cells were grown in knockout Dulbecco's modified Eagle's medium (Gibco, Grand Island, NY) supplemented with 20% serum replacement (Gibco), 1% nonessential amino acids (Gibco), 0.1 mmol/l 2-mercaptoethanol (Gibco), 1 mmol/l glutamine (Biological Industries, Bet-Haemek, Israel), 4 ng/ml human recombinant basic fibroblast growth factor (bFGF) (PeproTech, Rocky Hill, NJ). Cultures were grown in 5% CO_2, 95% humidity, and were routinely passaged every 4–5 days after disaggregation with 0.1% collagenase IV (Gibco).

Induction of differentiation in hES cells. Methods for the induction of differentiation in mouse ES cells were applied herein for the induction of hES differentiation (17,18). In brief, ~10^7 undifferentiated hES cells were disaggregated and cultured in suspension in 100-mm bacterial-grade petri dishes (Greiner, Frickenhausen, Germany), which resulted in induction of synchronous differentiation characterized by initial formation of small aggregates and followed by the acquisition of the configuration of embryoid bodies (EBs) (19). Alternatively, hES colonies were left unpassaged until confluence (~10 days) and were replated on gelatinized six-well tissue culture plates in the absence of a feeder layer. The cells spontaneously differentiated to an array of cell phenotypes. The growth media used in differentiation are described above.

Histological analysis. EBs were collected at indicated intervals, washed three times with ice-cold phosphate-buffered saline, fixed overnight in 10% neutral-buffered formalin, dehydrated in graduated alcohol (70–100%), and embedded in paraffin. For general histomorphology, 5-μm sections were stained with hematoxylin/eosin.

Immunohistochemistry. Deparaffinized 5-μm sections were incubated for 90 min at room temperature with the primary antibody: polyclonal guinea pig anti-swine insulin, 1:100 dilution (Dako), followed by incubation with goat anti-rabbit biotinylated secondary antibody. Detection was accomplished using streptavidin-peroxidase conjugate and aminoethyl carbazole (or diaminobenzidine tetrahydrochloride) as a substrate (Histostain-SP kit; Zymed Lab). Counterstaining was carried out with hematoxylin. Nonimmune serum was used as a negative control, and normal human pancreas paraffin sections were used as positive controls.

Morphometric studies. To estimate the relative percentage of cells that stained positive by immunohisochemistry, morphometric measurements were conducted as previously described (20).

Insulin detection assay. Adherent cells, MEFs, undifferentiated hES cells, and cells that had differentiated spontaneously in vitro for >20 days were grown in six-well plates. Cells were washed three times with serum-free medium containing 25 mmol/l glucose and incubated in 3 ml of serum-free medium for 2 h. For suspended EBs, experiments were performed in 50-mm bacterial-grade petri dishes. A total of 60–70 EBs per dish were exposed for 2 h to 3 ml of serum-free medium containing either 5.5 or 25 mmol/l glucose. Subsequently, conditioned media were collected, and insulin levels were measured using a microparticle enzyme immunoassay (AXSYM system Insulin kit code B2D010; Abbott) that detects human insulin with no crossreactivaty to proinsulin or C-peptide.

RT-PCR. Total RNA was isolated from undifferentiated hES cells and from in vitro differentiated hES cells growing as EBs or as high-density cultures at various stages of differentiation.

cDNA was synthesized from 7 μg total RNA using Moloney murine leukemia virus RT (Promega) in 1× transcription buffer containing 0.5 μmol/l oligo $dT_{(12-18)}$ (Gibco) and 400 μmol/l deoxyribonucleotides (dNTPs). Aliquots of cDNA were diluted 1:5 for IPF1/PDX1, neurogenin 3 (Ngn3), octamer-binding transcription factor (Oct4), GLUT1, and GLUT2 or 1:2 for insulin- and islet-specific glucokinase (GK). Subsequent PCR was as follows: 2.5 μl cDNA (for IPF1/PDX1, Ngn3, and Oct4) or 5 μl cDNA (for others), 1× PCR buffer, 400 μmol/l dNTPs, 100 ng of each primer pair, and 1 U *Taq* polymerase. After initial hot start for 5 min, amplification continued with 28 cycles for β-actin, 31 cycles for GLUT1, 40 cycles for GLUT2, 38 cycles for GK, 36 cycles for insulin, 37 cycles for Oct4, and 35 cycles for IPF1/PDX1 and Ngn3. Denaturation steps were at 94°C for 1 min, annealing at 58, 52, 50, 67,62, 55, 52, and 60°C for 1 min, respectively, and extension was at 72°C for 1 min and a final polymerization for 10 min. The amplified products were separated on 1.5% agarose gels. Each PCR was performed in duplicate and under linear conditions. The forward and reverse primer sequences used for determination of human insulin (hIns), IPF1/PDX1, Ngn3, and β-actin were as follows: hIns: 5′-GCC TTT GTG AAC CAA CAC CTG-3′, 5′-GTT GCA GTA GTT CTC CAG CTG-3′ (261-bp fragment); IPF1: 5′-CCC ATG GAT GAA GTC TAC C-3′, 5′-GTC CTC CTC CTT TTT CCA C-3′ (262-bp fragment); Ngn3: 5′-CTC GAG GGT AGA AAG GAT GAC GCC TC-3′, 5′-ACG CGT GAA TGG GAT TAT GGG GTG GTG-3′ (948-bp fragment); and β-actin: 5′-CAT CGT GGG CCG CTC TAG GCA C-3′, 5′-CCG GCC AGC CAA GTC CAG GAC GG-3′ (508-bp fragment). The primer sequences used for determination of GLUT1, GLUT2, GK, and Oct4 were as previously described (21–23), the amplified fragments being 310, 398, 380, and 320 bps, respectively.

Statistics. Results are expressed as means ± SE, and comparisons were conducted using the unpaired Student's *t* test.

RESULTS

The H9 line of hES cells was used. These cells grow as homogeneous and undifferentiated colonies when they are propagated on a feeder layer of MEFs. Accordingly, spontaneous in vitro differentiation of H9 cells was investigated after removal of cells from the MEF feeder layer using two different model systems. Cells grown under adherent conditions in tissue culture plates, in the absence of MEFs, displayed a pleiotropic pattern with numerous morphologies, as previously described (24). In contrast, in vitro differentiation in suspension culture resulted in a more consistent pattern, with the formation of discrete EBs. One day after transfer to bacterial-grade petri dishes, cells failed to adhere and formed small aggregates. After 3 days under these conditions, EBs acquired a simple structure with primitive endodermal layers surrounding inner cells (Fig. 1*A*) and then continued to grow in size and developed a more cystic structure (400–700 μm in diameter). Subsequent studies were carried out using immunohistochemistry to determine the spatial and temporal pattern and to

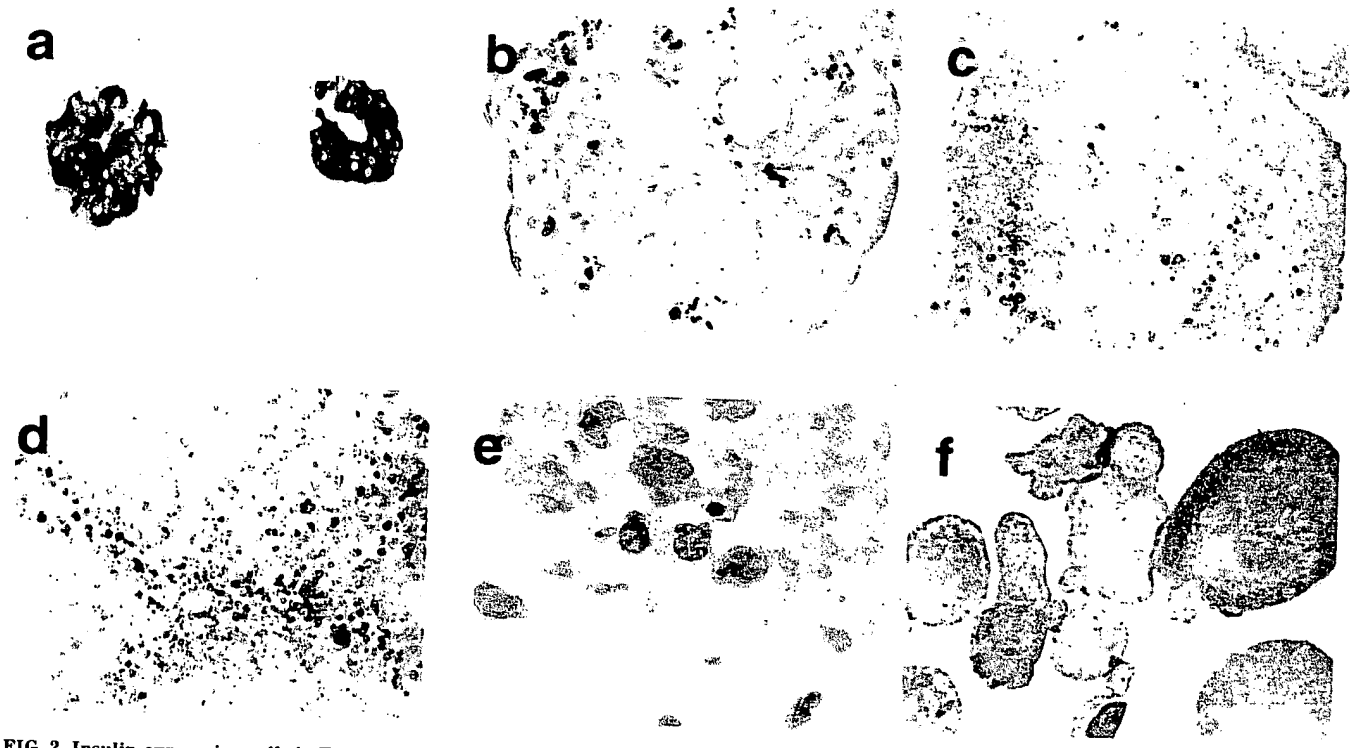

FIG. 2. Insulin-expressing cells in EBs. Immunohistochemistry was performed on paraffin sections as described in RESEARCH DESIGN AND METHODS. *A*: Normal human pancreas was used as a positive control (40× magnification). *B–D*: EBs at day 19 after differentiation (original magnification 40×). *E*: EB at 19 days after differentiation (100× magnification), where the plane of section shows cells in which the cytoplasmic localization of staining is evident. *F*: EBs at 19 days with nonimmune control serum (10× magnification).

obtain an estimate of the relative density of cells in suspension-cultured EBs with insulin-producing capability. Hematoxylin and eosin staining of paraffin-embedded sections was used to provide the overall histological morphology of EBs. Organization of EBs started as early as day 3 after removal from MEFs and transfer to suspension culture. With progressive days in suspension culture, more complex structures became evident, such as epithelial- or endothelial-like cells lining hollow structures or cysts (Fig. 1*B* and *C*).

After EB development, these cells were collected every 3 days until day 19 for immunohistochemistry using anti-insulin antibody. Pancreatic islets were used as a positive control (Fig. 2*A*), and no staining was evident using nonimmune serum (Fig. 2*F*). Occasional cells expressing insulin were evident as early as 14 days of differentiation, with a progressive increase in number through day 19. Insulin-expressing cells were found either scattered throughout the EBs or organized into small clusters (Fig. 2*B–D*). Higher magnification confirmed that immunohistochemical staining was cytoplasmic, as expected (Fig. 2*E*). Among EBs, which stained positively for insulin (60–70%), an average of 1–3% cells positively stained at maximum density. The remaining 30–40% of EBs were negative for insulin staining.

To characterize these insulin-containing cells, which are interspersed among the mixed population of spontaneously differentiating adherent hES, insulin elaborated into the medium was measured by enzyme immunoassay in undifferentiated hES, differentiated hES, and MEF cells. Growth medium contained serum replacement and 25 mmol/l glucose, which is essential for hES viability. Under each of the experimental conditions tested, immunoreactive insulin concentration was measured at the end of a 2-h incubation period in 3 ml of serum-free medium in either six-well plates (adherent cells) or 50-mm petri dishes (EBs). In adherent cells, insignificant immunoreactive insulin could be detected in media harvested from undifferentiated hES (5.6 ± 0.6 μU/ml, n = 6) (Fig. 3*A*); and none could be detected from a feeder layer without overlying hES. However, in media harvested after 22 and 31 days of differentiation, insulin concentrations were as follows: 126.2 ± 17.7 μU/ml (n = 12) and 315.9 ± 47 μU/ml (n = 7), respectively (Fig. 3*A*). Similarly, as shown in Fig. 3*B*, insulin release was significantly greater from 20- to 22-day EBs (60–70 EBs per dish), as compared with undifferentiated hES. No significant difference in insulin concentration was observed when incubations were carried out at a 5.5-mmol/l ambient medium glucose concentration (158 ± 16 μU/ml, n = 6) or at a 25-mmol/l ambient medium glucose concentration (146.2 ± 22.1 μU/ml, n = 6).

The foregoing results prompted us to examine the expression of other β-cell–related genes using RT-PCR analysis of total RNA extracted from undifferentiated and differentiated hES cells. As shown in Fig. 4, insulin mRNA was detected in differentiated cells but not in undifferentiated hES. In parallel, islet GK and GLUT2 genes were also identified after but not before differentiation. Similar results were obtained using either EBs or high-density adherent culture conditions. On the other hand, the GLUT1 isotype, a constitutive glucose transporter, was widely expressed in all forms of hES, as well as in human fibroblasts. Expression of three transcription factors was examined. As expected, mRNA expression of Oct4, a marker of the

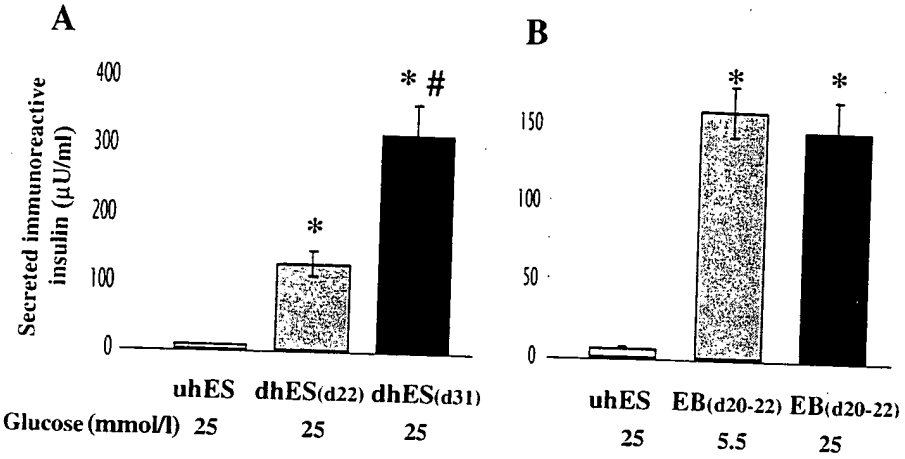

FIG. 3. Insulin secretion at various glucose concentrations and growth conditions. *A*: Undifferentiated hES (uhES) cells were cultured in knockout medium (n = 6) or were allowed to differentiate in high-density adherent conditions (dhES) for 22 (n = 12) and 31 days (n = 7). *B*: hES grown in suspension as EBs (60–70 EBs per dish) for 20–22 days (n = 6). Cultures were exposed to 3 ml of serum-free medium for 2 h containing either 25 or 5.5 mmol/l glucose, as indicated. The media were harvested after incubation, and insulin concentration was measured using enzyme immunoassay as described in RESEARCH DESIGN AND METHODS. Data are means ± SE. *P < 0.0001 vs. uhES; #P = 0.0004 vs. dhES-d22.

pluripotent state (25,26), was detected in undifferentiated hES but decreased progressively during the subsequent 3 weeks of differentiation (Fig. 4*C*). We also demonstrated that differentiating hES cells express IPF1/PDX1 and Ngn3 transcription factors (Fig. 4*C*); together they have been shown to contribute to the regulation of pancreatic and endocrine cell differentiation (27–30).

DISCUSSION

As has been shown during the past two decades, embryonic development of the pancreas is the result of several distinct but interacting mechanisms involving growth factors, epithelial-mesynchymal interactions (31), and extracellular matrix that eventually regulate the expression of diverse transcription factors (27,32–33). However, the initial signal in the cascade of events that eventuate in the commitment of gut endoderm to develop into pancreatic tissue is still obscure. In our study, we provide evidence that a pathway for producing insulin-secreting cells with additional β-cell features is not an infrequent outcome in the course of spontaneous differentiation of hES cells in culture, under the conditions that we used. This observation is a prerequisite for experimental strategies based on the enrichment of spontaneously appearing β-cells or their precursors for cell replacement therapy. The cells described herein produce and secrete insulin and express two essential genes, GLUT2 and islet-specific GK, that are believed to play an important role in β-cell function and glucose-stimulated insulin secretion (34–36). The possibility that the insulin-staining cells are unrelated to β-cells and are of extraembryonic or other origin (37) is highly unlikely, in view of the other markers identified, including the temporal course of appearance of β-cell developmental markers, and in view of the secretion of fully processed insulin.

Although we have not demonstrated glucose responsiveness, we cannot conclude that the cells are glucose unresponsive. As long as β-cells are not in a homogeneous or enriched state, rather presenting among other cell types, we cannot isolate the effects of glucose from countervening effects of other secretagogues. Furthermore, in the absence of homogeneous cell populations, comparisons based on different experimental conditions are not readily quantified because of the heterogeneity among EBs and the difficulty in normalizing insulin response to parameters such as protein or DNA content (38). The fine-tuning of insulin secretion in response to glucose requires cross-talk between adjacent β-cells caused by functional heterogeneity, and it has been shown that isolated β-cells function differently compared with β-cells found in clusters or pseudoislets (39,40). Moreover, long-term exposure to high glucose levels might affect the function of such insulin-producing cells and reduce their responsiveness to acute glucose changes, as has been previously reported in other systems (38). This high-glucose medium is needed to maintain the viable growth of hES in culture, but this does not rule out the possibility that protocols allowing growth of cells with insulin-producing capability in media containing lower glucose concentrations may restore glucose responsiveness. In any case, for treatment of diabetes with β-cell grafts derived from differentiated hES, it will be necessary to demonstrate stimulus-secretion coupling after obtaining enriched or homogeneous β-cell cultures, as has been demonstrated for mouse ES-derived β-cells (14).

Recently, islet cells were successfully generated in vitro from pancreatic stem cells of humans and adult mice (41,42). However, the major practical limitation of this approach is the restricted number of cells that can be cultivated from human pancreases. Hence, hES cells may represent a reasonable potential alternative.

Nevertheless, before proceeding with additional efforts to establish this system as an alternative resource, several issues need to be clarified. For instance, in contrast to the results of in vitro differentiation of hES-1 and -2 lines reported by Reubinoff et al. (12), our H9 suspension cultures did not induce prominent cell death and did result in EB formation. This observation may indicate different characteristics of each hES-derived cell line. Currently used hES cells are not of clonal origin, despite their homogenous appearance in the undifferentiated state, suggesting the need to examine the in vitro differentiation of each hES-derived cell line independently or the need to

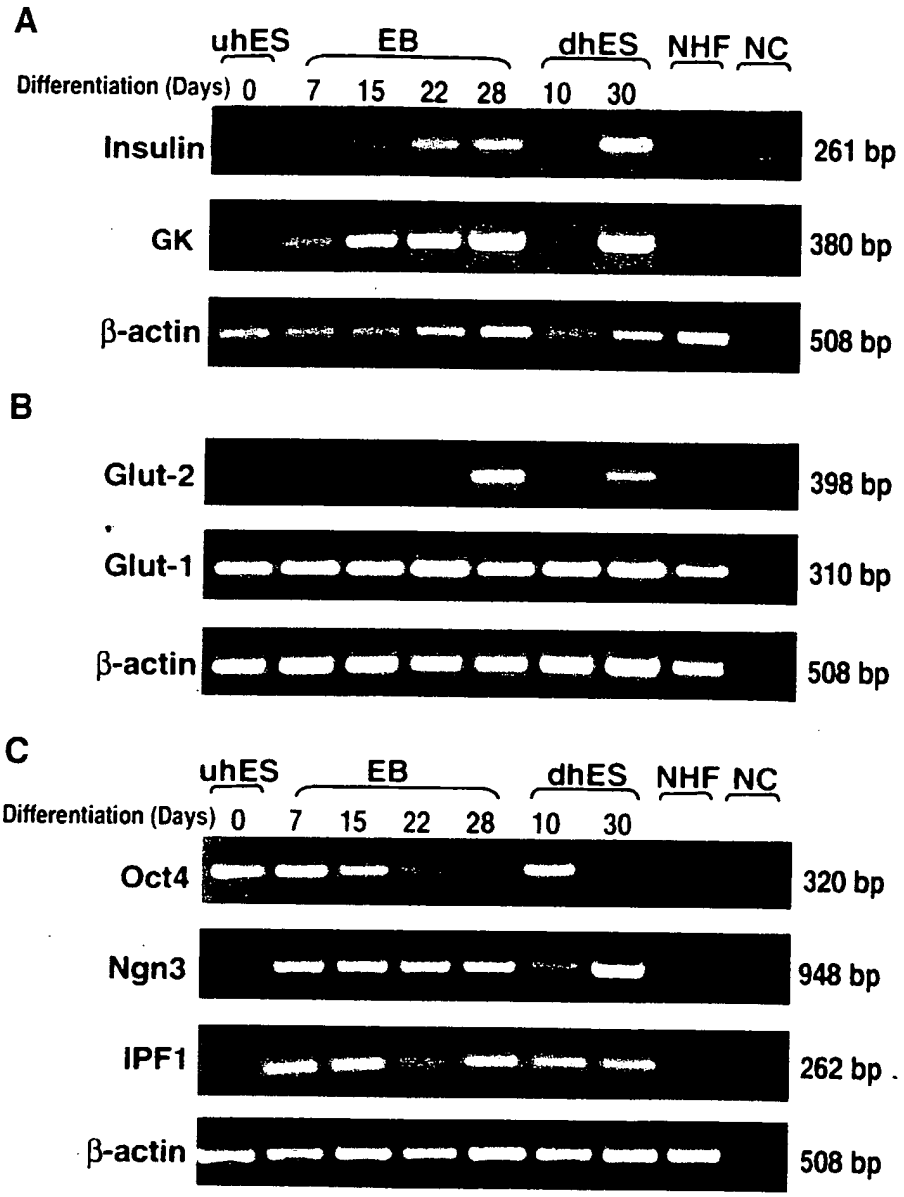

FIG. 4. Expression of β-cell-related genes. Total RNA was extracted from undifferentiated hES (uhES) cells, from differentiated hES growing either as EBs or as high-density adherent cell cultures (dhES) at various stages of differentiation, and from normal human fibroblasts (NHF). cDNA was synthesized from 7 μg total RNA and oligo dT primer. Aliquots of cDNA were diluted 1:2 for insulin and islet-specific GK or 1:5 for GLUT1, GLUT2, Oct4, Ngn3, and IPF1/PDX1 before PCR. β-actin served as an internal standard. NC indicates no cDNA. For insulin, GK, GLUT2, GLUT1, Oct4, Ngn3, IPF1/PDX1, and β-actin, 36, 38, 40, 31, 37, 35, 35, and 28 cycles were applied, respectively, for insulin, GK, and β-actin (*A*); for GLUT1, GLUT2, and β-actin (*B*); and Oct4, Ngn3, IPF1/PDX1, and β-actin (*C*).

examine clonal hES cell lines with well-defined differentiated responses to growth factors (43).

In terms of strategies for enriching the population of insulin-secreting hES-derived cell lines for further characterization and study, our results certainly indicate that the approach first described by Klug et al. (44) to enrich cardiomyocytes from mouse ES cells is potentially applicable. In the case of β-cells, the insulin promoter fused to a downstream selection marker could serve as the relevant selection tool. Indeed, this strategy was recently extended to enrichment of β-cells from mouse ES cells (14). Our findings indicate that even under conditions of spontaneous differentiation from nonclonal pluripotent hES cells, EBs are produced with a surprisingly high representation of cells with insulin-producing capacity, as compared with previous reports using mouse ES (6,14). Although this appears to occur spontaneously, it should be noted that the differentiation medium was supplemented with bFGF. Recently, Hart et al. (45) have suggested that FGF signaling may be involved in β-cell maturation, terminal differentiation, and post natal expansion. Tissue engineering estimates indicate that this is already a sufficient basis for enrichment protocols, based on the strategy described by Klug et al. (44). Certainly, additional protocols to enhance the starting number of β-cells in the mixed population of cells within the EBs can only improve the yield from enrichment strategies. Other limiting issues that may arise include possible senescence (46) of postdifferentiation

hES-cell derivatives attributed to loss of telomerase, as we have reported (24).

In conclusion, our findings clearly indicate that the complex differentiation pattern of hES cells includes a subset of cells that have many characteristics of β-cell function, including proinsulin and/or insulin production and insulin release, as well as the expression of other β-cell markers. Although not surprising, in view of the capacity of ES cells to differentiate into multiple different cell types, this finding is a necessary prerequisite for therapeutic strategies based on cell enrichment from hES cells as a source of cell replacement in type 1 diabetes.

ACKNOWLEDGEMENTS

We thank Z. Shen-Orr and S. Bar-Elan for performing the insulin assay (Endocrinology Laboratory, Rambam Medical Center); the Department of Pathology, Rambam Medical Center, for providing human pancreas paraffin blocks; and I. Reiter for excellent technical assistance.

REFERENCES

1. The Diabetes Control and Complication Trial Research Group: The effect of intensive treatment of diabetes on the development and progression of long-term complications in insulin-dependent diabetes mellitus. *N Engl J Med* 329:977–986, 1993
2. Fioretto P, Steffes MW, Sutherland DE, Goetz FC, Mauer M: Reversal of lesions of diabetic nephropathy after pancreas transplantation. *N Engl J Med* 339:69–75, 1998
3. Shapiro AMJ, Lakey JRT, Ryan EA, Korbutt GS, Toth E, Warnock GL, Kneteman NM, Rajotte RV: Islet transplantation in seven patients with type 1 diabetes mellitus using a glucocorticoid-free immunosuppressive regimen. *N Engl J Med* 343:230–238, 2000
4. Samstein B, Platt JL: Physiologic and immunologic hurdles to xenotransplantation. *J Am Soc Nephrol* 12:182–193, 2001
5. Efrat S: Prospects for gene therapy of insulin-dependent diabetes mellitus. *Diabetologia* 41:1401–1409, 1998
6. Efrat S: Genetically engineered pancreatic β-cell lines for cell therapy of diabetes. *Ann N Y Acad Sci* 875:286–293, 1999
7. Soria B, Andreu E, Berná G, Fuentes E, Gil A, León-Quinto T, Martín F, Montaya E, Nadal A, Reig JA, Ripoll C, Roche E, Sanches-Andrés J: Engineering pancreatic islets. *Pflügers Arch-Eur J Physiol* 440:1–18, 2000
8. Cheung AT, Dayanandan B, Lewis JT, Korbutt GS, Rajotte RV, Bryer-Ash M, Boylan MO, Wolfe MM, Kieffer TJ: Glucose-dependent insulin release from genetically engineered K cells. *Science* 290:1959–1962, 2000
9. Lee HC, Kim SJ, Kim KS, Shin HC, Yoon JW: Remission in models of type 1 diabetes by gene therapy using a single chain insulin-analogue. *Nature* 408:483–488, 2000
10. Ferber S, Halkin A, Cohen H, Ber I, Einav Y, Goldberg I, Barshack I, Seijffers R, Kopolovic J, Kaiser N, Karasik A: Pancreatic and duodenal homeobox gene 1 induces expression of insulin genes in liver and ameliorates streptozotocin-induced hyperglycemia. *Nat Med* 6:568–572, 2000
11. Thomson JA, Itskovitz-Eldor J, Shapiro SS, Waknitz MA, Swiergiel JJ, Marshal VS, Jones JM: Embryonic stem cell lines derived from human blastocysts. *Science* 282:1145–1147, 1998
12. Reubinoff BE, Pera MF, Fong CY, Trounson A, Bongso A: Embryonic stem cell lines from human blastocysts: somatic differentiation in vitro. *Nat Biotech* 18:399–404, 2000
13. Shamblott MJ, Axelman J, Wang S, Bugg EM, Littlefield JW, Donovan PJ, Blumenthal PD, Huggins GR, Gearhart JD: Derivation of pluripotent stem cells from cultured human primordial germ cells. *Proc Natl Acad Sci U S A* 95:13726–13731, 1998
14. Soria B, Roche E, Berná G, León-Quinto T, Reig JA, Martín F: Insulin-secreting cells derived from embryonic stem cells normalize glycemia in streptozotocin-induced diabetic mice. *Diabetes* 49:157–162, 2000
15. Shamblott MJ, Axelman J, Littlefield JW, Blumenthal PD, Huggins GR, Cui Y, Cheng L, Gearhart JD: Human embryonic germ cell derivatives express a broad range of developmentally distinct markers and proliferate extensively in vitro. *Proc Natl Acad Sci U S A* 98:113–118, 2001
16. Schuldiner M, Yanuka O, Itskovitz-Eldor J, Melton DA, Benvenisty N: Effects of eight growth factors on the differentiation of cells derived from human embryonic stem cells. *Proc Natl Acad Sci U S A* 97:11307–11312, 2000
17. Robertson EG (Ed.): *Teratocarcinomas and Embryonic Stem Cells: a practical approach*. Washington, D.C., IRL Press. 71–112, 1987
18. Keller GM: In vitro differentiation of embryonic stem cells. *Curr Op Cell Biol* 7:862–869, 1995
19. Itskovitz-Eldor J, Schuldiner M, Karsenti D, Eden A, Yanuka O, Amit M, Soreq H, Benvenisty N: Differentiation of human embryonic stem cells into embryoid bodies compromising the three embryonic germ layers. *Mol Med* 6:88–95, 2000
20. Green J, Maor G: Effect of metabolic acidosis on the growth hormone/IGF endocrine axis in skeletal growth centers. *Kidney Int* 57:2258–2267, 2000
21. Seino Y, Yamamoto T, Inoue K, Imamura M, Kadowaki S, Kojima H, Fujikawa J, Imura H: Abnormal facilitative glucose transporter gene expression in human islet cell tumors. *J Clin Endocrinol Metab* 76:75–78, 1993
22. Koranyi LI, Tanizawa Y, Welling CM, Rabin DU, Permutt MA: Human islet glucokinase gene: isolation and sequence analysis of full-length cDNA. *Diabetes* 41:807–811, 1992
23. Van Eijk Mj, Van Rooijen MA, Modina S, Scesi L, Folkers G, Van Tol HT, Bevers MM, Fisher SR, Lewin HA, Rakacolli D, Galli C, de Vaureix C, Trounson Ao, Mummery CL, Gandolfi F: Molecular cloning, genetic mapping and developmental expression of bovine POU5F1. *Biol Reprod* 60:1093–1103, 1999
24. Tzukerman M, Shachaf C, Ravel Y, Braunstein I, Cohen-Barak O, Yalon-Hacohen M, Skorecki KL: Identification of a novel transcription factor binding element involved in the regulation by differentiation of the human telomerase (hTERT) promoter. *Mol Biol Cell* 11:4381–4391, 2000
25. Yeom YI, Fuhrmann G, Ovitt CE, Brehm A, Kazuyuki O, Gross M, Hübner K, Schöler HR: Germline regulatory element of Oct-4 specific for the totipotent cycle of embryonal cells. *Development* 122:881–894, 1996
26. Niwa H, Miyazaki JI, Smith AG: Quantitative expression of Oct-3/4 defines differentiation, dedifferentiation or self-renewal of ES cells. *Nat Genet* 24:372–376, 2000
27. Edlund H: Transcribing pancreas. *Diabetes* 47:1817–1823, 1998
28. Apelqvist A, Li H, Sommer L, Beatus P, Anderson DJ, Honjo T, Hrabe de Angelis M, Lendhal U, Edlund H: Notch signalling controls pancreatic cell differentiation. *Nature* 400:877–881, 1999
29. Schwitzgebel VM, Scheel DW, Conners JR, Kalamaras J, Lee JE, Anderson DJ, Sussel L, Johnson JD, German MS: Expression of neurogenin3 reveals an islet cell precursor population in the pancreas. *Development* 127:3533–3542, 2000
30. Herrera PL: Adult insulin- and glucagon-producing cells differentiate from two independent cell lineages. *Development* 127:2317–2322, 2000
31. Scharfmann R: Control of early development of the pancreas in rodents and humans: implications of signals from the mesenchyme. *Diabetologia* 43:1083–1092, 2000
32. Edlund H: Pancreas: how to get there from the gut? *Curr Op Cell Biol* 11:663–668, 1999
33. Kim SK, Hebrok M: Intercellular signals regulating pancreas development and function. *Genes & Dev* 15:111–127, 2001
34. Efrat S: Making sense of glucose sensing. *Nat Genet* 17:249–250, 1997
35. Matschinsky FM, Glaser B, Magnuson MA: Pancreatic β-cell glucokinase: closing the gap between theoretical concepts and experimental realities. *Diabetes* 47:307–315, 1998
36. Shepherd PR, Kahn BB: Mechanism of disease: glucose transporters and insulin action: implication for insulin resistance and diabetes mellitus. *N Engl J Med* 341:248–257, 1999
37. Alarcón C, Serna J, Pérez-Villamil B, de Pablo F: Synthesis and differentially regulated processing of proinsulin in developing chick pancreas, liver and neuroretina (Letter). *FEBS* 436:361–366, 1998
38. Ling Z, Pipeleers DG: Prolonged exposure of human β cells to elevated glucose levels results in sustained cellular activation leading to a loss of glucose regulation. *J Clin Invest* 98:2805–2812, 1996
39. Jonkers FC, Jonas JC, Gilon P, Henquin JC: Influence of cell number on the characteristics and synchrony of Ca^{2+} oscillations in clusters of mouse pancreatic islet cells. *J Physiol* 520:839–849, 1999
40. Charollais A, Gjinovci A, Huarte J, Bauquis J, Nadal A, Martín F, Andreu E, Sánches-Andrés J, Calabrese A, Bosco D, Soria B, Wolheim CB, Herrera PL, Meda P: Junctional communication of pancreatic β cells contributes to the control of insulin secretion and glucose tolerance. *J Clin Invest* 106:235–243, 2000
41. Bonner-Weir S, Taneja M, Weir GC, Tatarkiewics K, Song KH, Sharma A, O'Neil JJ: In vitro cultivation of human islets from expanded ductal tissue. *Proc Natl Acad Sci U S A* 97:7999–8004, 2000
42. Ramiya VK, Maraist M, Arfors KE, Schatz DA, Peck AB, Cornelius JG:

Reversal of insulin-dependent diabetes using islet cells generated *in vitro* from pancreatic stem cells. *Nat Med* 6:278–282, 2000
43. Amit M, Carpenter MK, Inokuma MS, Chiu CP, Harris CP, Waknitz MA, Itskovitz-Eldor J, Thomson JA: Clonally derived human embryonic stem cell lines maintain pluripotency and proliferative potential for prolonged periods of culture. *Dev Biol* 227:271–278, 2000
44. Klug MG, Soonpaa MH, Koh GY, Field LJ: Genetically selected cardiomyocytes from differentiating embryonic stem cells form stable intracardiac grafts. *J Clin Inv* 98:216–224, 1996
45. Hart AW, Baeza N, Apelqvist Å, Edlund H: Attenuation of FGF signaling in mouse β-cells leads to diabetes. *Nature* 408:864–868, 2000
46. Halvorsen TL, Beattie GM, Lopez AD, Hayek A, Levine F: Accelerated telomere shortening and senescence in human pancreatic islet cells stimulated to divide *in vitro*. *J Endocrinol* 166:103–109, 2000